JOURNAL OF PETROLOGY | VOLUME 46 | NUMBER 7 | PAGES 1443–1487 | 2005 | doi:10.1093/petrology/egi022

Tertiary Ultrapotassic Volcanism in Serbia: Constraints on Petrogenesis and Mantle Source Characteristics

D. PRELEVIĆ[1,2]*, S. F. FOLEY[2], R. L. ROMER[3], V. CVETKOVIĆ[1] AND H. DOWNES[4]

[1]FACULTY OF MINING AND GEOLOGY, UNIVERSITY OF BELGRADE, DJUŠINA 7, 11000 BELGRADE, SERBIA & MONTENEGRO

[2]INSTITUTE OF GEOLOGICAL SCIENCES, UNIVERSITY OF MAINZ, BECHERWEG 21, 55099 MAINZ, GERMANY

[3]GEOFORSCHUNGSZENTRUM POTSDAM, TELEGRAFENBERG, D-14473 POTSDAM, GERMANY

[4]SCHOOL OF EARTH SCIENCES, BIRKBECK COLLEGE, MALET STREET, LONDON WC1E 7HX, UK

RECEIVED OCTOBER 10, 2003; ACCEPTED FEBRUARY 7, 2005
ADVANCE ACCESS PUBLICATION MARCH 18, 2005

The Serbian province of Tertiary ultrapotassic volcanism is related to a post-collisional tectonic regime that followed the closure of the Tethyan Vardar Ocean by Late Cretaceous subduction beneath the southern European continental margin. Rocks of this province form two ultrapotassic groups; one with affinities to lamproites, which is concentrated mostly in the central parts of the Vardar ophiolitic suture zone, and the other with affinities to kamafugites, which crops out in volcanoes restricted to the western part of Serbia. The lamproitic group is characterized by a wide range of $^{87}Sr/^{86}Sr_i$ (0·70735–0·71299) and $^{143}Nd/^{144}Nd_i$ (0·51251–0·51216), whereas the kamafugitic group is isotopically more homogeneous with a limited range of $^{87}Sr/^{86}Sr_i$ (0·70599–0·70674) and $^{143}Nd/^{144}Nd_i$ (0·51263–0·51256). The Pb isotope compositions of both groups are very similar ($^{206}Pb/^{204}Pb$ 18·58–18·83, $^{207}Pb/^{204}Pb$ 15·62–15·70 and $^{208}Pb/^{204}Pb$ 38·74–38·99), falling within the pelagic sediment field and resembling Mesozoic flysch sediments from the Vardar suture zone. The Sr and Nd isotopic signatures of the primitive lamproitic rocks correlate with rare earth element fractionation and enrichment of most high field strength elements (HFSE), and can be explained by melting of a heterogeneous mantle source consisting of metasomatic veins with phlogopite, clinopyroxene and F-apatite that are out of isotopic equilibrium with the peridotite wall-rock. Decompression melting, with varying contributions from depleted peridotite and ultramafic veins to the final melt, accounts for consistent HFSE enrichment and isotopic variations in the lamproitic group. Conversely, the most primitive kamafugitic rocks show relatively uniform Sr and Nd isotopic compositions and trace element patterns, and small but regular variations of HFSE, indicating variable degrees of partial melting of a relatively homogeneously metasomatized mantle source. Geochemical modelling supports a role for phlogopite, apatite and Ti-oxide in the source of the kamafugitic rocks. The presence of two contrasting ultrapotassic suites in a restricted geographical area is attributable to the complex geodynamic situation involving recent collision of a number of microcontinents with contrasting histories and metasomatic imprints in their mantle lithosphere. The geochemistry of the Serbian ultrapotassic rocks suggests that the enrichment events that modified the source of both lamproitic and kamafugitic groups were related to Mesozoic subduction events. The postcollisional environment of the northern Balkan region with many extensional episodes is consistent at regional and local levels with the occurrence of ultrapotassic rocks, providing a straightforward relationship between geodynamics and volcanism.

KEY WORDS: *kamafugite; lamproite; Mediterranean; Serbia; mantle metasomatism; veined mantle; petrogenesis*

INTRODUCTION

Ultrapotassic volcanism within the Mediterranean region is spatially and temporally associated with the Late Cretaceous–Cenozoic convergence of Africa–Arabia with Eurasia that resulted in the progressive closure of ocean basins, and ultimately in the collision of the Alpine orogen with the southern passive continental margin of

*Corresponding author. Present address: Johannes Gutenberg - Universitaet, Institut fuer Geowissenschaften, FB 22, Mineralogie, Becherweg 21, 55099 Mainz, Germany. Telephone: (49)(0)6131 39 24763. Fax: (49) (0)6131 39 23070. E-mail: prelevic@uni-mainz.de

Europe (Wilson & Bianchini, 1999). Ultrapotassic rocks of Tertiary–Quaternary age occur in numerous localities, but have been most thoroughly investigated in Italy (Venturelli *et al.*, 1984*b*; Peccerillo, 1985, 1990, 1995, 1998; Conticelli & Peccerillo, 1992; Conticelli *et al.*, 1992, 2002; Conticelli, 1998) and in southeastern Spain (Venturelli *et al.*, 1984*a*, 1988, 1991; Benito *et al.*, 1999; Turner *et al.*, 1999). The Tertiary province described and discussed in this paper occurs in the central Balkan Peninsula and is the third large ultrapotassic province to be described from the Mediterranean region (Prelević *et al.*, 2001*a*, 2001*b*, 2002*a*, 2002*b*, 2003).

Ultrapotassic volcanic rocks have some of the most extreme Sr, Nd and Pb isotopic compositions of any mantle-derived magmas. Lamproites are of special interest as they may represent extreme examples of partial melting of mixed enriched and depleted mantle source rocks. Many intracontinental mantle-derived magmatic rocks may be less extreme blends of these or similar end-members (Wilson & Downes, 1991; Foley, 1992*a*; Anderson, 1995) The incompatible element concentrations and Sr, Nd and Pb isotope systematics of the most primitive Mediterranean ultrapotassic rocks demonstrate that their mantle sources were enriched by metasomatic agents. Extensive investigations of the extremely diverse Italian ultrapotassic rocks (Rogers *et al.*, 1985; Peccerillo, 1992, 1995, 1999, 2003; Conticelli *et al.*, 2002) have indicated roles for shallow-level interaction of mantle-derived magmas with the subducting slab, the overlying mantle wedge and the continental crust in their genesis. There is a general consensus that the geochemistry and isotope characteristics of the most enriched Mediterranean ultrapotassic rocks are due to a crustal signature acquired by the mantle source (Vollmer, 1976, 1989, 1991; Ellam *et al.*, 1989). The location, nature and ultimate origin of this metasomatic reservoir is, however, a matter of debate (Nelson *et al.*, 1986; Vollmer, 1989; Nelson, 1992; Bell, 2002; Gasperini *et al.*, 2002; Murphy *et al.*, 2002; Bell *et al.*, 2003). Three groups of models have been proposed to explain Mediterranean ultrapotassic volcanism, mostly based on the example of the Italian rocks: (1) the multistage mantle evolution model explains the ultrapotassic rocks as melts of the sub-continental lithospheric mantle previously metasomatized by subducted upper continental crust (Peccerillo, 1999, 2003); (2) the single-stage mantle evolution model explains the generation of the Tertiary ultrapotassic and potassic magmatism as caused by a mantle plume head with a diameter approaching 1000 km centred under Italy (Vollmer, 1976; Bell, 2002; Bell *et al.*, 2003), whereby the crustal signature is incorporated in the deep-mantle plume source; a similar deep-mantle source for the crustal component in lamproites has been put forward recently for Gaussberg, Antarctica, and also for Spanish lamproites (Murphy *et al.*, 2002); (3) the slab-window model proposes that some melts are derived directly from mantle plumes, whereas the rest of the magmatism represents mixtures of plume material and subducted upper crustal components (Gasperini *et al.*, 2002).

The issue of asthenospheric or lithospheric mantle sources and the age of the crustal component can be addressed by studying cogenetic ultrapotassic rocks of similar age emplaced within different lithospheric terrane blocks. If considerable differences in isotopic and trace element characteristics exist among the primitive rock types, the magmas are more likely to reflect derivation from a lithospheric source.

In this study we present mineral chemistry, major and trace element and Sr–Nd–Pb isotope data for samples from the newly delineated Serbian ultrapotassic province, which contains rocks of both lamproitic and kamafugitic affinity, as in Italy. The Serbian ultrapotassic province has the potential for better location and definition of the nature of the mantle source than for other Mediterranean ultrapotassic rock provinces. Its major advantage is the spatial distribution of ultrapotassic volcanism across several lithospheric terrane blocks of different provenance (the western blocks are of Gondwana affinity, whereas the eastern blocks are derived from Eurasia). Additionally, the magmatism is post-collisional, intra-continental and postdates the last subduction events by at least 30 Myr (Karamata *et al.*, 1997*a*, 1997*b*, 1999). We argue that the Serbian ultrapotassic magmatism is derived from the lithospheric mantle, and demonstrate that the primary ultrapotassic melts result from partial melting of at least two distinct lithospheric mantle sources.

GEOLOGICAL BACKGROUND AND DISTRIBUTION OF MAGMATISM IN THE SERBIAN ULTRAPOTASSIC PROVINCE

The Balkan Peninsula reflects the complexity of the tectonic evolution of the Mediterranean region. Its central axis comprises several geotectonic units, some of which may be regarded as microcontinents (Fig. 1, inset): (1) the East Serbian composite terrane (or Carpatho-Balkanides; lower Palaeozoic units merged before the Upper Permian) and the Serbo-Macedonian composite terrane (a crystalline terrane that formed the late Mesozoic southern European continental margin), which are fragments of Eurasia to the east; (2) the Vardar ophiolitic suture zone, which is the main suture zone of the Balkan Peninsula; (3) the Jadar Block (an exotic terrane thought to be derived from further west); (4) the Drina–Ivanjica terrane (a microcontinent); (5) the Dinaride ophiolite belt terrane, the suture of a Middle Triassic–Late Jurassic marginal sea of Gondwana; (6) the External Dinarides. All these units merged at the end of the Mesozoic.

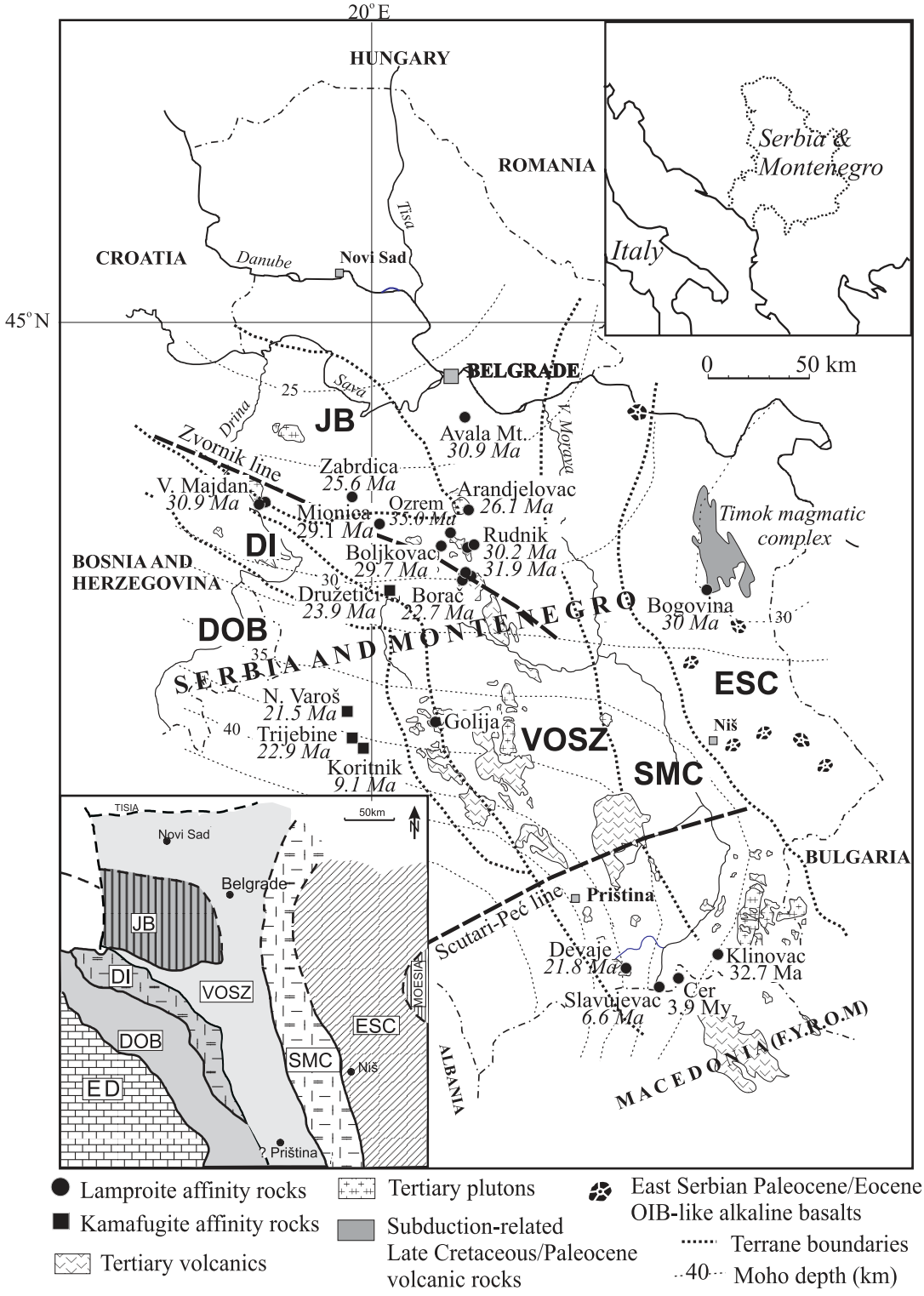

Fig. 1. Distribution and age of Serbian Tertiary ultrapotassic volcanism. The locations of Tertiary plutonic and volcanic formations in Serbia (mostly of intermediate and acid calc-alkaline composition) are also indicated. The inset is a sketch map of the terranes in the central part of the Balkan Peninsula according to Karamata & Krstić (1996) and Karamata *et al.* (1997*b*, 1999). ESC, East Serbian composite terrane; SMC, Serbo-Macedonian composite terrane; VOSZ, Vardar ophiolitic suture zone; JB, Jadar Block terrane; DI, Drina–Ivanjica terrane; DOB, Dinaride ophiolite belt; ED, External Dinarides. Moho depths according to Aljinović (1987). Zvornik line and Scutari–Peć line according to Marović *et al.* (2000, 2002); F.Y.R.O.M., Former Yugoslav Republic of Macedonia.

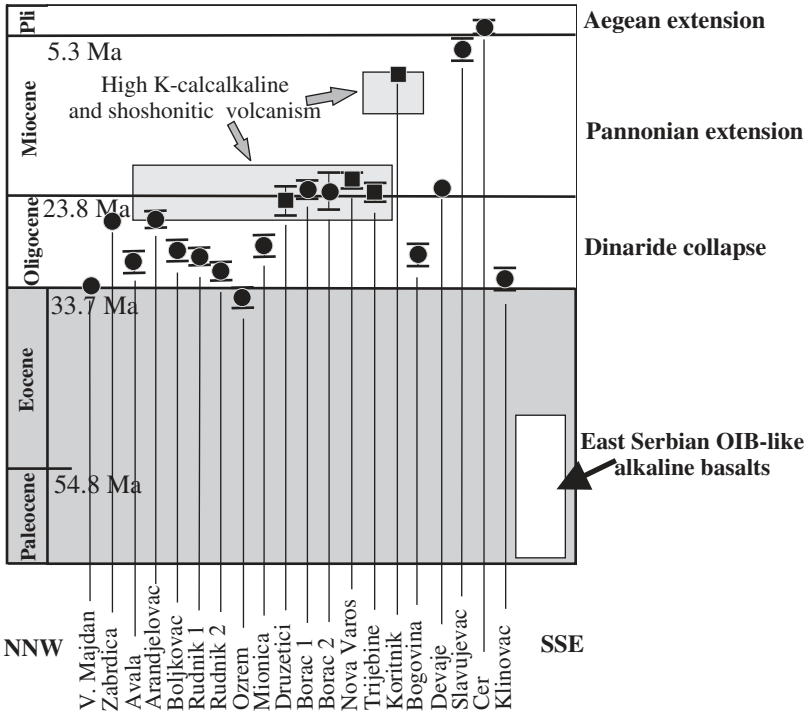

Fig. 2. Age-distribution of Serbian Tertiary ultrapotassic rocks relative to the major extensional episodes in the region [according to Marović *et al.* (2000, 2002)]. K–Ar age determinations are from Cvetković *et al.* (2004*a*). Symbols are as in Fig. 1.

The Tertiary history of basaltic and ultrapotassic magmatism in Serbia comprises three magmatic episodes, a first episode of Paleocene or Eocene alkaline basalts with sodic character, and two later (Oligocene or Miocene and Pliocene) episodes dominated by high-K calc-alkaline, shoshonitic and ultrapotassic magmatism (Cvetković *et al.*, 2004*a*). The sodic Paleocene–Eocene alkaline basalts are confined to the eastern tectonic units (Serbo-Macedonian and East Serbian composite terranes) where they form a trend broadly parallel to the terrane boundary (Fig. 1). Geochemically, the Paleocene–Eocene alkaline basalts show a clear ocean island basalt (OIB)-like Nd–Sr isotopic affinity (Cvetković *et al.*, 2004*a*), resembling rocks from other intracontinental European alkaline provinces such as the Massif Central and the Rhenish Massif in Germany (Wilson & Patterson, 2001). This magmatism generally postdates Late Cretaceous subduction-related volcanism of the Timok area, for which high-precision U–Pb age determinations have yielded ages from 86 to 70 Ma (von Quadt *et al.*, 2003); that is, they are at least 10 Myr older than the Palaeogene alkaline rocks. The alkaline basalts have been interpreted as being erupted during short relaxational phases between predominantly compressional conditions (Cvetković *et al.*, 2004*a*).

The Oligocene–Miocene and Pliocene rocks are dominated by high-K calc-alkaline, shoshonitic and ultrapotassic types. The Oligocene–Miocene volcanic episode started after a hiatus of at least 15 Myr (Fig. 2), indicating a distinct geodynamic trigger. Available radiometric ages (Cvetković *et al.*, 2004*a*) indicate the onset of ultrapotassic volcanism around 30 Ma in the northern part of the province along the WNW–ESE-trending Zvornik line (Fig. 2). The volcanism migrated southward over the next 20 Myr, during which plugs and flows of ultrapotassic rocks were emplaced within the SW part of Serbian Dinaride ophiolite belt. The Pliocene volcanic period is documented by K–Ar ages of 6·6 Ma and 3·9 Ma and these are most probably related to Macedonian magmatism to the south (Terzić & Svešnjikova, 1991; Altherr *et al.*, 2004). In Serbia, these rocks occur to the south of the Scutari–Peć line (Fig. 1), which is believed to be the northernmost limit of the influence of Aegean collapse (Kissel *et al.*, 1995). In terms of their mineralogy and geochemistry, the youngest volcanics are mostly of ultrapotassic character and cannot be distinguished from the older ultrapotassic rocks from the Vardar ophiolitic suture zone.

ANALYTICAL METHODS

Minerals were analysed on a CAMECA SX 100 microprobe at the GeoForschungsZentrum Potsdam using PAP correction procedures. Counting times for all

elements were 20 s for the peak position and 10 s for the background on each side of the peak. Operating conditions were 15 kV and 20 nA, and well-defined natural minerals were used as standards.

Whole-rock major elements and Cr, Ni, V, Co, Cu, Zn, Ba, Rb, Ga, Sr, Pb, Y, Zr and Nb [also U, Th, La, Ce and Nd in samples not analysed by inductively coupled plasma mass spectrometry (ICP-MS)] were determined by X-ray fluorescence (XRF) spectrometry on fused discs at the University of Greifswald using a sequential wavelength-dispersive Philips PW2404 X-ray spectrometer equipped with a single goniometer-based measuring channel, covering the complete measuring range. Details of the accuracy and analyses of international standards using this method have been reported by Prelević *et al.* (2004*a*).

Concentrations of rare earth elements (REE), Li, Sc, Cs, Hf, Th and U were measured by ICP-MS at the University of Bristol using standard operating conditions on a VG PlasmaQuad PQ2 Turbo-plus ICP-MS system with a Meinhard Nebulizer. Details of the accuracy and analyses of international standards using this method are given in Electronic Appendix 1, which may be downloaded from the *Journal of Petrology* web site at http://www.petrology.oupjournals.org.

Whole-rock Sr and Nd isotopic compositions were determined at the GeoForschungsZentrum Potsdam following procedures described by Romer *et al.* (2001). Unleached sample powders were dissolved with 52% HF for 4 days at 160°C on a hot plate; digested samples were dried and taken up in 6N HCl overnight. Sr and Nd were separated and purified using cation-exchange chromatography. $^{87}Sr/^{86}Sr$ and $^{143}Nd/^{144}Nd$ were analysed on a VG 54-30 Sector and a Finnigan MAT262 multicollector mass spectrometer, respectively, operated in dynamic mode. Ratios were normalized to $^{86}Sr/^{88}Sr = 0{\cdot}1194$ and $^{146}Nd/^{144}Nd = 0{\cdot}7219$, respectively. Multiple measurements of NBS 987 Sr reference material and La Jolla Nd reference material gave $0{\cdot}710277 \pm 0{\cdot}000009$ ($n = 4$) and $0{\cdot}511860 \pm 0{\cdot}000007$ ($n = 4$), respectively. Analytical uncertainties are 2σ mean. $^{87}Sr/^{86}Sr_i$ and $^{143}Nd/^{144}Nd_i$ were calculated for known K–Ar ages, using $^{87}Rb = 1{\cdot}42 \times 10^{-11}$ years^{-1} and $^{147}Sm = 6{\cdot}54 \times 10^{-12}$ years^{-1}.

Pb from unleached whole-rock sample powders was separated using anion exchange resin Bio Rad AG1-X8 (100–200 mesh) in 0·5 ml Teflon columns by HCl–HBr ion exchange chemistry using procedures described by Romer *et al.* (2001, and references therein). Pb was purified by a second pass over the column. Pb was loaded together with H_3PO_4 and silica gel, on single Re filaments. The isotopic composition of Pb was determined at 1200–1250°C on a Finnigan MAT262 multicollector mass spectrometer using static multicollection. Instrumental fractionation was corrected with 0·1% per a.m.u. as determined from repeated measurement of lead reference material NBS 981. Accuracy and precision of reported Pb ratios is better than 0·1% at the 2σ level.

CLASSIFICATION AND PETROLOGY OF SERBIAN ULTRAPOTASSIC ROCKS

All the studied rocks are ultrapotassic, following the criteria of Foley *et al.* (1987), with $K_2O > 3\%$, $MgO > 3\%$ and $K_2O/Na_2O > 2$, except for samples where analcimization of leucite has caused drastic reduction of the K_2O/Na_2O ratio. Two principal groups of Serbian Tertiary ultrapotassic rocks are recognized: (1) a group with lamproitic affinity (LAG); (2) a group with kamafugitic affinity (KAG). The term 'affinity' is used to signify similarity to one of the generally recognized ultrapotassic rock groups lamproites, kamafugites and Roman province type rocks (Foley *et al.*, 1987). It indicates probable similarities in the source characteristics of rocks with a given affinity despite considerable petrographic dissimilarities, both within the Serbian rock groups, and between some of the Serbian rocks and the ultrapotassic type rocks. Representative photomicrographs of the Serbian ultrapotassic rocks are given in Fig. 3, and detailed petrographic descriptions and further microphotographs are reported in Electronic Appendices 2 and 3, respectively, which may be downloaded from the *Journal of Petrology* web site at http://www.petrology.oupjournals.org.

The two Serbian ultrapotassic suites are restricted to specific geotectonic units (Fig. 1). The LAG rocks are concentrated within the central axis of the Balkans, within the Vardar ophiolitic suture zone and Jadar block terranes, with only one exception (Bogovina, situated in the East Serbian composite terrane), whereas the KAG rocks occur exclusively in the western terranes (Dinaridic ophiolite belt terrane and Drina–Ivanjica terrane).

The LAG comprises a variety of petrographically defined rock types, forming two subgroups: (1) primitive (plagioclase-free) and (2) evolved (plagioclase-bearing) LAG rocks, on the basis of the presence or absence of plagioclase in the groundmass and/or as a xenocryst, Cr and Ni content, and mineral chemistry. The primitive LAG rocks are lamproites, whereas the evolved LAG rocks cannot be considered as lamproites in the normal sense because of the presence of plagioclase (Foley *et al.*, 1987; Mitchell & Bergman, 1991). Evolved LAG rocks exhibit different degrees of differentiation and the variable, but common, presence of felsic xenoliths and xenocrysts. They may occur in composite intrusions in which decimetre-sized shoshonitic and latitic margins surround phenocryst-rich metre-sized dacitic interiors. The mafic parts of the composite dykes mineralogically

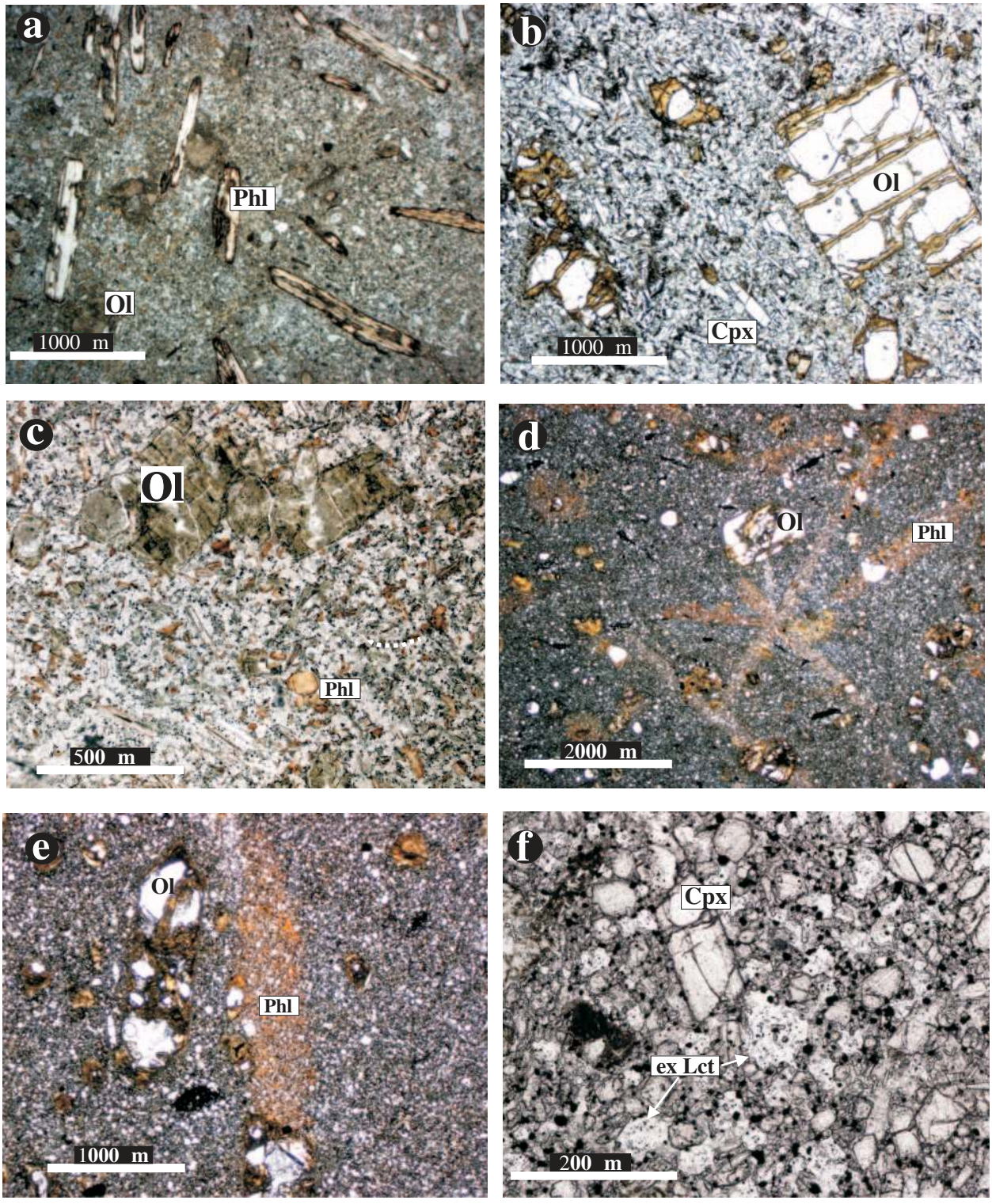

Fig. 3. Selected photomicrographs (plane-polarized light) of Serbian ultrapotassic rocks. (a) Sample Bo-3, Ol–Cpx–Phl–Lct–Sa–Amph-lamproite from Bogovina; (b) sample BK-01/3C, Ol–Cpx–Lct lamproite from Borač; (c) sample RO/1-II, Cpx-free Ol–Phl–Sa lamproite from Rudnik (note altered olivine); (d) and (e) samples KR01/3 and NV01/7, ugandites from Koritnik and Nova Varoš, respectively (note poikilitic phlogopite laths); (f) sample DZV/1, ankaratrite from Družetići (note rounded ex-leucite microphenocrysts pseudomorphed by analcime).

and geochemically resemble rocks from nearby minette and lamproite dykes. According to Prelević *et al.* (2004*a*) these mafic parts represent a wide spectrum of hybrid ultrapotassic and potassic magmas, generated by mixing of lamproitic mantle-derived magmas (primitive LAG) with magmas of silicic composition. These composite intrusions emphasize the role of magma-mixing in the evolution of Serbian LAG volcanism. Moreover, throughout the province, evolved LAG rocks host resorbed and reacted quartz, plagioclase, sanidine, biotite and salitic clinopyroxene, as well as partially digested cumulate nodules of two types: olivine–phlogopite + clinopyroxene + chromite (Type 1) and salitic-Cpx–biotite–plagioclase (Type 2) (Electronic Appendix 3-m, o-Type 1 and p-Type 2). Partial melting of quartz xenocrysts, crystallization of clinopyroxene coronas and resorption of plagioclase xenocrysts are almost ubiquitous (Electronic Appendix 3-n, q and r).

The KAG rocks mostly form 100–1000 m size volcanic flows. Although their exact petrographic name should, in most cases, be analcimite, we term them ugandites (olivine leucitites), leucite basanites and ankaratrites (Fig. 3d–f; Electronic Appendix 3-h, i, j, k and l), as the analcime originates by transformation of previously existing primary leucite (Prelević *et al.*, 2004*b*). Leucite occurs only in the freshest lavas at Koritnik. KAG rocks are not kamafugites *sensu stricto* because they lack characteristic kamafugitic minerals such as melilite and kalsilite (Woolley *et al.*, 1996; Le Maitre, 2002). The common occurrence of ugandite, leucite basanite and ankaratrite is, however, reminiscent of the alkaline mafic volcanics of the Toro–Ankole volcanic province, where kamafugites were originally described (Holmes & Harwood, 1937). Thus, we refer to the 'kamafugitic affinity' of the Serbian suite to emphasize the resemblance to kamafugites, although still using IUGS terminology (Woolley *et al.*, 1996; Le Maitre, 2002).

MINERAL CHEMISTRY

Below is a brief summary of the mineralogy and mineral chemistry of Serbian ultrapotassic rocks. Detailed descriptions are included in Electronic Appendix 4. Also, representative mineral composition data are reported in Electronic Appendix 5, and more comprehensive electron microprobe analyses are included in two supplementary datasets. All these files can be downloaded from the *Journal of Petrology* web site at http://www.petrology.oupjournals.org. Mineral abbreviations are after Kretz (1983).

In the LAG rocks, phenocrysts of high-Mg olivine (Fo mostly 90–93; Fig. 4a), with a modal abundance of 10–15 vol. %, usually host Mg-chromite inclusions with high Cr-number [atomic Cr/(Cr + Al)] as high as 0·94 and Fe^{3+}-number ($Fe^{3+}/\Sigma Fe$) of 0–0·40 (Fig. 5). The most extreme composition with Cr-number up to 0·99 and Fe^{3+}-number = 0 occurs in samples from Arandjelovac. Mica phenocrysts from primitive LAG samples show lamproitic core–rim compositional trends (Mitchell & Bergman, 1991). Cores have Mg-number 90–80, Al_2O_3 11·7–14·0 wt %, and Cr_2O_3 up to 2·15 wt %, whereas rims and poikilitic groundmass crystals have TiO_2 up to 10 wt %, high FeO_T (around 11 wt %) and BaO (up to 3 wt %), low Al_2O_3 (around 10 wt %) and MgO (around 17 wt %). The core compositions of the evolved LAG phlogopites resemble phlogopite cores in the primitive LAG rocks, but their core–rim trend is towards higher Al contents, resembling calc-alkaline lamprophyres and Roman province lavas (Mitchell & Bergman, 1991) (Fig. 6a). Clinopyroxene encompasses phenocrysts and megacrysts, glomeroporphyritic clusters, accumulations of acicular quench crystals, groundmass crystals and also xenocrysts of sieve-structured green salite, usually mantled by diopside, that originated from Type 2 cumulate nodules (Fig. 3b; Electronic Appendix 3c, d, e, f, m, n, o, p, q). Microphenocrysts, phenocrysts and megacrysts (0·5–10 mm) in primitive LAG rocks usually have Mg-number around 90, Al is <0·025 Al atoms per formula unit (Fig. 6c), insufficient to compensate for the deficiency of Si in the tetrahedral site. Line analyses across zoned Cpx grains (Fig. 4c) illustrate normal zoning trends, sometimes repetitive, with restricted zones of lower Mg composition with Mg-number down to 85, TiO_2 up to 1·5 wt % and Cr_2O_3 abundances <0·1 wt %, but without variation of Al_2O_3 content (Fig. 4c). In contrast, Cpx phenocrysts and microphenocrysts from evolved LAG samples are commonly intensely zoned (Fig. 4e): cores have similar compositions to phenocrysts from the LAG, and show more than one episode of gradual evolution towards lower Mg-number (down to 75), higher Al_2O_3 (up to 3 wt %) and TiO_2 (up to 2·5 wt %), disrupted by narrow zones of the primitive, core-like compositions. The behaviour of both Ti and Al with Si is conspicuously antipathetic (Fig. 4e), in contrast to Cpx from primitive LAG rocks where only Ti varies (Fig. 4c). Green salitic clinopyroxene ($En_{30–36}Fs_{11–20}Wo_{45–47}$, up to 7% Al_2O_3) forms single crystals usually mantled by clinopyroxene of composition similar to the acicular clinopyroxenes (Fig. 4f). It is resorbed, sieved and embayed to different extents.

In primitive lamproitic rocks, the groundmass commonly contains Fe-rich alkali feldspar (up to 3% FeO_T), sanidine (sometimes hyalophane with up to 23 vol. % celsian), and leucite (universally pseudomorphed by analcime). Plagioclase occurs only in the groundmass of evolved LAG rocks ($Ab_{40–44}An_{40–45}Or_{10–15}$) together with low-Fe sanidine and leucite pseudomorphed by analcime. Moreover, primitive LAG rocks contain rare rutile, ilmenite and Ti-magnetite; in some samples these minerals coexist.

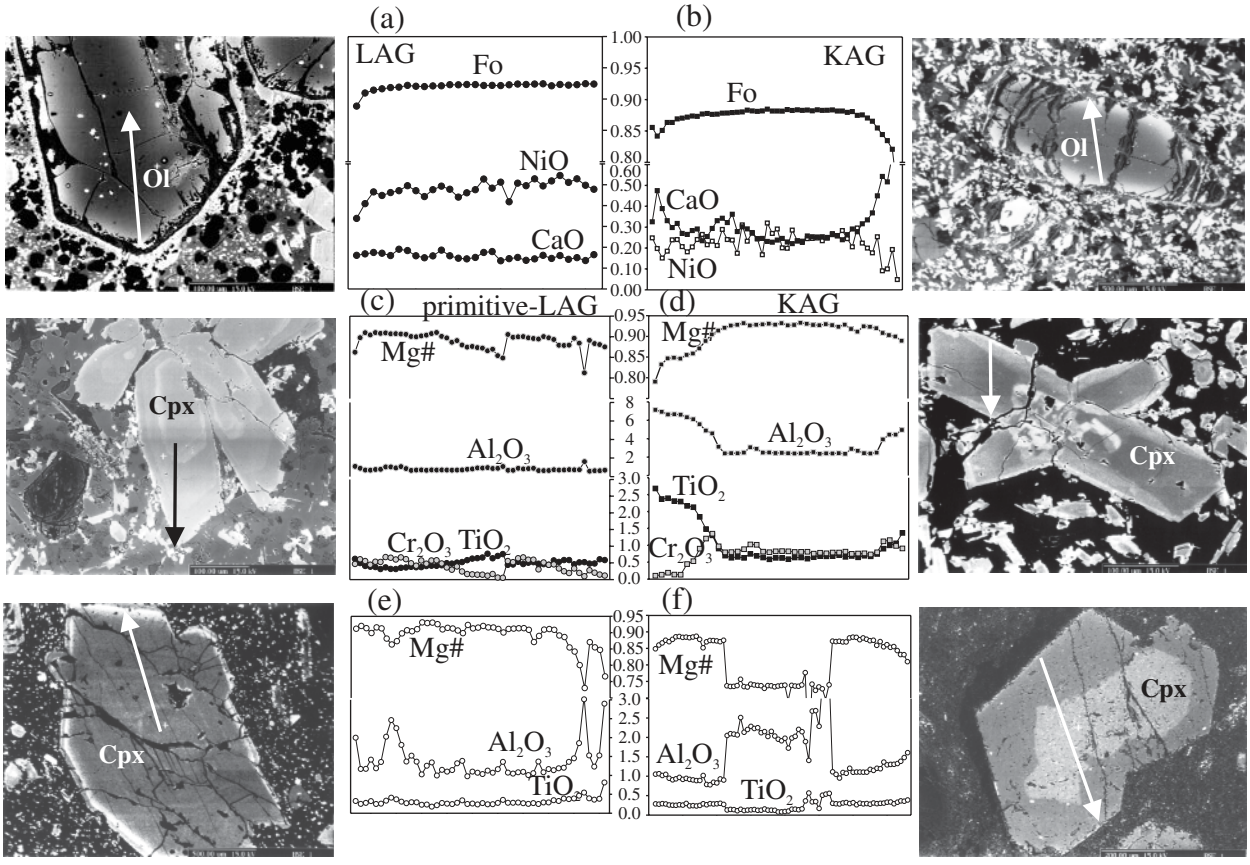

Fig. 4. Line analyses across selected minerals from Serbian ultrapotassic rocks. Olivine from (a) primitive LAG, sample BK-01/3a; (b) KAG, sample KR01/3; Cpx from (c) primitive LAG, sample M00-3; (d) KAG, sample NV01/7; (e) evolved LAG, sample Blj-2; (f) salitic Cpx from evolved LAG, sample BK/1. The arrows denote rim–core (a), core–rim (c and e) and cross-sectional compositional trends (b, d and f) for selected macrocrysts.

In the rocks with kamafugitic affinity, olivine, consistently less magnesian than in LAG rocks (Fo 88–89), appears as phenocrysts, with a modal abundance of 5–15 vol. % (Fig. 4b). It hosts Mg-chromites with significantly lower Cr-number than spinels from LAG rocks, with values not exceeding 0·81, and having higher Fe^{3+} and slightly higher TiO_2 contents (Fig. 5b). Phlogopite is not a phenocryst phase in the KAG rocks, but appears as large millimetre-sized poikilitic laths enclosing earlier minerals in ugandites, interstitially in the groundmass of leucite basanites, and also in vesicle fillings and rare centimetre-sized amoeboid pegmatitic segregations in ankaratrites (Fig. 3d and e; Electronic Appendix 3h, i and j). The large poikilitic phlogopites in ugandites have uniform compositions with high Mg-number in the range of 88–84, low Al_2O_3 contents down to 7 wt %, high TiO_2 up to 7 wt % and variable BaO and high F contents of 2–3 wt % and up to 6 wt %, respectively (Electronic Appendix 5). The interstitial tiny phlogopitic plates in leucite basanites always have lower Mg-number in the range 70–75, higher Al_2O_3 contents (up to 15 wt %) and similar TiO_2 and F contents, but are enriched in BaO (up to 6 wt %). The most exotic compositions with Mg-number around 75, Al_2O_3 15 wt %, high TiO_2 (up to 10 wt %), low SiO_2 (down to 33 wt %), but high BaO (up to 12 wt %) are found in phlogopites from ankaratrites (Fig. 6b). Clinopyroxene in KAG rocks occurs as phenocrysts. Core compositions have Mg-number 82–88, Al_2O_3 is mostly >2%, and TiO_2 2–3%, and trend towards rims with Mg-number 80–70, and higher Al_2O_3 and TiO_2 contents (Fig. 4d). In contrast to clinopyroxenes from the lamproitic group, KAG clinopyroxenes contain sufficient Al to balance silica deficiencies in the tetrahedral site and have higher Ti content for the same Mg-number. Clinopyroxenes from ugandite and leucite basanite occupy distinct areas on a plot of Al vs Ti (Fig. 6d).

The presence of both leucite and nepheline in the groundmass is a common feature of rocks with kamafugitic affinity. In ugandite, leucite is mostly pseudomorphed by analcime, and only in ugandites from the Koritnik volcano has fresh leucite been found. Nepheline varies in modal

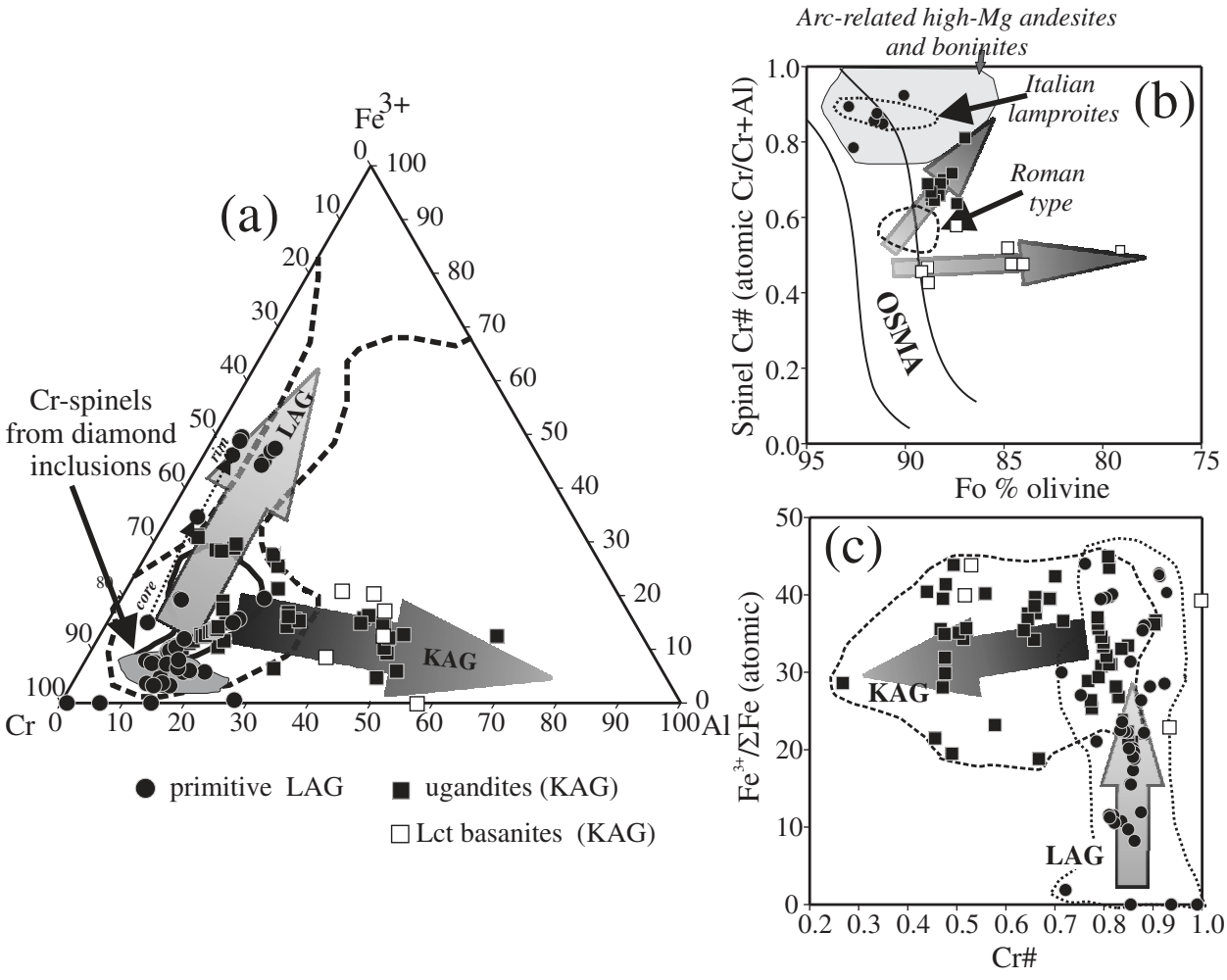

Fig. 5. (a) Spinel Cr–Al–Fe^{3+} ion plot for Serbian ultrapotassic rocks; continuous and dashed lines correspond to respectively the 50th and 90th percentile contours for the kimberlite and lamproite dataset of Barnes & Roeder (2001); dotted arrow denotes core–rim trend across some larger grains resembling the general trend with more reduced and Cr-enriched core, and an oxidized rim with lower Cr-number. (b) Position of olivine–spinel pairs from the Serbian ultrapotassic rocks on the olivine-Fo vs spinel-Cr-number diagram with the olivine–spinel mantle array (OSMA) defined by Arai (1994). (c) Cr-number [ionic Cr/(Cr + Al)] vs $Fe^{3+}/\Sigma Fe$ in spinel diagram for Serbian ultrapotassic rocks; grey shaded arrows denote core–rim evolutionary trends for LAG and KAG samples.

abundance and composition between lithologies. In ugandites, it is least abundant and has the highest proportion of kalsilite component (≤38 mol %), whereas the kalsilite component decreases with increasing nepheline abundance in other KAG rocks. Minor phases in the groundmass are Ti-magnetite with 30–60 mol % ulvöspinel, hyalophane in ugandites ($Or_{53·4}Cn_{34·6}Ab_{8·6}An_{3·4}$), and plagioclase in leucite basanites.

GEOCHEMICAL CHARACTERISTICS

Major and trace element compositions of Serbian ultrapotassic rocks are listed in Tables 1–3. Sr and Nd isotopic analyses of selected samples are given in Table 4, and Pb isotope data in Table 5. In the discussion, we include previously published Sr and Nd isotope data (Cvetković *et al.*, 2004*a*) for samples from the same localities.

Major and compatible trace elements

Primitive LAG samples are slightly silica-undersaturated to -saturated, with SiO_2 in the range of 43–52 wt %, Mg-number up to 80 [$100Mg/(Mg + 0{\cdot}85Fe_T)$], Al_2O_3 contents 10–13 wt % and Cr and Ni up to 1200 and 550 ppm, respectively (Fig. 7a, b and d). TiO_2 is around 1 wt % in most primitive lamproitic samples, although a few display higher contents (>2 wt %). With respect to major elements, the majority of the primitive lamproitic rocks resemble lamproites from Spain (Venturelli *et al.*, 1984*a*, 1988; Benito *et al.*, 1999; Turner *et al.*, 1999) and

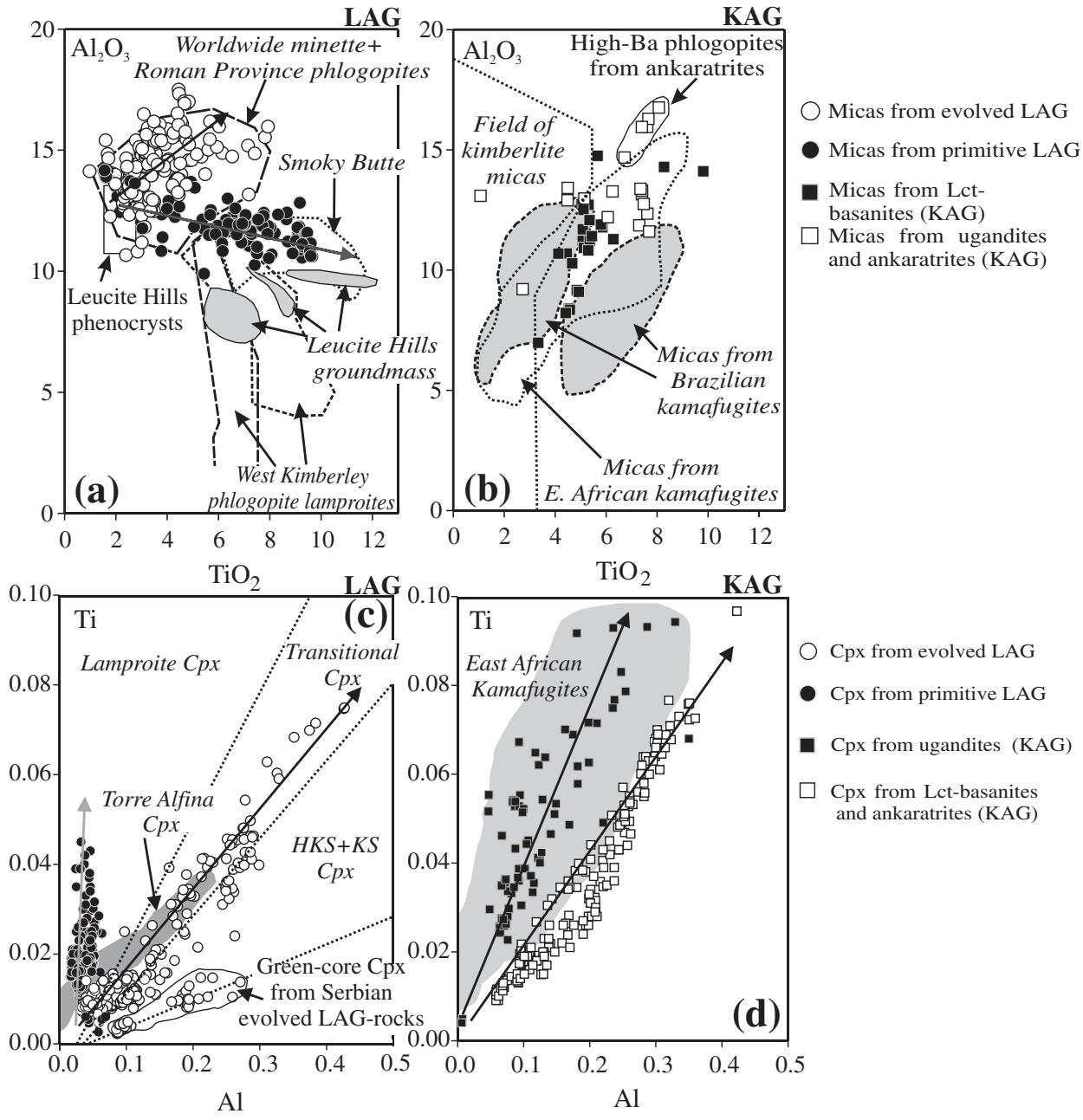

Fig. 6. (a) and (b) Al_2O_3 vs TiO_2 plots for phlogopites from Serbian ultrapotassic rocks. Data fields are from Mitchell *et al.* (1987), Mitchell & Bergman (1991), Araujo *et al.* (2001) and Tappe *et al.* (2003). (c) and (d) Plots of Al vs Ti atomic proportions for clinopyroxenes from Serbian ultrapotassic rocks. Field for lamproite clinopyroxene is after Mitchell & Bergman (1991); data for the clinopyroxenes from Italian provinces: high potassium series (HKS), potassium series (KS) and transitional rocks after Perini & Conticelli (2002, and references therein); Torre Alfina clinopyroxenes after Conticelli (1998); clinopyroxenes from East African kamafugites after Tappe *et al.* (2003); arrows denote core–rim trends for phenocrysts.

Italy (Venturelli *et al.*, 1984; Conticelli & Peccerillo, 1992; Conticelli *et al.*, 1992, 2002; Peccerillo, 1995). They mostly plot in the lamproite field on the classification diagrams of Foley *et al.* (1987) (Fig. 7c, e and f), although in some diagrams they plot largely in the Roman province field (Fig. 7c). Evolved LAG rocks have higher SiO_2 contents, mostly around 55%, but up to 62 wt %. Mg-number is <70, mostly around 65, Al_2O_3 ranges from 11 to 15 wt % and Cr and Ni are less than 500 and 250 ppm, respectively. Their TiO_2 contents are mostly <1 wt %. They mainly plot in the Roman province field, resembling the potassium series (KS), transitional rocks (TRANS)

Table 1: Whole-rock major (%) and trace element (ppm) analyses of primitive LAG rocks

Locality:	Bogovina			Borač			Zabrdica		Rudnik	
Age (Ma):	30			22·6			25·6		30·21	
Rock type:	Ol–Cpx–Phl–Lct–Sa-lamproite			Ol–Cpx–Lct-lamproite			Ol–Cpx–Phl–Lct–Sa-lamproite		Ol–Phl–Sa-lamproite	
Sample:	Bo-3	Bo2-1	Bo2-2	BK01/3-1	BK01/3C	BK01/3A-2	ZB01/2	ZB01/1	RO/1-II	RO00/1-A
SiO_2	48·5	49·4	48·9	50·4	49·9	54·0	51·5	50·4	46·7	47·3
TiO_2	2·20	2·10	2·07	1·47	1·44	1·29	1·45	1·41	1·63	1·64
Al_2O_3	10·09	9·78	9·73	10·16	10·67	11·41	10·73	10·57	10·80	10·94
$Fe_2O_3^*$	7·18	7·02	7·40	6·66	7·28	6·16	7·28	6·83	7·04	6·95
MnO	0·10	0·09	0·09	0·11	0·11	0·10	0·10	0·07	0·08	0·07
MgO	9·13	9·68	9·68	12·85	10·97	9·91	10·30	8·50	9·84	10·40
CaO	7·78	8·15	7·99	6·20	6·92	5·60	6·30	6·84	3·82	3·82
Na_2O	3·21	3·18	2·91	2·34	4·13	2·62	2·96	1·77	0·57	0·55
K_2O	2·90	2·79	2·78	4·62	1·23	5·00	4·36	4·01	6·77	6·77
P_2O_5	0·79	0·85	0·80	0·65	0·69	0·56	0·52	0·52	0·70	0·71
LOI	7·03	7·04	7·27	3·77	6·50	2·90	4·06	8·56	11·19	10·15
Sum	98·93	100·09	99·64	99·24	99·82	99·56	99·56	100·04	99·12	99·27
Mg-no.	73·9	75·6	74·5	81·8	77·3	78·6	76·1	73·4	75·8	77·2
Cr	483	490	492	728	613	557	837	802	695	689
Ni	288	301	293	466	405	376	427	465	486	530
Co	33	37	36	38	38	27	33	36	33	40
V	157	160	167	118	138	109	131	137	137	145
Cu	50	60	64	0	33	6	17	10	25	42
Zn	81	71	65	72	87	68	79	79	75	78
Ba	3505	3895	3673	1455	1953	1100	826	1128	1153	1119
Ga	19	17	20	14	15	17	18	16	17	17
Li	12	15	n.d.	30	30	36	87	194	107	102
Sc	17	17	n.d.	20	22	18	22	22	26	26
Rb	169	102	106	217	319	287	194	191	221	218
Sr	820	856	842	825	740	824	586	608	598	599
Y	22	20	22	41	56	53	23	23	24	24
Zr	1035	954	894	694	656	619	649	736	676	675
Nb	69	63	50	33	31	28	32	33	38	40
Cs	9·4	4·8	n.d.	38·3	68·8	33·9	47·7	103·1	8·1	3·2
Hf	26·3	24·3	n.d.	18·8	16·8	16·4	19·9	20·1	19	18·9
Pb	32	36	31	40	41	41	19	20	31	31
Th	35·5	33·7	36·0	57·3	50·6	51·3	43·0	45·0	53·1	52·9
U	4·0	6·3	2·0	15·8	13·2	17·5	12·3	14·5	11·3	11·1
La	98·5	86·7	93·0	82·9	82·2	74·3	68·0	66·6	80·6	82·3
Ce	206·9	190·1	184·0	199·9	197·6	175·9	168·7	167·2	201·2	204·7
Pr	25·8	23·5	n.d.	26·8	26·4	23·2	23·7	23·3	26·1	26·6
Nd	112·3	102·2	88·0	109·1	109·2	95·0	98·9	97·6	114·9	116·2
Sm	19·8	18·3	n.d.	18·7	19·2	16·2	16·5	15·7	19·5	20·7
Eu	5·4	5·3	n.d.	3·1	3·3	2·8	2·9	3·0	3·3	3·4
Gd	12·6	11·4	n.d.	10·2	10·5	9·2	9·7	9·6	11·9	12·1
Tb	1·5	1·4	n.d.	1·2	1·3	1·1	1·2	1·2	1·5	1·5
Dy	5·1	4·6	n.d.	5·6	6·1	5·3	4·7	4·7	5·3	5·4
Ho	0·8	0·7	n.d.	0·8	0·9	0·7	0·8	0·8	0·9	0·9
Er	1·8	1·7	n.d.	2·2	2·5	2·1	2·0	2·0	2·0	2·1
Tm	0·2	0·2	n.d.	0·3	0·3	0·3	0·3	0·3	0·3	0·3
Yb	1·5	1·4	n.d.	1·7	2·0	1·7	1·8	1·9	1·8	1·8
Lu	0·2	0·2	n.d.	0·3	0·3	0·3	0·3	0·3	0·3	0·2

Table 1: continued

Locality:	Mionica				Arandjelovac					
Age (Ma):	29·1				26·0					
Rock type:	Ol–Cpx–Phl–Lct–Sa-lamproite				primitive minette					
Sample:	M00/3	M00/3-II	Mionica81a	Mionica81B	Ar99/2	Ar99	Ar96/1	Ar96/2	Ar99/4	Ar96/4
SiO_2	51·2	51·7	51·0	51·9	42·4	46·9	46·5	43·3	44·4	45·7
TiO_2	1·44	1·46	1·43	1·46	0·79	0·87	0·83	0·80	0·81	0·84
Al_2O_3	11·91	11·92	11·92	11·95	10·21	11·12	10·78	10·62	10·28	10·89
$Fe_2O_3^*$	6·89	7·15	7·05	6·92	7·57	8·45	8·37	7·86	9·33	8·36
MnO	0·09	0·09	0·09	0·09	0·12	0·15	0·14	0·13	0·13	0·12
MgO	5·38	5·30	5·22	5·24	10·05	11·81	13·36	10·30	12·60	11·06
CaO	8·69	6·91	8·70	7·87	9·54	8·56	7·74	9·85	8·18	8·32
Na_2O	1·31	1·39	1·23	1·33	1·28	2·03	0·81	1·09	0·39	0·76
K_2O	6·57	6·62	6·55	6·59	3·06	4·43	5·66	3·15	5·93	5·70
P_2O_5	0·70	0·67	0·68	0·68	0·96	1·11	1·08	0·99	1·02	1·04
LOI	3·85	4·34	5·83	5·05	11·07	4·82	3·94	11·79	6·25	6·71
Sum	97·99	97·58	99·70	99·08	97·04	100·24	99·17	99·88	99·30	99·48
Mg-no.	61·4	61·4	61·4	61·9	74·8	75·8	78·4	74·5	75·1	74·7
Cr	486	544	579	578	824	868	1176	925	1124	1038
Ni	399	406	376	408	275	260	299	298	392	329
Co	29	28	35	32	42	43	48	58	53	44
V	113	133	139	147	159	185	182	179	188	187
Cu	10	4	33	66	186	59	19	378	23	49
Zn	75	81	83	80	71	64	72	66	89	77
Ba	984	1117	1160	1133	1276	1647	2437	1316	2634	2986
Ga	14	18	18	19	10	15	16	12	17	14
Li	57	n.d.	46	n.d.	109	n.d.	n.d.	n.d.	49	n.d.
Sc	19	n.d.	20	n.d.	26	n.d.	n.d.	n.d.	28	n.d.
Rb	254	240	278	281	148	193	218	153	236	240
Sr	916	861	1165	1111	516	711	783	521	516	587
Y	45	65	42	60	25	33	29	22	29	30
Zr	676	665	691	672	202	208	195	201	197	214
Nb	31	30	32	31	12	11	10	11	11	13
Cs	162·4	n.d.	211·6	n.d.	10·3	n.d.	n.d.	n.d.	20·2	n.d.
Hf	19·6	n.d.	18·1	n.d.	4·5	n.d.	n.d.	n.d.	5·2	n.d.
Pb	31	34	33	30	33	18	22	32	7	16
Th	46·9	40·6	41·9	41·1	15·9	18·0	15·0	17·0	18·4	21·0
U	12·8	7·5	11·7	6·9	6·1	2·0	3·0	2·0	6·4	3·0
La	117·4	n.d.	98·8	n.d.	28·7	35·0	32·0	25·0	33·3	23·0
Ce	261·3	237·1	203·0	198·6	60·0	48·0	80·0	52·0	68·6	69·0
Pr	33·7	n.d.	26·8	n.d.	7·6	n.d.	n.d.	n.d.	8·8	
Nd	133·6	n.d.	107·4	n.d.	32·0	49·0	46·0	43·0	36·3	35·0
Sm	21·9	n.d.	17·5	n.d.	6·5	n.d.	n.d.	n.d.	7·5	n.d.
Eu	4·2	n.d.	3·6	n.d.	2·0	n.d.	n.d.	n.d.	3·1	n.d.
Gd	15·6	n.d.	12·5	n.d.	5·1	n.d.	n.d.	n.d.	6·3	n.d.
Tb	2·1	n.d.	1·7	n.d.	0·7	n.d.	n.d.	n.d.	0·9	n.d.
Dy	9·1	n.d.	7·2	n.d.	3·3	n.d.	n.d.	n.d.	4·2	n.d.
Ho	1·6	n.d.	1·2	n.d.	0·6	n.d.	n.d.	n.d.	0·7	n.d.
Er	4·1	n.d.	3·3	n.d.	1·6	n.d.	n.d.	n.d.	1·8	n.d.
Tm	0·6	n.d.	0·5	n.d.	0·3	n.d.	n.d.	n.d.	0·3	n.d.
Yb	3·9	n.d.	2·9	n.d.	1·6	n.d.	n.d.	n.d.	1·7	n.d.
Lu	0·6	n.d.	0·4	n.d.	0·2	n.d.	n.d.	n.d.	0·3	n.d.

*Total iron as Fe_2O_3.
Ages are from Cvetković *et al.* (2004*a*). Mg-number = atomic 100 Mg/(Mg + 0·85Fe_T); n.d., not determined.

Table 2: Whole-rock major (%) and trace element (ppm) analyses of evolved LAG rocks

Locality:	Klinovac		Cer	Slavujevac[2]	Ozrem		Borač							
Age (Ma):[1]	32·7		3·9	6·6	35·0		22·6							
Rock type:	Phl-trachybasalt				Ol–Cpx–Phl–Lct–Sa-lamp.		Phl-basaltic trachyandesite							
Sample:	Klin124	Klin133	Cer114	S153	Oz204	Oz205	BK-3	BK01/12	BK/1	BK01/2-4	BK01/2-4A	BK01/3-3	BK01/4-B-II	BK01/4B
SiO_2	48·2	47·9	52·5	51·2	50·9	50·9	54·9	53·0	54·5	53·1	52·8	56·7	53·3	53·3
TiO_2	0·89	0·89	1·17	0·95	1·07	1·06	0·96	1·34	0·94	0·97	1·02	0·90	1·11	1·12
Al_2O_3	12·99	13·03	14·02	14·29	13·20	13·04	13·14	11·71	13·10	14·24	14·56	14·87	14·40	14·42
$Fe_2O_3^*$	7·03	6·60	9·61	9·84	6·24	6·16	6·04	7·43	6·42	6·29	6·42	5·63	7·08	7·15
MnO	0·12	0·12	0·12	0·13	0·16	0·16	0·09	0·08	0·08	0·10	0·11	0·08	0·11	0·11
MgO	5·64	5·35	6·35	6·15	6·27	6·23	5·93	5·58	5·52	6·56	6·65	4·20	5·96	5·93
CaO	9·59	10·87	7·47	8·09	8·74	8·85	8·25	5·68	7·91	6·75	7·03	6·55	7·76	7·74
Na_2O	2·92	2·81	3·83	4·64	2·95	3·01	2·47	1·57	2·24	2·49	2·55	3·16	2·56	2·55
K_2O	4·26	4·34	3·71	3·64	2·79	2·82	5·29	6·24	5·25	3·61	3·66	4·84	4·84	4·85
P_2O_5	1·31	1·41	1·23	1·16	0·69	0·70	0·66	0·74	0·67	0·47	0·48	0·49	0·67	0·68
LOI	4·59	5·64	0·26	0·24	5·95	6·38	1·90	5·77	2·36	5·18	4·79	2·31	1·65	1·51
Sum	97·57	98·97	100·30	100·13	97·66	97·74	99·62	99·11	99·02	99·71	100·03	99·76	99·48	99·40
Mg-no.	63·4	63·6	56·8	56·6	68·7	68·9	68·2	61·7	65·0	69·6	69·4	61·6	64·5	64·2
Cr	327	375	337	154	383	357	361	430	370	341	353	202	430	436
Ni	101	141	181	97	195	187	132	249	118	83	83	56	130	139
Co	20	31	n.d.	n.d.	36	32	17	25	25	23	21	13	26	21
V	171	172	n.d.	n.d.	194	200	129	118	134	147	163	130	135	139
Cu	9	90	n.d.	n.d.	79	66	11	0	54	4	22	7	12	10
Zn	61	55	n.d.	n.d.	94	98	73	88	60	100	106	177	92	88
Ba	2060	2144	1570	1731	1573	1565	1233	1309	1245	1018	1068	998	1428	1455
Ga	12	18	n.d.	n.d.	18	19	17	15	22	16	17	19	17	18
Li	55	126	n.d.	n.d.	29	n.d.	29	40	25	100	n.d.	47	n.d.	n.d.
Sc	20	24	n.d.	n.d.	26	n.d.	20	22	20	21	n.d.	19	n.d.	n.d.
Rb	119	125	155	165	131	n.d.	157	237	188	135	126	180	149	148
Sr	1250	1344	972	1322	1055	n.d.	1389	919	1420	885	911	1002	1163	1164
Y	26	21	27	38	32	34	44	49	36	37	35	37	54	54
Zr	317	238	304	244	462	464	488	649	406	296	308	387	422	416
Nb	15	17	18	20	24	28	19	33	23	24	25	20	26	27
Cs	53	16·2	n.d.	n.d.	920·7	n.d.	4·4	2·3	5·2	5·7	n.d.	8·1	n.d.	n.d.
Hf	6·5	6·8	n.d.	n.d.	13·1	n.d.	13·7	15·9	11·3	6·7	n.d.	n.d.	n.d.	n.d.
Pb	49	58	48	n.d.	39·3	n.d.	56	45	47	42	33	38	20	25
Th	18·2	23·3	n.d.	n.d.	42·7	41·0	63·8	46·7	46·0	42·6	36·6	31·1	50·8	51·3
U	4·6	5·2	n.d.	n.d.	11·6	2·0	16·4	15·6	11·7	10·7	9·4	9·2	8·1	10·4

Table 2: continued

Locality:	Klinovac		Cer	Slavujevac[2]	Ozrem		Borač							
Age (Ma):[1]	32·7		3·9	6·6	35·0		22·6							
Rock type:	Phl-trachybasalt				Ol–Cpx–Phl–Lct–Sa-lamp.		Phl-basaltic trachyandesite							
Sample:	Klin124	Klin133	Cer114	S153	Oz204	Oz205	BK-3	BK01/12	BK/1	BK01/2-4	BK01/2-4A	BK01/3-3	BK01/4-B-II	BK01/4B
La	37·2	55·9	50·0	n.d.	90·2	n.d.	115·3	98·7	117·4	84·8	n.d.	82·0	n.d.	n.d.
Ce	73·1	107·0	95·1	n.d.	194·5	n.d.	228·8	209·9	242·1	167·5	n.d.	158·9	n.d.	n.d.
Pr	8·8	12·4	10·6	n.d.	24·5	n.d.	28·2	27·6	28·8	19·1	n.d.	18·9	n.d.	n.d.
Nd	35·3	48·1	49·3	n.d.	96·4	86·0	106·8	111·6	111·5	72·5	n.d.	71·4	n.d.	n.d.
Sm	6·5	8·5	8·5	n.d.	16·1	n.d.	18·4	19·3	18·8	12·9	n.d.	13·3	n.d.	n.d.
Eu	2·6	2·9	2·0	n.d.	3·6	n.d.	4·0	3·5	4·1	2·8	n.d.	3·0	n.d.	n.d.
Gd	5·1	6·2	6·0	n.d.	11·1	n.d.	11·9	11·4	12·1	8·8	n.d.	8·9	n.d.	n.d.
Tb	0·7	0·9	1·0	n.d.	1·5	n.d.	1·5	1·4	1·5	1·2	n.d.	1·2	n.d.	n.d.
Dy	3·5	4·0	5·4	n.d.	6·2	n.d.	7·4	6·8	7·5	6·2	n.d.	5·7	n.d.	n.d.
Ho	0·6	0·7	1·1	n.d.	1·1	n.d.	1·1	1·1	1·1	1·0	n.d.	0·8	n.d.	n.d.
Er	1·7	2·0	2·8	n.d.	2·7	n.d.	3·0	3·0	3·0	2·9	n.d.	2·3	n.d.	n.d.
Tm	0·3	0·3	0·4	n.d.	0·4	n.d.	0·4	0·4	0·4	0·4	n.d.	0·3	n.d.	n.d.
Yb	1·7	2·0	2·5	n.d.	2·4	n.d.	2·4	2·6	2·4	2·6	n.d.	1·8	n.d.	n.d.
Lu	0·3	0·3	0·3	n.d.	0·4	n.d.	0·4	0·4	0·4	0·4	n.d.	0·3	n.d.	n.d.

Locality:	Avala						Avala		Boljkovac		
Age (Ma):[1]	30·9						22·0[2]		29·7		
Rock type:	minette						Phl-trachybasalt		Phl-trachyandesite		
Sample:	AV-1	AV97/2	AV 1-2	AV 1-5	AV 2-1	AV 2-3	AV00/5	AV00/8	Blj2	Blj1	Blj3
SiO_2	56·5	55·8	56·0	56·5	56·0	55·5	49·0	49·7	62·3	62·0	62·0
TiO_2	1·39	1·33	1·40	1·40	1·37	1·40	1·51	1·53	0·82	0·82	0·80
Al_2O_3	12·90	12·55	13·08	13·12	13·11	12·86	15·27	15·04	13·70	13·83	13·79
$Fe_2O_3^*$	5·44	5·23	5·58	5·55	5·51	5·61	8·91	8·06	4·92	4·91	4·30
MnO	0·09	0·09		0·09	0·09	0·09	0·13	0·13	0·11	0·09	0·09
MgO	5·98	5·36	5·79	5·82	5·79	5·86	5·38	5·79	3·56	3·61	2·87
CaO	3·92	4·34	3·88	3·82	3·88	4·01	8·61	10·75	4·22	4·19	4·04
Na_2O	1·81	1·47	1·92	1·91	1·90	1·91	2·38	2·55	2·47	2·47	2·62
K_2O	7·45	7·21	6·96	7·17	6·82	7·13	4·48	3·67	5·35	5·40	5·51
P_2O_5	0·45	0·44	0·45	0·44	0·44	0·45	0·65	0·66	0·32	0·32	0·32
LOI	3·50	4·72	4·21	3·50	4·39	4·52	3·31	2·09	2·21	2·09	2·39
Sum	99·47	98·57	99·25	99·35	99·28	99·31	99·63	99·96	99·93	99·69	98·68
Mg-no.	70·7	69·2	69·4	69·7	69·7	69·6	56·2	60·6	60·8	61·2	58·8

Locality:	Avala						Avala		Boljkovac		
Age (Ma):[1]	30·9						22·0[2]		29·7		
Rock type:	minette						Phl-trachybasalt		Phl-trachyandesite		
Sample:	AV-1	AV97/2	AV 1-2	AV 1-5	AV 2-1	AV 2-3	AV00/5	AV00/8	Blj2	Blj1	Blj3
Cr	354	325	439	408	401	411	130	113	236	223	226
Ni	128	85	90	91	90	116	78	54	111	105	113
Co	21	22	22	23	21	23	19	7	18	16	17
V	126	114	114	113	113	107	159	167	93	93	94
Cu	11	43	49	42	38	52	11	15	23	28	41
Zn	74	74	79	80	78	80	172	408	55	65	50
Ba	1008	931	844	849	815	841	1205	995	831	855	831
Ga	18	20	21	21	21	21	15	13	18	17	23
Li	35	37	36	36	39	36	154	108	50	52	n.d.
Sc	19	18	18	18	18	17	22	20	12	12	n.d.
Rb	556	544	1020	1020	1020	995	243	232	359	372	n.d.
Sr	432	482	421	410	460	435	820	987	596	604	597
Y	22	20	20	21	20	20	35	30	25	25	29
Zr	490	612	671	676	634	358	254	246	371	367	367
Nb	22	31	33	33	33	33	52	55	27	26	28
Cs	11·5	11·5	12·2	12·7	11·1	11·2	22·5	32·4	21·8	22·2	n.d.
Hf	13·1	10·5	13·0	13·1	11·6	11·8	5·5	5·0	9·7	10·1	n.d.
Pb	30	27	26	27	25	27	59	202	44	46	42
Th	48·8	46·0	44·1	43·8	43·8	43·8	18·5	16·3	34·7	35·6	39·0
U	12·4	11·4	12·6	12·0	13·6	12·0	5·3	4·8	13·8	14·4	n.d.
La	73·3	58·2	56·0	55·5	54·6	56·0	73·8	64·3	57·8	51·1	44·0
Ce	191·0	145·8	141·0	138·0	139·0	140·0	136·5	122·5	114·6	111·9	108·0
Pr	25·3	19·4	19·8	19·8	19·7	19·9	15·8	14·0	14·4	13·5	n.d.
Nd	104·0	81·2	82·5	82·4	82·0	82·1	59·6	54·3	56·6	53·6	70·0
Sm	17·2	13·3	14·5	14·6	14·4	14·4	11·1	9·8	10·0	9·6	n.d.
Eu	3·0	2·3	2·2	2·3	2·3	2·3	3·2	2·6	2·0	1·9	n.d.
Gd	9·7	8·0	8·8	8·9	8·9	8·8	9·3	8·0	6·8	6·4	n.d.
Tb	1·3	1·0	1·0	1·0	1·0	1·0	1·3	1·1	0·9	0·8	n.d.
Dy	4·7	3·9	4·2	4·2	4·2	4·3	6·1	5·5	4·3	4·0	n.d.
Ho	0·8	0·7	0·7	0·7	0·7	0·7	1·1	0·9	0·8	0·8	n.d.
Er	1·9	1·5	1·9	1·9	1·9	1·9	2·8	2·5	2·0	1·9	n.d.
Tm	0·3	0·2	0·3	0·3	0·2	0·2	0·4	0·4	0·3	0·3	n.d.
Yb	1·7	1·5	1·5	1·5	1·5	1·5	2·4	2·3	1·9	1·8	n.d.
Lu	0·2	0·2	0·2	0·2	0·2	0·2	0·4	0·3	0·3	0·3	n.d.

Table 2: continued

Locality:	Golija		Devaje	Devaje–Visoča	Veliki Majdan							Rudnik		Avala
Age (Ma):[1]			21·8		33·5							31·9		
Rock type:	kersantite		leucitite		minette	leucominette						minette	leuco-minette	sandstone
Sample:	D4	D5	Dev	Vi-1	VM01/3	VM VI/2	VM VI/7	VM XII/3	VM XIV/2	VM XIV/4	VM XIV/6	R97x/424	R2	AV01
SiO_2	53·7	53·7	48·6	51·6	52·9	50·6	53·4	55·6	57·0	60·0	61·1	51·4	57·8	57·5
TiO_2	1·03	1·00	1·37	0·74	1·08	1·15	1·04	0·88	0·78	0·75	0·98	0·98	0·83	0·72
Al_2O_3	15·37	15·07	13·28	15·78	11·60	10·99	12·11	12·47	12·91	13·87	12·58	12·22	13·47	18·66
Fe_2O_3*	7·12	7·31	9·25	7·80	11·57	4·35	2·28	4·60	4·57	3·80	3·50	7·28	4·10	6·61
MnO	0·19	0·18	0·20	0·10	0·09	0·18	0·15	0·14	0·11	0·10	0·09	0·10	0·06	0·24
MgO	5·11	5·14	3·55	2·06	7·27	7·55	2·64	6·76	5·71	3·99	4·51	8·29	3·40	2·89
CaO	7·50	7·47	8·55	8·06	1·42	9·33	9·55	5·60	5·40	4·72	4·33	4·47	4·55	1·01
Na_2O	2·02	2·06	1·09	3·82	0·51	0·30	0·09	0·59	1·37	1·53	1·42	0·16	2·56	5·87
K_2O	5·21	4·70	8·79	6·48	6·51	7·10	6·95	5·89	4·98	5·27	6·48	9·14	6·09	3·17
P_2O_5	0·76	0·75	0·73	0·20	0·66	0·61	0·55	0·39	0·45	0·40	0·45	1·04	0·63	0·07
LOI	1·76	1·88	2·97	3·27	6·08	7·54	11·28	7·06	6·53	5·71	4·46	3·98	5·59	3·66
Sum	99·77	99·24	98·38	99·91	99·64	99·71	100·00	99·99	99·83	100·12	99·92	99·08	99·06	100·38
Mg-no.	60·6	60·1	44·6	34·4	57·2	80·0	71·9	76·8	73·5	69·7	74·2	71·5	64·2	60·6
Cr	67	73	108	48	384	454	371	420	290	220	258	424	106	99
Ni	19	18	33	12	257	257	212	206	176	101	137	136	80	83
Co	11	19	30	3	18	21	17	24	22	14	16	36	13	17
V	184	184	247	60	86	94	87	93	86	78	66	157	79	148
Cu	10	28	78	80	11	12	13	13	76	10	4	52	7	11
Zn	95	99	107	b.d.	102	98	45	62	61	191	79	64	39	116
Ba	1311	1144	3302	2132	1853	1007	1914	1072	1060	1155	1034	2129	1141	637
Ga	17	17	26	b.d.	15	24	18	19	18	18	18	21	17	21
Li	39	48	23	23	46	35	35	57	41	30	33		19	134
Sc	20	21	b.d.	b.d.	12	14	12	12	12	10	9	21	10	17
Rb	169	180	443	643	260	380	275	283	226	251	359	411	200	216
Sr	1271	1321	1783	1799	307	587	418	399	450	490	417	554	700	810
Y	40	31	39	51	21	21	19	18	18	17	15	30	31	22
Zr	342	334	642	671	539	568	515	379	365	311	527	423	404	100
Nb	15	15	33	34	32	36	36	25	28	29	33	25	18	14
Cs	9·4	14·8	21·9	25·1	15·4	17·0	19·8	18·9	7·1	17·9	9·2	13·0	9·3	2·4

Locality:	Golija		Devaje	Devaje–Visoča	Veliki Majdan							Rudnik		Avala
Age (Ma):[1]			21·8		33·5							31·9		
Rock type:	kersantite		leucitite		minette	leucominette						minette	leuco-minette	sandstone
Sample:	D4	D5	Dev	Vi-1	VM01/3	VM VI/2	VM VI/7	VM XII/3	VM XIV/2	VM XIV/4	VM XIV/6	R97x/424	R2	AV01
Hf	7·7	8·3	16·1	16·5	6·1	16·2	12·8	9·6	8·7	7·0	12·9	5·4	3·4	3·0
Pb	19	29	52	48	56	74	50	18	18	31	26	36	6	34
Th	32·8	33·3	64·2	64·5	18·5	43·7	37·8	32·6	33·0	33·5	44·4	18·8	11·8	12·6
U	7·4	7·4	5·9	9·7	6·2	13·7	13·3	11·3	10·0	10·4	14·7	4·0	3·1	2·4
La	113·4	115·3	101·3	100·5	62·8	56·4	54·4	54·3	64·6	55·1	62·1	45·7	89·5	25·5
Ce	241·7	245·7	237·7	220·5	154·0	141·0	136·5	121·5	139·3	118·6	148·4	97·6	187·9	66·5
Pr	27·3	27·8	29·2	26·8	19·6	20·4	17·7	14·7	16·3	13·9	18·7	11·9	21·7	6·6
Nd	105·0	106·7	121·4	109·1	84·3	85·8	77·1	62·2	67·6	57·1	81·3	50·1	88·2	25·8
Sm	17·3	17·4	23·9	22·0	14·6	15·2	13·9	10·8	11·4	9·8	14·0	10·8	15·6	4·9
Eu	3·8	4·0	5·2	4·9	2·7	2·7	2·8	2·2	2·3	2·0	2·5	2·1	3·5	1·3
Gd	12·1	12·0	15·6	15·5	9·3	9·5	8·9	7·1	7·7	6·5	8·1	6·5	11·6	3·7
Tb	1·5	1·5	2·0	2·0	1·2	1·0	1·1	0·9	1·0	0·9	1·0	0·8	1·5	0·6
Dy	6·8	6·8	9·2	9·7	4·4	4·3	4·1	3·6	3·7	3·3	3·4	3·6	6·2	3·6
Ho	1·2	1·2	1·6	1·8	0·7	0·7	0·7	0·6	0·6	0·6	0·5	0·6	1·0	0·7
Er	3·0	2·9	3·8	4·3	1·8	1·8	1·7	1·5	1·6	1·5	1·2	1·4	2·7	2·1
Tm	0·4	0·4	0·5	0·6	0·2	0·2	0·2	0·2	0·2	0·2	0·2	0·2	0·4	0·4
Yb	2·4	2·4	3·1	3·8	1·6	1·4	1·5	1·4	1·5	1·3	1·1	1·0	2·4	2·1
Lu	0·4	0·4	0·5	0·6	0·2	0·2	0·2	0·2	0·2	0·2	0·2	0·2	0·4	0·3

*Total iron as Fe_2O_3.
[1]Cvetkovič *et al*. (2004*a*).
[2]Vaskovič *et al*. (1996).
Mg-number = atomic 100 Mg/(Mg + 0·85 Fe_T); n.d., not determined; b.d., below detection.

Table 3: Whole-rock major (%) and trace element (ppm) analyses of KAG rocks

Locality:	Koritnik					Nova Varoš[2]					
Age (Ma):[1]	9·12					21·5					
Rock type:	ugandites			Lct-basanites		ugandites		Lct-basanites			
Sample:	KOR-56	KR01/3	KR01/1	KR01/2	KOR-47	NV01/7	NV01/4	NV01/6C	NV01/3	NV01/6A	NV01/5
SiO_2	42·4	42·3	42·3	43·8	44·3	42·8	44·2	43·1	44·5	45·3	45·8
TiO_2	2·18	2·20	2·20	1·95	1·89	1·86	1·59	1·53	1·59	1·44	1·46
Al_2O_3	10·00	10·29	10·24	11·70	11·88	10·16	11·30	11·34	11·45	13·36	13·84
$Fe_2O_3^*$	10·41	10·50	10·45	10·12	9·85	10·55	9·59	9·37	9·68	8·97	8·58
MnO	0·16	0·16	0·16	0·16	0·16	0·16	0·15	0·16	0·15	0·14	0·13
MgO	12·90	12·53	12·29	11·32	11·12	11·52	11·33	10·68	11·27	10·31	9·57
CaO	10·20	10·45	10·57	10·03	10·02	9·78	9·55	10·30	9·65	9·65	10·07
Na_2O	2·17	2·00	2·27	2·56	2·89	3·04	3·54	3·26	3·34	3·46	3·60
K_2O	5·29	5·15	5·02	4·46	4·52	1·74	1·93	1·69	2·19	0·97	0·89
P_2O_5	1·30	1·48	1·46	1·29	1·24	1·18	1·39	1·29	1·38	0·84	0·83
LOI	2·38	2·07	1·95	1·92	1·50	6·80	5·28	7·19	4·84	5·68	5·18
Sum	100·01	99·71	99·48	99·83	99·92	99·56	99·80	99·92	99·99	100·09	100·00
Mg-no.	73·4	72·6	72·2	71·1	71·3	70·6	72·3	71·5	72·0	71·7	71·1
Cr	536	506	512	481	530	652	563	549	550	462	442
Ni	340	308	286	245	210	290	255	271	269	197	156
Co	44	43	41	38	38	44	40	40	40	38	34
V	212	196	225	229	219	186	184	188	192	205	213
Cu	49	17	30	b.d.	26	40	28	34	28	24	16
Zn	165	160	160	133	134	187	149	141	152	105	103
Ba	1178	1215	1165	1044	1119	1251	1029	1014	1588	1092	1015
Ga	14	15	15	14	13	13	14	11	13	13	14
Li	n.d.	16	16	15	n.d.	56	42	72	n.d.	n.d.	33
Sc	n.d.	30	30	32	n.d.	24	24	25	n.d.	n.d.	26
Rb	175	152	165	178	162	38	99	60	94	60	62
Sr	1236	1153	1159	1015	1016	1250	969	742	1209	801	837
Y	51	39	40	38	46	21	24	21	24	25	25
Zr	578	549	555	478	446	370	320	305	322	254	255
Nb	44	49	48	43	41	57	39	35	40	32	32
Cs	n.d.	3·5	3·9	3·3	n.d.	3·4	9·4	12·9	n.d.	n.d.	21
Hf	n.d.	12·7	12·8	10·9	n.d.	10·1	8·1	7·4	n.d.	n.d.	6·0
Pb	9	11	12	12	11	9	11	9	8	9	7
Th	27·3	22·1	24·1	19·2	22·8	22·2	17·0	14·6	n.d.	n.d.	14·6
U	1·4	5·3	5·3	4·3	b.d.	4·9	2·5	2·3	n.d.	n.d.	3·4
La	119·1	123·1	128·3	98·9	n.d.	116·8	118·4	79·1	n.d.	n.d.	62·4
Ce	281·1	271·3	285·4	216·3	202·0	237·0	241·7	164·1	n.d.	n.d.	126·0
Pr	27·9	33·7	35·4	26·7	n.d.	24·3	25·2	17·3	n.d.	n.d.	13·9
Nd	136·3	128·5	135·8	103·9	n.d.	83·6	87·4	61·4	n.d.	n.d.	50·6
Sm	20·9	20·1	21·0	16·4	n.d.	11·4	12·3	9·3	n.d.	n.d.	8·8
Eu	5·5	4·7	4·9	4·0	n.d.	2·6	3·0	2·3	n.d.	n.d.	2·3
Gd	13·0	14·3	14·8	12·2	n.d.	7·9	8·6	7·0	n.d.	n.d.	7·0
Tb	n.d.	1·9	1·9	1·6	n.d.	1·1	1·2	1·0	n.d.	n.d.	1·0
Dy	8·4	7·4	7·7	6·8	n.d.	5·0	5·7	4·8	n.d.	n.d.	5·1
Ho	1·5	1·2	1·3	1·2	n.d.	0·9	1·1	0·9	n.d.	n.d.	1·1
Er	3·8	2·9	3·1	3·0	n.d.	2·2	2·6	2·3	n.d.	n.d.	2·6
Tm	n.d.	0·4	0·4	0·4	n.d.	0·3	0·4	0·3	n.d.	n.d.	0·4
Yb	2·4	2·7	2·7	2·6	n.d.	1·9	2·1	2·0	n.d.	n.d.	2·3
Lu	0·4	0·4	0·4	0·4	n.d.	0·3	0·3	0·3	n.d.	n.d.	0·4

Locality:	Trijebine[2]				Družetići[2]					
Age (Ma):	22·9				23·9					
Rock type:	Lct-basanites				ankaratrites					
Sample:	TRIJEB-32	TR01/2	TR01/5	TR01/1	Druz-103	Druz-88	DZIII/2	DZV/1	DZI/2	Druz-106
SiO_2	43·3	43·7	44·6	45·7	41·7	40·9	41·5	41·7	42·1	42·2
TiO_2	1·75	1·71	1·67	1·37	1·41	1·40	1·42	1·43	1·39	1·43
Al_2O_3	11·54	11·79	12·54	13·37	13·05	12·63	12·82	13·25	12·80	13·63
Fe_2O_3*	9·39	8·97	9·05	8·67	9·41	9·18	9·26	9·26	9·23	9·68
MnO	0·15	0·15	0·11	0·14	0·19	0·21	0·16	0·18	0·18	0·19
MgO	10·82	9·38	8·28	9·65	8·50	9·25	9·11	9·73	8·69	8·90
CaO	10·47	11·21	10·87	9·98	12·88	12·57	12·19	12·66	12·55	12·68
Na_2O	3·46	4·03	3·31	3·18	4·34	3·65	3·79	3·79	3·99	4·10
K_2O	0·90	0·99	0·74	1·39	0·46	0·52	0·08	0·62	0·44	0·23
P_2O_5	1·13	1·08	1·03	0·75	1·54	1·51	1·57	1·35	1·49	1·30
LOI	6·70	6·28	7·35	5·38	5·50	5·78	7·16	5·48	6·17	5·51
Sum	100·07	99·82	100·04	100·00	98·97	97·64	99·08	99·43	99·02	99·81
Mg-no.	71·8	69·6	66·5	71·0	66·2	68·8	68·2	69·7	67·2	66·6
Cr	454	460	455	464	200	193	190	185	179	192
Ni	210	209	191	143	167	159	170	156	160	160
Co	38	32	37	33	33	31	39	32	28	39
V	221	199	223	204	218	227	200	218	220	217
Cu	34	21	25	b.d.	13	5	23	16	10	108
Zn	130	123	114	97	102	89	90	87	91	95
Ba	1068	1086	1057	904	1726	1676	5807	2327	2127	1028
Ga	14	16	15	16	15	14	13	12	13	16
Li	n.d.	19	41	26	217	n.d.	178	n.d.	n.d.	103
Sc	n.d.	27	29	30	22	n.d.	24	n.d.	n.d.	23
Rb	84	135	68	86	8	14	4	21	16	5
Sr	905	1014	1010	841	1489	1167	1062	1435	1252	1259
Y	31	32	32	27	40	36	35	38	33	51
Zr	398	402	377	267	546	494	510	511	501	432
Nb	37	39	36	31	54	50	52	57	51	30
Cs	n.d.	3·1	4	2·8	15·5	n.d.	9·5	n.d.	n.d.	12·5
Hf	n.d.	10·0	9·6	6·2	11·0	n.d.	11·1	n.d.	n.d.	11·0
Pb	11	13	14	12	34	21	39	9	23	48
Th	18·5	19·1	18·2	13·2	55·8	n.d.	45·0	n.d.	n.d.	57·1
U	b.d.	4·8	2·6	3·1	12·3	n.d.	5·4	n.d.	n.d.	11·9
La	85·3	92·8	89·5	65·1	112·2	n.d.	91·2	n.d.	n.d.	103·0
Ce	200·9	200·5	193·6	137·0	369·7	n.d.	333·4	n.d.	n.d.	336·6
Pr	19·6	24·6	23·9	16·4	42·2	n.d.	39·4	n.d.	n.d.	38·3
Nd	92·1	94·1	92·3	62·5	165·1	n.d.	153·0	n.d.	n.d.	149·2
Sm	14·9	14·7	14·8	10·0	27·8	n.d.	30·0	n.d.	n.d.	25·1
Eu	3·9	3·7	3·7	2·7	6·7	n.d.	6·5	n.d.	n.d.	6·2
Gd	9·7	10·7	10·6	7·6	19·6	n.d.	17·9	n.d.	n.d.	18·3
Tb	n.d.	1·4	1·4	1·0	2·5	n.d.	2·3	n.d.	n.d.	2·3
Dy	6·7	6·1	6·1	4·9	11·1	n.d.	11·0	n.d.	n.d.	10·6
Ho	1·3	1·1	1·0	0·9	2·0	n.d.	1·6	n.d.	n.d.	1·9
Er	3·4	2·6	2·7	2·4	4·5	n.d.	4·3	n.d.	n.d.	4·4
Tm	n.d.	0·4	0·4	0·4	0·6	n.d.	0·5	n.d.	n.d.	0·6
Yb	2·3	2·4	2·4	2·2	3·5	n.d.	3·4	n.d.	n.d.	3·5
Lu	0·4	0·4	0·4	0·3	0·5	n.d.	0·5	n.d.	n.d.	0·5

*Total iron as Fe_2O_3.
Mg-number = atomic 100 Mg/(Mg + 0·85Fe_T); b.d., below detection; n.d., not determined.
[1]Cvetković *et al*. (2004*a*).
[2]Highly analcimized samples.

Table 4: Whole-rock Rb, Sr, Nd, Sm concentration (ppm) and Sr and Nd isotope data for Serbian ultrapotassic rocks, recalculated for the given ages

Sample	Locality	Rock type	Age*	Rb	Sr	$^{87}Sr/^{86}Sr$ measured	$^{87}Sr/^{86}Sr_i$	Sm	Nd	$^{143}Nd/^{144}Nd$ measured	$^{143}Nd/^{144}Nd_i$
LAG rocks											
BK-3	Borač	Phl-basaltic trachyandesite	23	157	1389	0·706274 ± 4	0·70617	18·4	106·77	0·512581 ± 7	0·51257
BK01/12	Borač	Phl-basaltic trachyandesite	23	237	919	0·710267 ± 9	0·71003	19·28	111·61	0·512283 ± 6	0·51227
BK01/3-1	Borač	Ol–Cpx–Lct–lamproite	23	217	825	0·711863 ± 6	0·71162	18·74	109·08	0·512204 ± 7	0·51219
BK01/3C	Borač	Ol–Cpx–Phl–Lct–Sa-lamproite	23	319	740	0·711090 ± 4	0·71069	19·21	109·18	0·512219 ± 7	0·5122
M00/3	Mionica	Ol–Cpx–Phl–Lct–Sa-lamproite	29	254	916	0·710693 ± 4	0·71036	21·86	133·56	0·512316 ± 6	0·5123
ZB01/2	Zabrdica	Ol–Cpx–Phl–Lct–Sa-lamproite	26	194	586	0·711917 ± 6	0·71157	16·54	98·92	0·512178 ± 5	0·51216
Ar99/2	Arandjelovac	primitive minette	26	148	516	0·707760 ± 11	0·70745	6·46	31·96	0·512536 ± 5	0·51252
AV-1	Avala	minette	31	556	432	0·713316 ± 8	0·71169	17·18	103·95	0·512178 ± 5	0·51216
AV00/5	Avala	Phl-trachybasalt	22	243	820	0·707770 ± 5	0·7075	11·13	59·63	0·512614 ± 4	0·5126
AV00/8	Avala	Phl-trachybasalt	22	232	987	0·707393 ± 6	0·70718	9·82	54·25	0·512622 ± 3	0·51261
Klin124	Klinovac	Phl-trachybasalt	33	119	1250	0·708830 ± 6	0·708703	6·51	35·34	0·512375 ± 9	0·512336
Bo-3	Bogovina	Ol–Cpx–Phl–Lct–Sa–Amph-lamp.	30	169	820	0·709021 ± 9	0·70877	19·77	112·34	0·512336 ± 6	0·51232
Blj2	Boljkovac	Phl-trachyandesite	30	359	596	0·710276 ± 5	0·70954	10	56·62	0·512281 ± 6	0·51226
VM01/3	V. Majdan	minette	34	260	307	0·714162 ± 13	0·71299	14·61	84·32	0·512200 ± 4	0·51218
VM VI/2	V. Majdan	leucominette	34	380	587	0·710807 ± 5	0·70992	15·2	85·8	0·512211 ± 6	0·51221
VM VI/7	V. Majdan	leucominette	34	275	418	0·710963 ± 6	0·71006	13·91	77·1	0·512235 ± 5	0·51224
VM XII/3	V. Majdan	leucominette	34	283	399	0·711137 ± 5	0·71016	10·8	62·22	0·512252 ± 5	0·51225
VM XIV/2	V. Majdan	leucominette	34	226	450	0·710764 ± 5	0·71007	11·42	67·57	0·512256 ± 6	0·51226
VM XIV/4	V. Majdan	leucominette	34	251	490	0·711280 ± 4	0·71058	9·79	57·09	0·512261 ± 6	0·51226
VM XIV/6	V. Majdan	leucominette	34	359	417	0·712072 ± 5	0·71089	13·98	81·29	0·512213 ± 5	0·51221
RO/1-II	Rudnik	Ol–Phl–Sa-lamproite	30	221	598	0·711973 ± 4	0·71152	19·49	114·89	0·512208 ± 6	0·51219
R97x/424	Rudnik	minette	30	411	554	0·709550 ± 4	0·70863	10·82	50·07	0·512393 ± 4	0·51237
R2	Rudnik	leucominette	22	200	700	0·705709 ± 6	0·70545	15·64	88·22	0·512672 ± 6	0·51266
D4	Golija	kersantite	20	169	1271	0·706493 ± 5	0·70638	17·29	105·02	0·512530 ± 6	0·51252
D5	Golija	kersantite	20	180	1321	0·706424 ± 4	0·70631	17·37	106·7	0·512542 ± 6	0·51253
Dev	Devaje	leucitite	22	443	1783	0·708411 ± 5	0·70819	23·87	121·42	0·512393 ± 5	0·51238
Vi-1	Devaje–Visoča	leucitite	22	643	1799	0·708315 ± 6	0·708	22·01	109·09	0·512422 ± 6	0·5124
KAG rocks											
KR01/3	Koritnik	ugandite	9	152	1153	0·706061 ± 6	0·70601	20·05	128·51	0·512619 ± 6	0·51261
KR01/1	Koritnik	ugandite	9	165	1159	0·706052 ± 4	0·706	21·02	135·79	0·512597 ± 5	0·51259
NV01/7	Nova Varoš	ugandite	20	38	1250	0·707113 ± 1	0·70709	11·44	83·64	0·512640 ± 6	0·51263
NV01/6C	Nova Varoš	ugandite	20	60	742	0·706289 ± 4	0·70622	9·31	61·36	0·512639 ± 7	0·51263
NV01/4	Nova Varoš	Lct-basanite	20	99	969	0·706637 ± 5	0·70655	12·32	87·36	0·512627 ± 6	0·51262
TR01/1	Trijebine	Lct-basanite	23	86	841	0·705919 ± 5	0·70582	10·03	62·51	0·512616 ± 6	0·5126
Tr01/2	Trijebine	Lct-basanite	23	135	1014	0·706145 ± 5	0·70602	14·72	94·08	0·512600 ± 6	0·51259
DZV/1	Družetići	ankaratrite	24	8	1489	0·706567 ± 5	0·70656	27·76	165·06	0·512573 ± 6	0·51256
DZI/2	Družetići	ankaratrite	24	4	1062	0·706741 ± 5	0·70674	30·04	152·98	0·512578 ± 7	0·51256
Flysch sediments											
AV01	Avala	sandstone	50	216	810	0·712261 ± 6	0·71193	4·94	25·78	0·512192 ± 8	0·51217

Ages from Cvetković *et al.* (2004*a*). Subscript i indicates initial values.

Table 5: Whole-rock Pb, Th and U concentration (ppm) and Pb isotope ratios of Serbian ultrapotassic rocks, recalculated for the given ages

				Measured			Age-corrected		
Sample	Pb	Th	U	$^{206}Pb/^{204}Pb$	$^{207}Pb/^{204}Pb$	$^{208}Pb/^{204}Pb$	$^{206}Pb/^{204}Pb$	$^{207}Pb/^{204}Pb$	$^{208}Pb/^{204}Pb$
LAG rocks									
BK-3	56	63·8	16·4	18·821	15·677	38·990	18·755	15·674	38·905
BK01/12	45	46·7	15·6	18·786	15·685	38·957	18·706	15·681	38·879
BK01/3-1	40	57·3	15·8	18·818	15·682	38·987	18·729	15·678	38·880
BK01/3C	41	50·6	13·2	18·788	15·671	38·932	18·715	15·667	38·840
M00/3	31	46·9	12·8	18·808	15·701	39·023	18·687	15·696	38·877
ZB01/2	19	43·0	12·3	18·865	15·675	39·000	18·701	15·667	38·812
Ar99/2	33	15·9	6·1	18·630	15·669	38·899	18·581	15·667	38·857
AV-1	30	48·8	12·4	18·823	15·667	38·958	18·695	15·661	38·792
AV00/5	59	18·5	5·3	18·735	15·651	38·827	18·683	15·656	38·785
AV00/8	202	16·3	4·8	18·645	15·672	38·918	18·700	15·685	38·877
Klin124	49	18·2	4·6	18·711	15·665	38·999	18·680	15·664	38·959
Bo-3	32	35·5	3·9	18·810	15·626	38·905	18·772	15·624	38·795
Blj2	44	34·7	13·8	18·768	15·677	38·904	18·675	15·673	38·827
VM01/3	56	18·5	6·2	18·718	15·665	38·868	18·681	15·663	38·832
VM VI/2	74	43·7	13·7	18·701	15·688	38·909	18·639	15·685	38·844
VM VI/7	50	37·8	13·3	18·724	15·680	38·901	18·635	15·676	38·818
VM XII/3	18	32·6	11·3	18·945	15·677	39·073	18·734	15·667	38·873
VM XIV/2	18	33·0	10·0	18·865	15·662	39·000	18·678	15·653	38·797
VM XIV/4	31	33·5	10·4	18·749	15·661	38·863	18·637	15·656	38·744
VM XIV/6	26	44·4	14·7	18·906	15·674	39·057	18·716	15·665	38·868
RO/1-II	31	53·1	11·3	18·779	15·672	38·947	18·669	15·666	38·777
R97x/424	36	18·8	4·0	18·716	15·648	38·804	18·683	15·646	38·752
R2	6	11·8	3·1	18·853	15·685	39·033	18·732	15·679	38·884
D4	19	32·8	7·4	18·765	15·676	38·985	18·686	15·672	38·870
D5	29	33·3	7·4	18·734	15·675	38·953	18·684	15·673	38·878
Dev	52	64·2	5·9	18·756	15·674	38·965	18·731	15·673	38·877
Vi-1	48	64·5	9·7	18·783	15·688	39·019	18·739	15·686	38·922
KAG rocks									
KR01/3	11	22·1	5·3	18·814	15·656	38·933	18·814	15·656	38·933
KR01/1	12	24·1	5·3	18·817	15·661	38·959	18·817	15·661	38·959
NV01/7	9	22·2	4·9	18·863	15·662	39·000	18·751	15·657	38·834
NV01/6C	9	14·6	2·3	18·813	15·679	39·007	18·761	15·676	38·898
NV01/4	11	17·0	2·5	18·791	15·670	38·969	18·745	15·668	38·865
TR01/1	12	13·2	3·1	18·738	15·637	38·822	18·738	15·637	38·822
Tr01/2	13	19·1	4·8	18·779	15·651	38·883	18·779	15·651	38·883
DZV/1	34	55·8	12·3	18·832	15·668	38·987	18·832	15·668	38·987
DZI/2	39	45·0	5·4	18·758	15·676	38·922	18·758	15·676	38·922
Flysch									
AV01	34	13·0	2·0	18·735	15·651	38·827	18·696	15·649	38·760

and high-potassium series (HKS) rocks of the Italian province (Conticelli & Peccerillo, 1992; Peccerillo, 1995, 2003; Conticelli *et al.*, 2002).

In contrast to the highly variable LAG rocks, ugandites and leucite basanites of the kamafugitic group are remarkably uniform in composition. They are silica-undersaturated, commonly showing normative feldspathoid contents up to 30%. SiO_2 contents are in the range 42–46 wt %, Mg-number 66–73 (mostly >70), and Cr and Ni up to 550 and 300 ppm, respectively. CaO contents

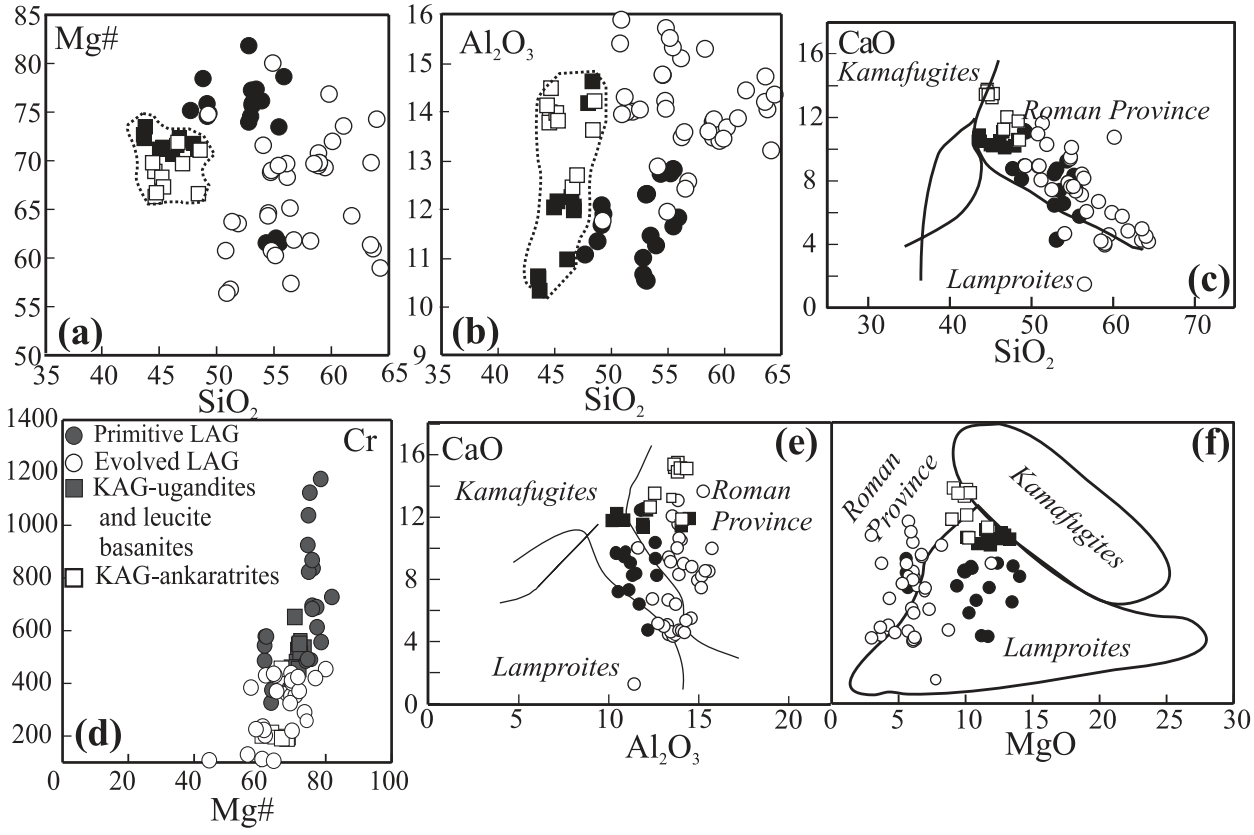

Fig. 7. Whole-rock variation diagrams for Serbian ultrapotassic rocks recalculated on volatile-free basis: SiO_2 vs (a) Mg-number, (b) Al_2O_3, (c) CaO; (d) Mg-number vs Cr; (c), (e) and (f) are plots of Serbian ultrapotassic rocks on the classification diagrams of Foley *et al.* (1987).

are elevated but never exceed 12 wt %, whereas alumina contents range from 10 to 14 wt %. There is no significant correlation of either SiO_2 or Al_2O_3 content with Mg-number or Cr content, indicating that fractionation of mafic minerals is not the major cause of the SiO_2 and Al_2O_3 variations (Fig. 7a and b). Compared with ugandites and leucite basanites, ankaratrites have lower Mg-number (down to 58–68), and considerably lower Cr and Ni contents, below 200 and 150 ppm, respectively. These samples also show ubiquitously higher CaO contents, up to 14 wt %. The alkalis are disturbed in most rocks with kamafugitic affinity as a result of analcimization of leucite. This is most intense in ankaratrites, which show a decrease of K_2O content down to 0·05% and K_2O/Na_2O ratio to 0·03. Analcimization has not occurred in the Koritnik samples, whose K_2O content of 5·3% indicates the original K_2O content of the other KAG rocks.

High volatile contents (loss on ignition; LOI) are characteristic of most of the Serbian ultrapotassic rocks. This is due to a combination of the high modal abundance of phlogopite and two major alteration processes: analcimization of leucite and iddingsitization of olivine. In some melanocratic varieties of LAG, phlogopite makes more than 30 vol. % of the rocks, and olivine is almost universally iddingsitized (Electronic Appendix 3-g). The influence of analcimization on LOI values is best illustrated by the analcime-bearing KAG samples from Nova Varoš, Trijebine and Družetići: these have LOI values that are substantially higher (4·8–7·2 wt %) than in the analcime-free samples from Koritnik (1·8–2·3 wt %).

Incompatible trace elements

Incompatible trace element variations are summarized in Fig. 8. Primitive mantle normalized patterns for the primitive LAG rocks from the Vardar ophiolitic suture zone are similar but abundances vary widely. They exhibit extreme enrichment in large ion lithophile elements (LILE; Cs, Rb, Ba, Th and U), in the range of 300–1000 times primitive mantle for most samples. The level of enrichment is highest for Cs (>5000 times primitive mantle), Th and U, giving rise to troughs in the patterns at Rb and Ba. Primitive lamproitic rocks display characteristic Pb peaks (Fig. 8a and b) and Sr and P troughs of variable intensity. They are depleted in high field strength elements (HFSE), with Nb and Ti troughs and high LILE/HFSE ratios, resembling other Italian and

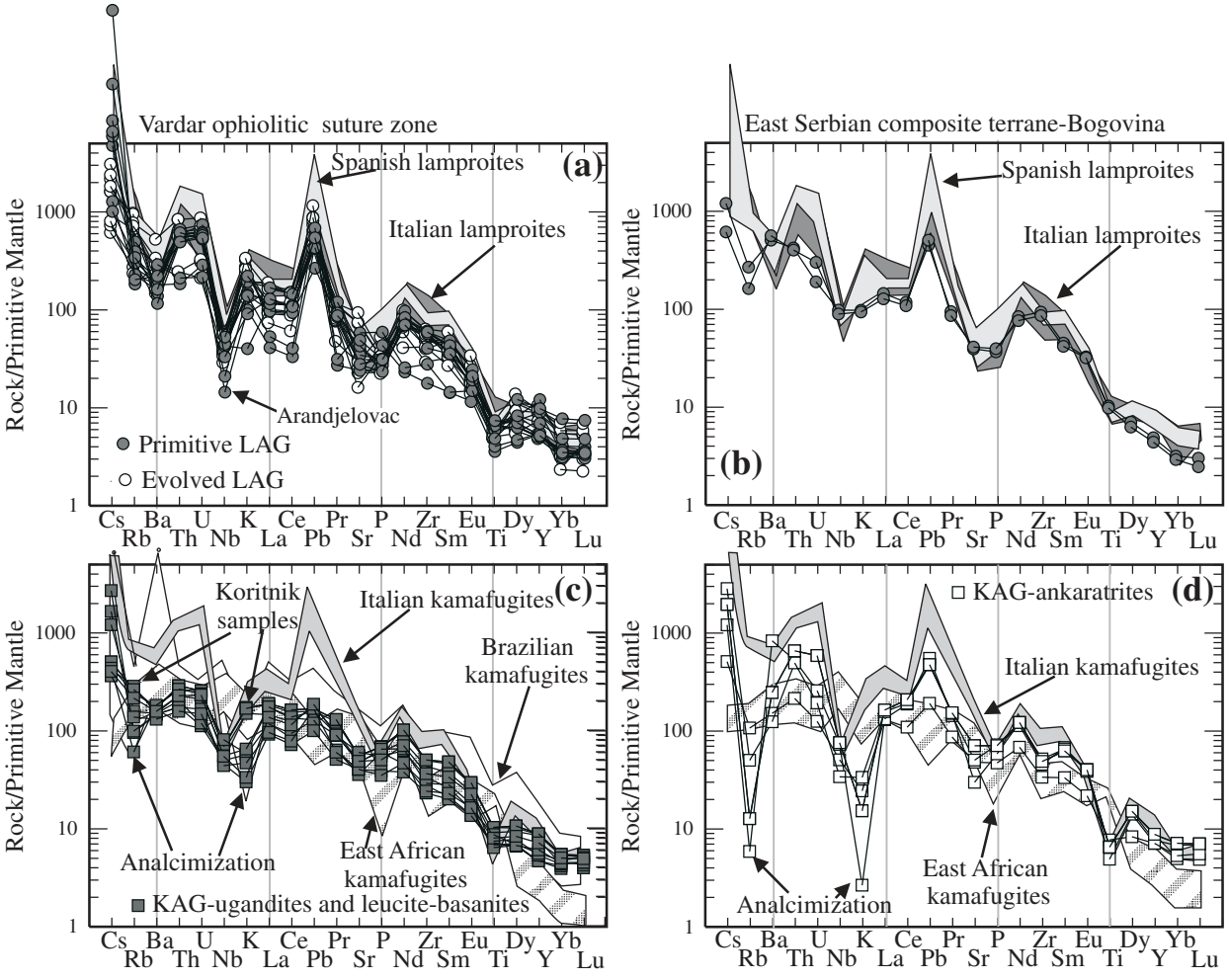

Fig. 8. Primitive mantle-normalized trace element variation diagrams for representative samples of Serbian Tertiary ultrapotassic rocks. (a) Primitive LAG rocks from Vardar ophiolitic suture zone; (b) primitive LAG rocks from Bogovina–East Serbian composite terrane; (c) KAG ugandites and leucite basanites; (d) KAG ankaratrites. Coefficients for normalization are after Sun & McDonough (1989) and McDonough & Sun (1995). Fields for Italian and Spanish lamproites are from Conticelli *et al.* (2002) and Turner *et al.* (1999), respectively. Fields for Italian, Brazilian and East African kamafugites are from Conticelli & Peccerillo (1992), Stoppa & Cundari (1995), Carlson *et al.* (1996), Di Battistini *et al.* (1998, 2001) and Tappe *et al.* (2003).

Spanish Mediterranean-type lamproites (Fig. 8a). Ba, P and Sr troughs correlate with the level of general enrichment of incompatible elements (including REE, see also below), disappearing in the samples from Arandjelovac, which are most HFSE depleted. The patterns for the samples from Bogovina (in the East Serbian composite terrane) are slightly different from other LAG rocks in that the Ti, Nb and Ba troughs are much less pronounced (Fig. 8b). The evolved LAG rocks show similar incompatible element patterns but with slightly higher levels of enrichment. La/Yb ratios of primitive LAG rocks range from 20 to 60 but are mostly around 40 (Fig. 9a and b). The extent of REE fractionation for all primitive LAG rocks, except Bogovina, and their level of enrichment correlate with Nb, Zr, Hf and TiO_2, with the most depleted samples coming from the Arandjelovac dyke (Fig. 9a). The most enriched samples display a Eu trough, which passes into a slight positive anomaly in the Arandjelovac samples (Fig. 9a). The rocks from Bogovina do not show a Eu anomaly and also display considerable depletion in heavy REE (HREE), with Lu_N below 10 times chondrite (Fig. 9b). Evolved LAG rocks show a large range of REE enrichment and are fractionated to different extents (Fig. 9c). They also show different intensities of Eu anomaly.

Incompatible elements in KAG rocks are generally similar to those in LAG rocks, but with less pronounced LILE enrichment and LILE/HFSE fractionation (Fig. 8c). Troughs at K and Rb are apparent in analcime-bearing samples (Fig. 8c), and are extremely large in the ankaratrites (Fig. 8d), but absent in non-analcimized samples. All KAG samples have Nb and Ti

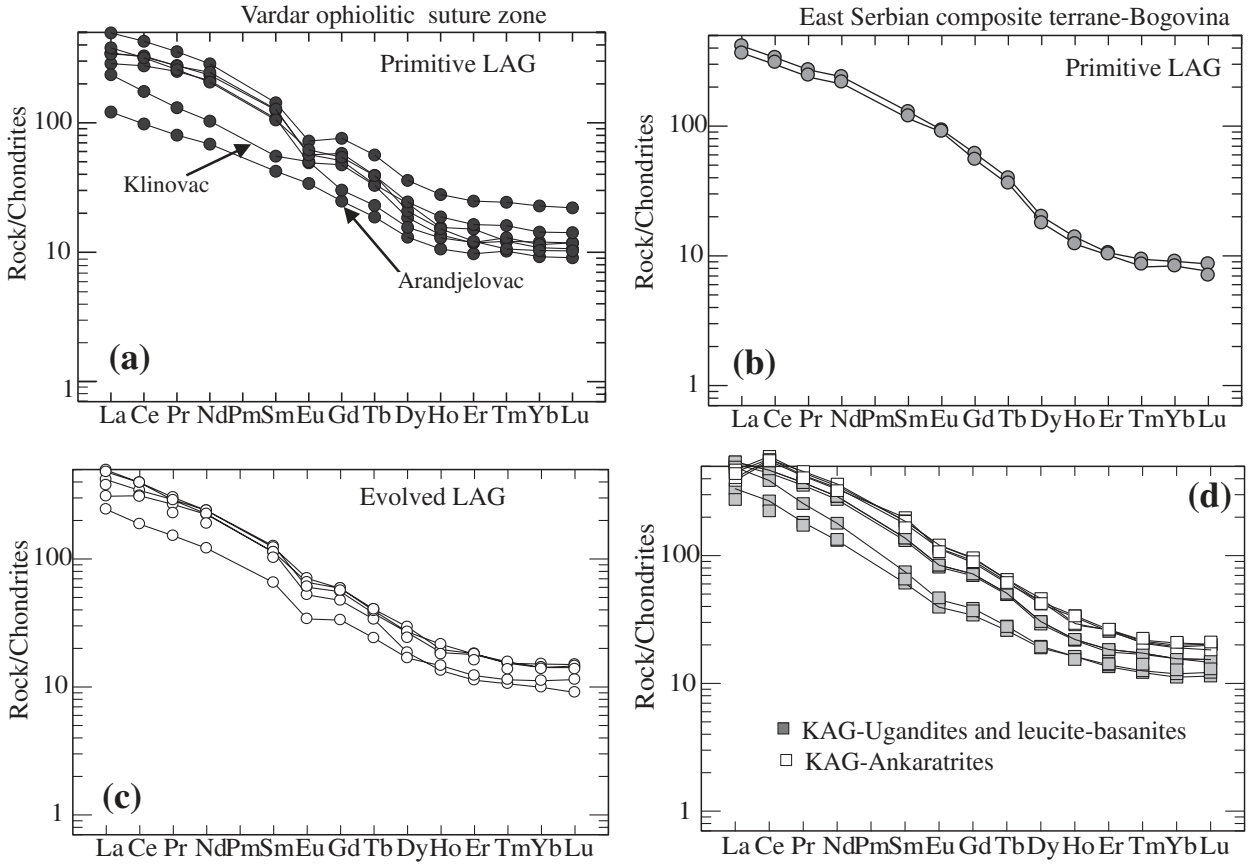

Fig. 9. Chondrite-normalized REE patterns for representative samples of Serbian Tertiary ultrapotassic rocks. (a) Primitive LAG rocks from the Vardar ophiolitic suture zone; (b) primitive LAG rocks from Bogovina–East Serbian composite terrane; (c) evolved LAG rocks; (d) KAG rocks. Coefficients for normalization are after Sun & McDonough (1989).

troughs and a Pb peak, but all these anomalies are much less pronounced than in the LAG rocks. The incompatible element patterns are broadly similar to those of Italian kamafugitic rocks, but not those from East African. Light REE (LREE) concentrations in KAG rocks are high (up to 500 times chondrite), and overall pattern shapes are steeply and consistently fractionated with only a slight Eu anomaly (Fig. 9d). Concentrations of HREE are low, but mostly slightly above 10 times chondrite.

Radiogenic isotopes

LAG rocks vary widely in $^{87}Sr/^{86}Sr_i$ (0·70735–0·71299) and $^{143}Nd/^{144}Nd_i$ (0·51251–0·51216) (Fig. 10). Primitive lamproitic samples plot in the enriched quadrant, clearly trending towards the space usually occupied by upper crustal rocks. Evolved LAG rocks are dispersed in the same space, with a few samples showing less radiogenic Sr and more radiogenic Nd isotopic values. In contrast to the wide variation of $^{87}Sr/^{86}Sr$ and $^{143}Nd/^{144}Nd$, the LAG rocks display only slight variations in $^{206}Pb/^{204}Pb$, $^{207}Pb/^{204}Pb$ and $^{208}Pb/^{204}Pb$ ratios (Fig. 11). They plot above the northern hemisphere reference line (NHRL) on $^{206}Pb/^{204}Pb$ vs $^{207}Pb/^{204}Pb$ and $^{208}Pb/^{204}Pb$ diagrams (Fig. 11) and fall within the pelagic sediment field of Ben Othman *et al.* (1989).

The radiogenic isotopic signatures of Serbian LAG rocks with a large range of Sr and Nd isotopic values and a restricted variation of Pb isotopes highlight a strong similarity to other Mediterranean ultrapotassic provinces (Nelson *et al.*, 1986; Conticelli *et al.*, 2002). They are more enriched in radiogenic Sr and depleted in radiogenic Nd than any known basaltic volcanics or/and mantle xenoliths in the region, including those from Macedonia and the Pannonian basin (Fig. 10). Although primitive LAG samples have higher Nd and lower Sr isotopic ratios than Italian and Spanish lamproites, Pb isotope systematics are almost identical to Italian and Spanish samples. It is interesting to note that primitive Serbian LAG samples lie on an extension of the Sr–Nd isotopic trend exhibited by lamproitic rocks from Spain, Tibet and Italy.

KAG rocks display considerably less variable Sr and Nd isotopic ratios than LAG rocks. The ugandites and leucite basanites have relatively uniform Nd and Pb

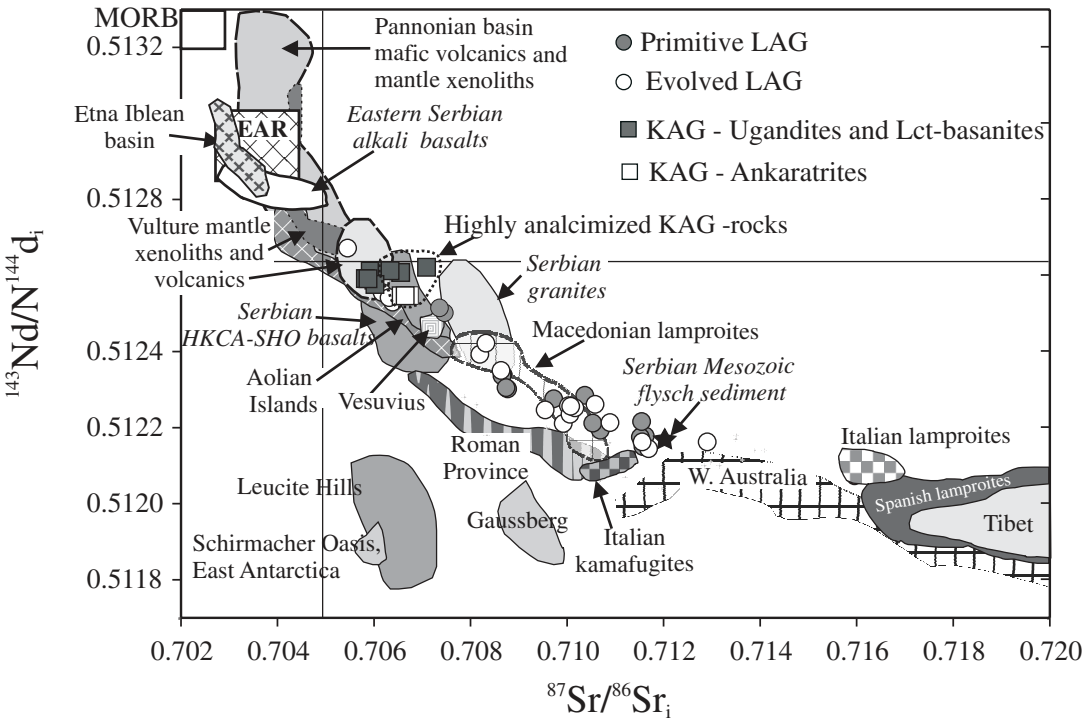

Fig. 10. Nd–Sr isotope diagram (initial values) for Serbian Tertiary ultrapotassic rocks. Also shown for comparison are fields for: East Serbian alkali basalts of Paleocene or Eocene age and Serbian HKCA–SHO basalts (high-K calc-alkaline to shoshonitic basalts) of Oligocene or Miocene age (Cvetković *et al.*, 2004*a*); Serbian granites of Oligocene or Miocene age (Karamata *et al.*, 1990); Schirmacher Oasis, East Antarctica, minette (Hoch *et al.*, 2001); Gaussberg (Murphy *et al.*, 2002); Leucite Hills lamproites (Nelson *et al.*, 1986); Italian lamproites and kamafugites (Conticelli *et al.*, 2002); Tibetan ultrapotassic rocks (Turner *et al.*, 1996; Miller *et al.*, 1999); Spanish lamproites (Benito *et al.*, 1999; Turner *et al.*, 1999); West Australian lamproites (Fraser *et al.*, 1985); Vulture mantle xenoliths and volcanics (Downes *et al.*, 2002); Pannonian Basin alkaline mafic volcanics and mantle xenoliths (Vaselli *et al.*, 1995; Harangi, 2001); Macedonian lamproites (Altherr *et al.*, 2004); MORB (Zindler & Hart, 1986); EAR, European asthenospheric reservoir (Cebria & Wilson, 1995).

isotopic compositions, whereas Sr isotope ratios vary within the range 0·70599–0·70655 with analcimized samples having the highest values (Fig. 10). Prelević *et al.* (2004*b*) interpreted decoupling of Sr and Nd isotopes to be a result of analcimization. The ankaratrites are enriched in radiogenic Sr, but depleted in radiogenic Nd, possibly indicating that assimilation–fractional crystallization (AFC) processes could have operated during their evolution. Compared with the isotopic composition of alkaline volcanic rocks from the broad surrounding areas, the data for KAG rocks most closely resemble samples from Monte Vulture carbonatites and melilitic rocks as well as xenoliths that they host (Downes *et al.*, 2002). The Pb isotope compositions of KAG rocks overlap almost completely with those of the LAG rocks, and also cluster within the pelagic sediment field. In contrast to Sr isotopes, the lack of considerable differences in Pb isotope values between analcimized and non-analcimized rocks suggests that Pb isotopes reflect primary compositions inherited from the mantle and are not affected by low-pressure processes.

As the Pb isotope compositions of both suites resemble those of pelagic sediments (Ben Othman *et al.*, 1989), we also analysed Mesozoic flysch sediments from the Vardar ophiolitic suture zone (sample AV01; Table 5), which give very similar results. The flysch sediments are part of the overstep sequence above the ophiolitic mélange and are primarily derived from the continental margin, sometimes as completely preserved turbidites. They represent a plausible crustal end-member reflecting the average composition of local upper-crustal sediments that may have been involved in the origin of Serbian LAG rocks.

Finally, no correlation of Pb isotope data is seen that could indicate that the type of binary mixing between HIMU and DM reservoirs invoked for Italian volcanic rocks [Aeolian Islands, Etna–Iblean province and Vesuvius (Gasperini *et al.*, 2002)] may be relevant for Serbian ultrapotassic rocks.

The impact of analcimization on the geochemistry of Serbian ultrapotassic rocks

Analcimization of leucite of the Serbian ultrapotassic rocks is very intense: fresh leucite survives only in

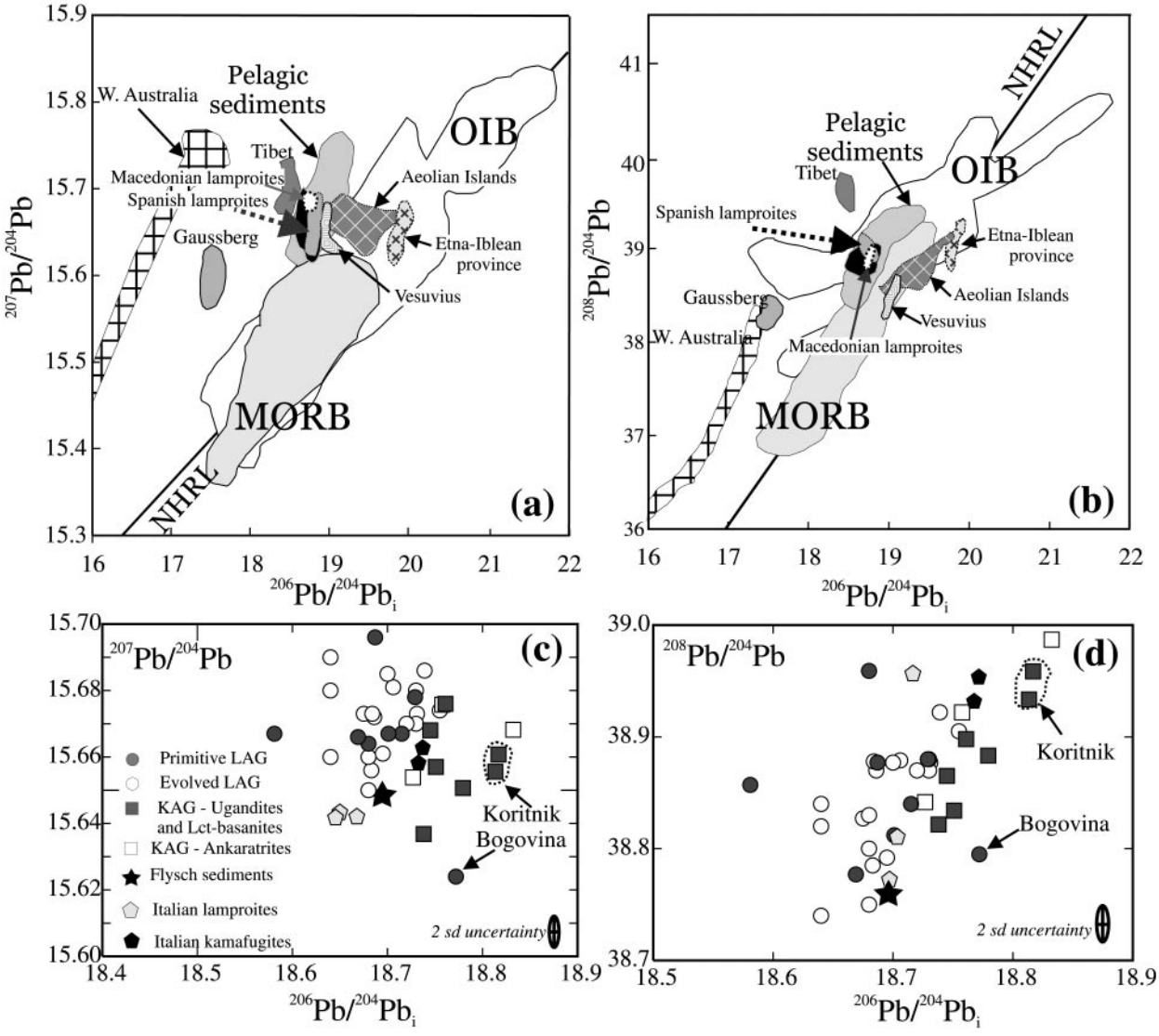

Fig. 11. (a) and (b) Variation of $^{207}Pb/^{204}Pb$ vs $^{206}Pb/^{204}Pb$ and $^{208}Pb/^{204}Pb$ vs $^{206}Pb/^{204}Pb$ (initial values) for the Serbian Tertiary ultrapotassic rocks (black field delineated with grey line). Data fields for MORB and OIB are from Zindler & Hart (1986), and for pelagic sediments are from Ben Othman *et al.* (1989). Data for ultrapotassic provinces worldwide are from the same sources as in Fig. 10; (c) and (d) show data from this study enlarged. The Koritnik volcanics, which are the only nonanalcimized KAG rocks, and the Bogovina sample, the only primitive LAG rock analysed for Pb isotopes from East Serbian composite terrane, are highlighted. NHRL is the Northern Hemisphere Reference Line, according to Hart (1984).

ugandites from the Koritnik lava flows as well as in rare leucite inclusions in Cpx. Analcimization has had a great impact on the geochemistry of the rocks, but affects only a restricted number of chemical parameters. Analcimization causes changes in the K_2O/Na_2O ratio, fractionation of LILE, the $^{87}Sr/^{86}Sr$ enrichment and the increase in the whole-rock $\delta^{18}O$ values (Prelević *et al.*, 2004*b*).

Leucite is a major reservoir of Rb and K but not for Ba (D_{Rb} up to 7·8 but D_{Ba} around 0·04; Foley & Jenner, 2004), and these elements are lost during alteration because they cannot be incorporated into analcime. This is confirmed by the absence of relative depletion of Rb and K in leucite-bearing Koritnik rocks (Fig. 8c). Moreover, extreme enrichment of Cs in some analcime-bearing samples (up to 900 ppm) is unusual, and may be related to analcimization (Prelević *et al.*, 2004*b*). Similar selective enrichment of Cs in hydrothermal analcimes has been reported in Yellowstone Park (Keith *et al.*, 1983), and it is explained by the zeolitic behaviour of the analcime and its high sorption potential for Cs and also for Sr (Redkin & Hemley, 2000). Analcimization is also recognized by an increase in whole-rock $\delta^{18}O$ values of around 3‰, which correlates with the level of whole-rock hydration (Prelević *et al.*, 2004*b*). Finally, the $^{87}Sr/^{86}Sr$ enrichment

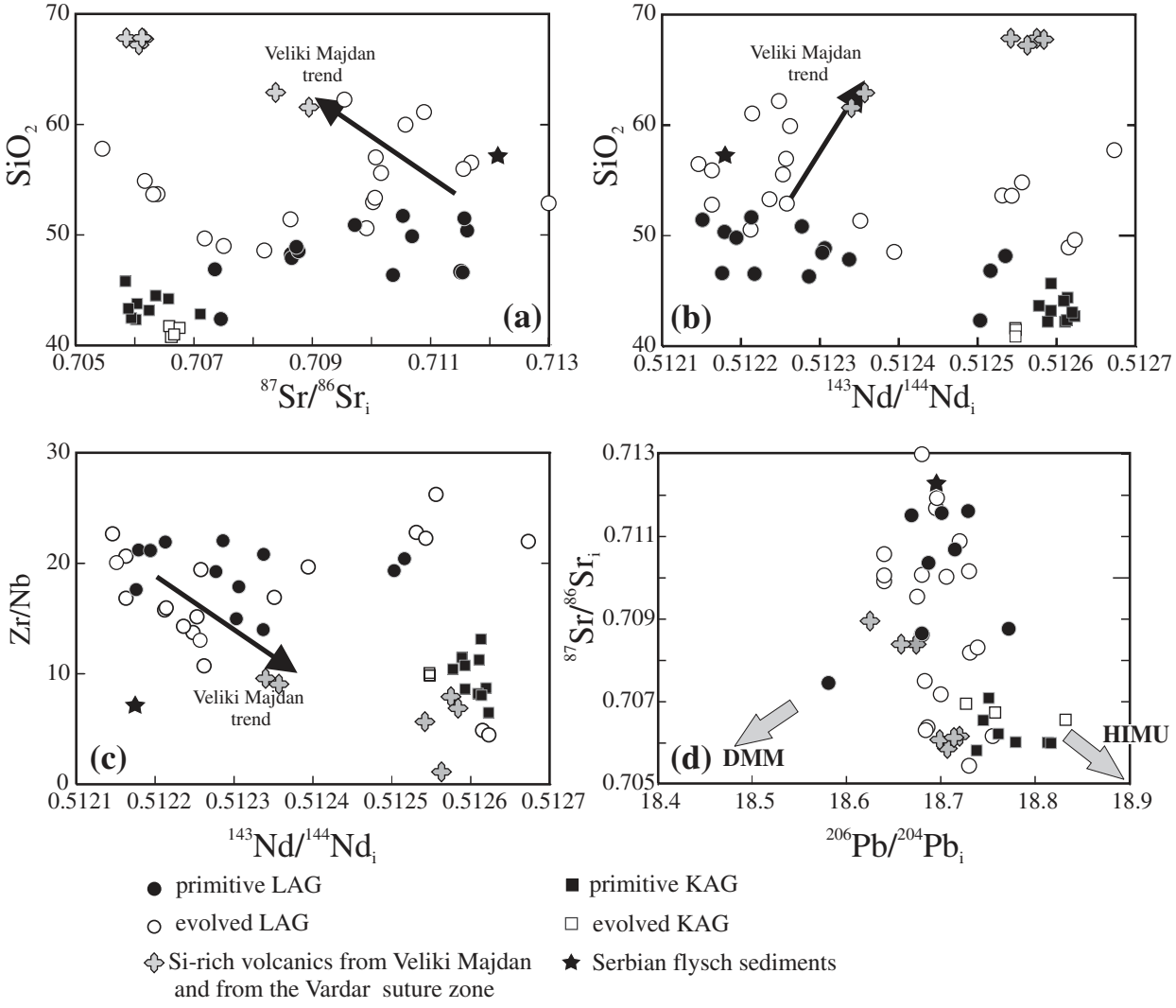

Fig. 12. Variation of $^{87}Sr/^{86}Sr_i$ and $^{143}Nd/^{144}Nd_i$ vs SiO_2 (a and b), $^{143}Nd/^{144}Nd_i$ vs Zr/Nb (c) and $^{206}Pb/^{204}Pb_i$ vs $^{87}Sr/^{86}Sr_i$ (d) for the Serbian ultrapotassic rocks. Data for the Si-rich volcanics from the Veliki Majdan and from the Vardar suture zone are from Prelević *et al.* (2004*a*) and D. Prelević (unpublished data, 2004), respectively. Arrows denote trends for Veliki Majdan samples.

at nearly constant $^{143}Nd/^{144}Nd$ exhibited by some KAG rocks also results from analcimization of leucite. All samples with higher $^{87}Sr/^{86}Sr$ are from the Nova Varoš lava flows, where $^{87}Sr/^{86}Sr$ values correlate with the modal analcime abundance, LOI of whole rocks and the whole-rock $\delta^{18}O$ values. The leucite-bearing rocks of Koritnik have lower $^{87}Sr/^{86}Sr$, LOI and $\delta^{18}O$ values.

DISCUSSION

Low-pressure processes

The two Serbian ultrapotassic suites are characterized by contrasting styles of low-pressure magmatic evolution. The LAG magmas erupted within a region (Fig. 1; Veliki Majdan, Borač-Kotlenik, Kopaonik) that produced mainly dacitic, andesitic and basaltic extrusions of high-K calc-alkaline affinity in Oligocene–Miocene times (Cvetković *et al.*, 2000, 2004*a*). It is likely that the different magma types used the same conduits, providing much potential for magmatic interaction. In contrast, KAG rocks occur exclusively in the western tectonic units, where no contemporaneous magmatism of other types has been detected.

The large range of isotopic variation correlates in some cases positively, but in others negatively, with indices of differentiation (Mg-number, SiO_2), indicating that fractional crystallization alone cannot account for the variation in major element composition of the LAG rocks (Figure 12a and b). Several lines of evidence, including the occurrence of composite intrusives, and the common presence of resorbed felsic xenocrysts and xenoliths (see

Electronic Appendix 3m, n, o, p, q and r), indicate that mixing between primitive LAG melts and contemporaneous high-K calc-alkaline felsic and intermediate magmas is an important process in the petrogenesis of the evolved LAG magmas. Petrography, mineral chemistry and bulk-rock geochemistry at Veliki Majdan (Prelević *et al.*, 2004*a*) and Rudnik (Prelević *et al.*, 2001*a*) provide evidence that the lamprophyric and shoshonitic volcanics of the composite intrusives formed by hybridization between dacitic and primitive LAG magmas. The hybridization patterns in these composite intrusions imply a significant role for such hybridization processes throughout the region. Whereas clinopyroxenes and phlogopites from primitive lamproitic rocks clearly follow typical lamproite compositional trends (alumina deficiency), the evolved LAG rocks show an opposite trend towards higher Al contents (Fig. 6a and c) from similar core compositions. The differences may be attributed to late-stage changes in Al_2O_3 content from similar parental lamproite magmas. Similar trends have been recognized at Torre Alfina in Italy, where low-Al clinopyroxenes from the least contaminated samples are typical of lamproites, but more contaminated rocks trend towards the Al-enriched field typical for the Roman province clinopyroxenes (Conticelli, 1998). Comparable variation occurs in phlogopites from LAG rocks (Fig. 6a). In the Veliki Majdan composite intrusions, similar variation in phlogopites has been attributed to hybridization of lamproite melt with peraluminous granitic magma (Prelević *et al.*, 2004*a*). Furthermore, Type 2 cumulate nodules and resorbed xenocrysts originating by disaggregation of these nodules are common in the evolved LAG rocks. These are peraluminous and consist of assemblages of calc-alkaline character, defining similar trends of increasing Al, Ca and Na content to those seen during hybridization of lamproite and dacite magmas. These xenoliths may be interpreted as high-pressure cumulates of near-liquidus phases associated with hybridization of lamproitic melts and calc-alkaline basalts (Prelević *et al.*, 2001*b*).

The scattered Sr–Nd–Pb isotope compositions (Fig. 12) preclude a single straightforward model for the evolution of all the LAG magmas. If we look only at the Nd–Sr isotopes (Fig. 10), contamination of primitive lamproitic rocks by felsic magmas resembling Serbian Si-rich (granitic) rocks results in a Nd–Sr isotope signature that does not resemble that usually expected for crustal contamination processes; the samples would be shifted into the mantle array from the position of uncontaminated (mantle-derived) LAG rocks, because of the radiogenic Sr and unradiogenic Nd isotope signature of the LAG rocks. Figure 12a and b shows that many evolved LAG rocks plot along the trend line delineated by the primitive rocks, but appear to be contaminated to varying degrees. The Veliki Majdan volcanics define a trend of decreasing $^{87}Sr/^{86}Sr$ and increasing $^{143}Nd/^{144}Nd$ with increasing SiO_2, subparallel to that of some of the evolved LAG rocks (Fig. 12a and b). This further confirms that contamination, most probably involving mixing of primitive LAG melts with Si-rich melts, may be a significant process during the evolution of the LAG magmas. Figure 12 demonstrates that such hybridization has had a significant impact on the geochemistry of the primitive LAG rocks, affecting not only major elements, but also Nd–Sr isotopes and HFSE ratios (Fig. 12c). In Figure 12d, both primitive and evolved LAG rocks have rather constant $^{206}Pb/^{204}Pb$ ratios ($\sim 18{\cdot}7 \pm 0{\cdot}1$) showing a trend between primitive LAG rocks and the Si-rich volcanics with unradiogenic $^{87}Sr/^{86}Sr$ (0·705) and $^{206}Pb/^{204}Pb$ isotope values between depleted mid-ocean ridge basalt (MORB) mantle (DMM) and HIMU-like mantle signatures. The major obstacle to a more quantitative assessment of the evolution of Serbian LAG rocks is the incompleteness of the isotope dataset for coeval magmatic rocks that represent potential contaminants.

The mineral chemistry and whole-rock compositions (lower Mg-number, Cr and Ni contents) of the ankaratrites indicate that they are more evolved than the other KAG rocks. They contain lower modal Ol and Cpx contents, and have evolved Cpx compositions and high-Ba phlogopites. Fractionation of olivine from either ugandites or leucite basanites would result in near-constant SiO_2 contents, decreasing MgO, Ni and Cr contents, and a slight increase in CaO, Al_2O_3 and P_2O_5, as found in ankaratrites. The low silica contents and similar incompatible element ratios (e.g. Zr/Nb and La/Yb) to other KAG rocks suggest that no interaction with LAG melts could be involved in the evolution of the ankaratrites. The relative increase in $^{87}Sr/^{86}Sr$ and decrease in $^{143}Nd/^{144}Nd$ of the evolved KAG relative to the primitive KAG (Fig. 12a and b) suggests instead the involvement of an AFC process. The nearly constant Pb isotope compositions are explained by the high Pb abundances and the dominance of a crustal Pb isotope signal in the mantle source of the magmas (see below). Although their major element compositions do not allow significant contamination with crustal materials, their Sr and Nd isotopic systematics require a minor effect of a crustal component. Alternatively, the more radiogenic Sr and unradiogenic Nd composition of the ankaratrites might indicate a locally more radiogenic mantle source than for the rest of the KAG localities.

The case for distinct mantle sources for the two ultrapotassic suites

Differences in oxidation state of the mantle sources

Oxygen fugacity is recognized as an important parameter in the origin of ultrapotassic magmas, controlling the speciation of C–O–H volatile components in the melt at high pressures and temperatures (Foley, 1985; Foley *et al.*,

1986). Oxygen fugacity can exert a strong influence on the mineral assemblage in the mantle source (Foley, 1989, 1992*a*, 1992*b*), as well as on melt compositions by controlling the level of silica saturation (Eggler, 1974, 1983). However, the redox state of ultrapotassic rocks varies, with evidence in some cases for highly oxidized conditions (Carmichael *et al.*, 1996; Righter & Rosas-Elguera, 2001), whereas in other cases reduced conditions apply (Foley, 1985). Experimental studies of the influence of oxygen fugacity on the composition of Mg-chromites in ultrapotassic rocks show that fO_2 is strongly reflected in the ferric-number (atomic $Fe^{3+}/\Sigma Fe$) and Cr-number [Cr/(Cr + Al)] of spinel (Foley, 1985). Lamproite spinel compositions show considerable variation of ferric-number value, the most reduced resembling Cr-rich, Fe^{3+}-poor compositions similar to spinel inclusions in diamonds (Barnes & Roeder, 2001).

Mg-chromites from the LAG and KAG samples indicate substantial differences in fO_2 in their parental melts. The ferric-number of early Cr-spinel inclusions in olivine phenocrysts is considerably lower in LAG rocks than KAG rocks (Fig. 5c). Moreover, the spinels show contrasting evolutionary trends (Fig. 5a): the trend of LAG spinels indicates dominance of the trivalent substitution $Cr \leftrightarrow Fe^{3+}$ on the Cr-number, emphasizing the significance of increasing fO_2 in the melt during ascent. The general trend recognized between spinels from different localities also occurs in line analyses across large grains (Fig. 5a) showing that the most primitive spinels are the most reduced. Such trends may be accounted for by oxidation of melts during emplacement caused by dissociation of water (Sato, 1978) driven by diffusion of H_2, which is more than a thousand times faster than water, and nearly a million times faster than oxygen (Wendlandt, 1991). This kind of 'auto-oxidation' can produce oxidation of lamproitic magmas by dissociation of only 0·1 wt % H_2O (Foley *et al.*, 1986).

Spinels from the KAG rocks have higher $Fe^{3+}/\Sigma Fe$ ratios (Fig. 5c) and noticeably lower Cr-number. They display an evolutionary trend (Fig. 5a) resulting from equilibration of spinel with olivine, clinopyroxene and other Al-bearing minerals. This may indicate a longer residence time of the KAG melts in low-pressure magma chambers.

The oxygen fugacity of the Serbian ultrapotassic rocks was estimated using the spinel–olivine Fe–Mg exchange oxybarometer (Ballhaus *et al.*, 1991) for spinel inclusions and their host olivine phenocrysts (olivine analysed <20 μm from the spinel inclusions). Temperatures were calculated by means of the olivine–chromite geothermometers of Ballhaus *et al.* (1991) and Poustovetov & Roeder (2001), assuming the pressure to be 20 kbar. For LAG rocks, we also estimated oxygen fugacity from coexisting Ti-magnetite and ilmenite using QUILF software (Andersen *et al.*, 1993); a summary of estimates is shown in Fig. 13. All results confirm substantial differences between the LAG and KAG groups, but there is a discrepancy between the results for the LAG obtained with different oxybarometers. Coexisting ilmenite and Ti-magnetite pairs from the LAG rocks consistently indicate oxygen fugacities in the range of the quartz–fayalite–magnetite (QFM) to magnetite–wüstite (MW) buffer (around QFM −3 log units fO_2; Fig. 13), whereas the spinel–olivine Fe–Mg exchange oxybarometer gives more variable values for fO_2 for the same rocks. The discrepancy may be accounted for by post-entrapment equilibration of Cr-spinel with the melt and silicate minerals (Kamenetsky *et al.*, 2001) following crystallization of Fe–Ti oxides that still record low fO_2. Alternatively, the olivine–spinel oxybarometer may be less accurate for lamproites as a result of compositional differences from those used in calibration of the method. The fO_2 for LAG rocks estimated from coexisting Ti–Fe oxides is in excellent agreement with the empirical spinel oxybarometer developed for lamproites (Foley, 1985), which predicts equilibration at the MW buffer for the LAG. The spinel–olivine pairs from the KAG rocks are equilibrated at consistently more oxidized conditions of nickel–nickel oxide (NNO) +1 to 2 (Fig. 13).

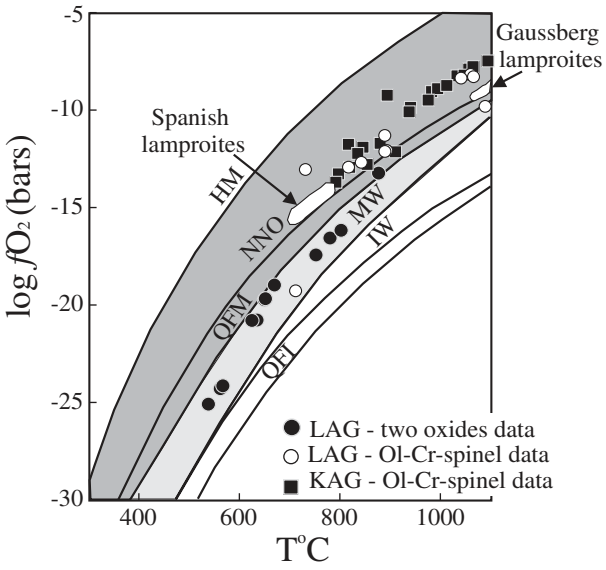

Fig. 13. A summary of oxygen fugacity estimates for Serbian ultrapotassic rocks. Data field for Spanish lamproites is after Venturelli *et al.* (1984*a*, 1988); that for Gaussberg is after Foley (1985). Oxygen buffers: HM, haematite–magnetite; NNO, nickel–nickel oxide; QFM, quartz–fayalite–magnetite; MW, magnetite–wüstite; WI, wüstite–iron; QFI, quartz–fayalite–iron; according to Andersen & Lindsley (1988).

Differences in fertility of the sources

Olivines and their Mg-chromite inclusions may be used as proxies for the mantle-source characteristics of the

Serbian ultrapotassic rocks. The idiomorphic tabular shape and homogeneous chemical composition of olivines from primitive LAG rocks indicate that they represent equilibrium phenocrysts (Fig. 3b; Electronic Appendix 3e and f). They have Fo contents up to 93 (Fig. 4a), and host chromite inclusions with Cr-number around 90. Such highly magnesian olivines are known from komatiites (Arndt *et al.*, 1977) and mantle xenoliths (Gaul *et al.*, 2000), but are known to host such high Cr-spinels only in boninites (Arai, 1994; Falloon & Danyushevsky, 2000; Barnes & Roeder, 2001; Kamenetsky *et al.*, 2002) and lamproites (Kuehner *et al.*, 1981; Jaques *et al.*, 1984; Venturelli *et al.*, 1984*a*, 1984*b*; Thy *et al.*, 1987; Mitchell & Bergman, 1991). Their presence is in apparent conflict with the relatively high SiO_2 content and LILE-enriched character of the host magma from which they crystallized, but only if taken to indicate large degrees of melting of a lherzolitic mantle source, which would result in high MgO in the melt and depletion of the LILE. Such extensive melting would require temperatures above 1500°C, which should be further indicated by whole-rock Ni contents >500 ppm, and Cr_2O_3 in olivine >0·2% (Arndt *et al.*, 1977; Campbell *et al.*, 1979; Murck & Campbell, 1986; Campbell, 2001). The primitive LAG rocks have lower whole-rock Ni contents (highest value 480 ppm, average 390 ppm), and Cr_2O_3 contents in olivine lower than 0·15% (maximum 0·14%, average 0·12%), which may reflect considerably lower temperature melting. This clearly suggests that a normal peridotite mantle source and/or high-temperature melting are not appropriate for the primitive LAG olivines and Cr-spinels, whereas they do indicate that refractory, depleted peridotite forms one component of the mantle source, as for boninites (Cameron *et al.*, 1983; Arai, 1994; Barnes & Roeder, 2001; Kamenetsky *et al.*, 2002). Similarities in high MgO and SiO_2 and low CaO, Al_2O_3 and Na_2O have been interpreted previously as evidence for a strongly depleted mantle source for boninites and silica-rich lamproites of Mediterranean type (Foley & Venturelli, 1989). Furthermore, low-Al spinels together with low Al_2O_3 contents in the bulk rocks are typical for both lamproites and boninites; their spinel compositions overlap with those of spinel inclusions in diamonds, and are the most Cr-enriched compositions found in nature. The olivine–spinel pairs from primitive LAG rocks plot in the most refractory part of the olivine–spinel mantle array diagram (Arai, 1994; Fig. 5b) together with mineral pairs from boninites and arc-related high-Mg, high-Si magmas. This accords with the recent study of ultramafic xenoliths hosted by East Serbian Palaeogene basanites (Cvetković *et al.*, 2004*b*), which shows that the lithospheric mantle beneath Serbia is more refractory than normal European lithosphere.

We may further extend the parallels between lamproites and boninites considering the similarities in models for their origin. In addition to depleted peridotitic mantle, a second, fluid or melt component must be involved in the origin of both rock types, which has considerably higher levels of incompatible elements in the case of lamproites. The additional hydrous component causes reduction of the solidus temperature. According to current interpretations, lamproites are the melting products of refractory mantle intersected by phlogopite- and clinopyroxene-bearing veins, the so-called vein + wall-rock melting model (Foley, 1992*a*; Mitchell, 1995). This model was prompted by the failure of experimental studies to locate multiphase saturation in peridotite minerals on the liquidi of ultrapotassic rocks, which should be found for purely peridotitic sources. According to the vein + wall-rock model, vein assemblages consisting principally of non-peridotitic, but ultramafic mineralogy, melt at lower temperatures than the surrounding peridotite, and the alkaline melt produced infiltrates and dissolves the peridotite. Accordingly, the second, 'fluxing' component may correspond to the content of the vein, with the presence of hydrous minerals.

The KAG olivine–spinel pairs are less refractory, more scattered, and mostly plot away from the mantle array (Fig. 5b), consistent with derivation from a less refractory mantle source. The large differences in the Cr-number of spinels from the KAG and LAG result from differences in both Cr and Al contents, whereas the Ti contents of the spinels from both groups are similar. These differences indicate that the KAG source is less refractory.

The source characteristics of Serbian ultrapotassic rocks and partial melting processes

To minimize the blurring effects of low-pressure processes on geochemical trends inherited from the mantle source, we restrict our attention to samples screened to have high Cr (>400 ppm) and Ni (>200 ppm) contents and the absence of felsic or crustally derived xenoliths and xenocrysts. In the case of the LAG rocks, this chemical screen is almost equivalent to our subclassification into primitive and evolved rocks; all primitive LAG rocks are included with the single exception of rocks from Klinovac. Although the Klinovac samples do not pass our chemical filter, we have included them in the discussion of mantle source characteristics because they are the most primitive samples from the southern part of the ultrapotassic province. For the KAG rocks, most of the ugandites and leucite basanites pass the chemical filter, whereas the ankaratrites are more evolved and were omitted.

The trace element characteristics and isotopic compositions of the screened samples are in agreement with the interpretations, based on mineral chemistry, that the two Serbian ultrapotassic suites (KAG and LAG) were

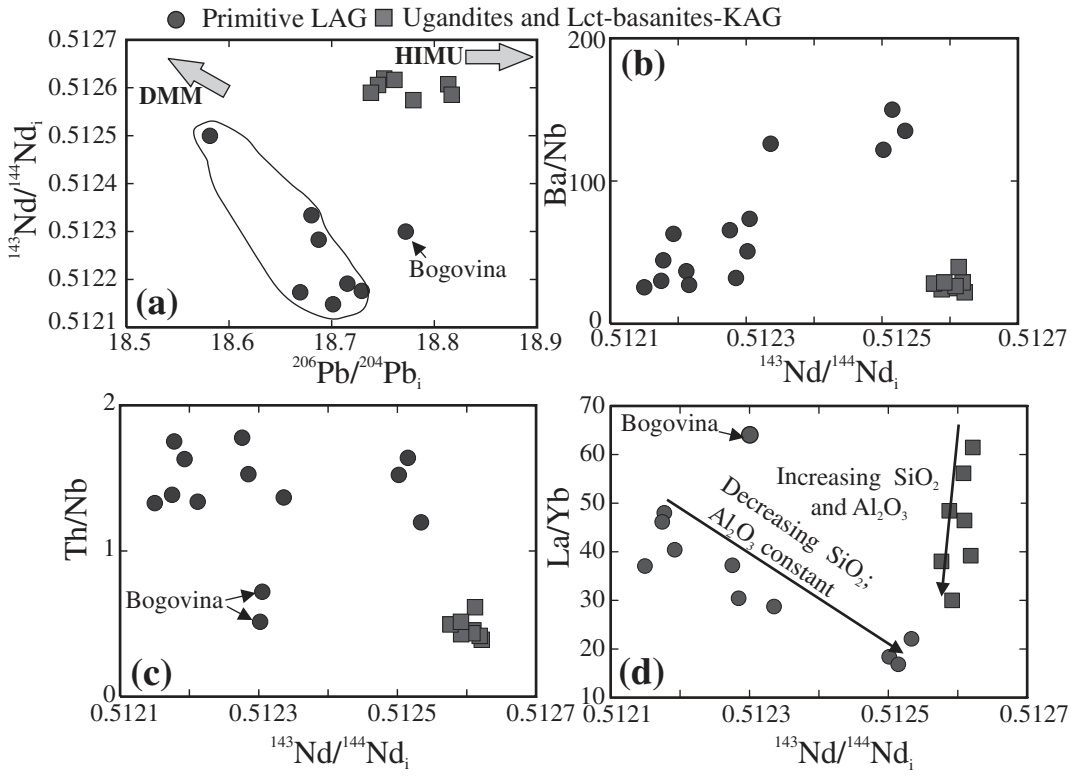

Fig. 14. (a–d) Variation of $^{206}Pb/^{204}Pb_i$ vs $^{143}Nd/^{144}Nd_i$, $^{143}Nd/^{144}Nd_i$ vs Ba/Nb, Th/Nb and La/Yb, of screened samples of Serbian ultrapotassic rocks. Samples are screened according to Cr and Ni contents (>400 and >200, respectively) and the absence of granitic or crustally derived xenoliths and xenocrysts.

derived from distinct mantle sources. No combination of fractionation of observed phenocryst phases, coupled with assimilation effects, can relate the observed groups geochemically. This is illustrated by the Nd–Sr isotope compositions of the screened samples: LAG rocks span a wide range of Nd–Sr isotopic ratios, whereas the KAG rocks have very restricted compositions. The $^{206}Pb/^{204}Pb$ vs $^{143}Nd/^{144}Nd$ diagram (Fig. 14a) clearly highlights the two different groups: the LAG rocks with less radiogenic Nd isotope compositions define a trend towards a mid-ocean ridge basalt-like (DMM) composition (with the exception of one Bogovina sample), whereas the KAG rocks display very little change in Nd–Pb isotopic values. The variations in Ba/Nb, Th/Nb and La/Yb vs $^{143}Nd/^{144}Nd$ (Fig. 14b–d) all efficiently discriminate between the two Serbian ultrapotassic groups.

The crustal signature in the mantle source

The geochemistry and isotope characteristics of Tertiary Mediterranean ultrapotassic igneous rocks are frequently explained as being due to a crustal signature acquired by the mantle source through subduction of continental materials (Nelson *et al.*, 1986; Ellam *et al.*, 1989; Peccerillo, 1992). Likewise, numerous geochemical features of the Serbian ultrapotassic rocks might be interpreted to indicate a role for subduction-related processes in their petrogenesis. Arguments include relatively low Ti and Nb concentrations, high Cs concentrations, high Cs/Rb and Pb/Ce, and the presence of a trough at Eu.

Pb isotopes are one of the most sensitive indices of contamination of the mantle by sediments (Ben Othman *et al.*, 1989), because of the huge contrast of Pb abundance between sediments and the mantle. An extremely small addition of sediment will significantly affect the mantle Pb isotope ratios and the source will assume the isotopic characteristics of the sediments. The Serbian ultrapotassic rocks show a relatively limited range of $^{206}Pb/^{204}Pb$ with radiogenic and slightly variable $^{207}Pb/^{204}Pb$. These characteristics may be readily explained by mixing of sources, but not by closed-system decay of U. A radiogenic $^{207}Pb/^{204}Pb$ signature requires the existence of a long-term variation in U/Pb, which would give rise to a large variation in $^{206}Pb/^{204}Pb$ (Nelson *et al.*, 1986). A single-stage extraction process with the metasomatic imprint originating from a depleted mantle source cannot explain the radiogenic $^{207}Pb/^{204}Pb$ together with relatively unradiogenic $^{206}Pb/^{204}Pb$. The major argument against such a scenario is that the ancient isotopic signature demonstrated by the high $^{207}Pb/^{204}Pb$ values

demands proportionally higher values of $^{206}Pb/^{204}Pb$. On the other hand, Nelson *et al.* (1986) suggested that the metasomatic component that enriched the mantle source of the Spanish lamproites already had high $^{207}Pb/^{204}Pb$, radiogenic Sr and unradiogenic Nd.

The strong similarity between the Pb isotope signature of Mesozoic flysch sediments and the screened Serbian ultrapotassic rocks is a strong argument for the influence of subducted sedimentary material. This crustal isotopic signature would have been introduced via Mesozoic subduction and stored in the form of metasomatic minerals in the mantle source. The different Sr and Nd isotope compositions of the two groups are interpreted below as depending upon the type of crustal material involved, and on the nature of the melting process. The involvement of Mesozoic flysch sediments explains mantle domains with high Rb/Sr, U/Pb and Th/Pb that have not yet evolved Sr and Pb isotopic ratios that differ considerably from those of the sediments.

The mantle source of the LAG rocks

The chemically screened LAG rocks show considerable isotopic variations that correlate with incompatible trace elements and their ratios (Fig. 14b–d). Given the high Sr, Nd and Pb concentrations, we may consider these isotopic compositions as representative of near primary mantle-derived melts. This variable isotopic composition of the primary melts indicates mixing between distinct mantle components in their source. Moreover, the coupling of isotopic and trace element ratios and abundances exhibited by the primitive LAG rocks is characteristic of mixing in the mantle (Nelson *et al.*, 1986). The mineralogy and geochemistry of primitive LAG rocks indicates the involvement of at least two mantle end-members: the first is a highly refractory harzburgitic mantle source indicated by the extreme compositions of olivines and Cr-spinels. It is in accordance with the recent study of ultramafic xenoliths hosted by East Serbian Palaeogene basanites (Cvetković *et al.*, 2004*b*), which indicates highly refractory lithospheric mantle underneath Serbia. Isotopically this component should have a signature similar to the depleted MORB mantle (DMM) of Zindler & Hart (1986). The second component should be responsible for the extreme enrichment in K_2O and LILE and other incompatible elements such as TiO_2 and HFSE, and is probably hydrous. It incorporates the crustal isotopic signature, probably stored in minerals such as phlogopite, amphibole, apatite and clinopyroxene (see below). Samples with radiogenic Sr and Pb and unradiogenic Nd isotope signatures resemble Serbian flysch sediments; this component we refer to as 'Serbian enriched mantle' (SEM; Fig. 15a and b). Samples with low $^{87}Sr/^{86}Sr$ and high $^{143}Nd/^{144}Nd$ ratios generally have the lowest $^{206}Pb/^{204}Pb$ (Fig. 15a and b, inset) suggesting involvement of a DMM component (Zindler & Hart, 1986) in their petrogenesis. Although the LAG trend suggests some affinity with the KAG mantle source in the Sr–Nd isotope covariation diagram (Fig. 10), similar trends do not occur on diagrams of $^{143}Nd/^{144}Nd$ or $^{87}Sr/^{86}Sr$ vs $^{206}Pb/^{204}Pb$ (Figs 14a, 15a and b). This further indicates that the two Serbian ultrapotassic suites do not have a common mantle end-member (Fig. 14).

Figure 15a and b illustrates a range of mixing curves in $^{87}Sr/^{86}Sr_i$ and $^{143}Nd/^{144}Nd_i$ vs $^{206}Pb/^{204}Pb_i$ plots for the Serbian ultrapotassic rocks between the two mantle end-members (DMM and SEM). The end-members used in the modelling in Fig. 15 are given in the figure caption. Hyperbolae of different curvature are the result of different Sr/Pb and Nd/Pb elemental ratios between DMM and SEM. The mixing trends for isotopic ratios will be nearly linear if the contributing components have similar elemental ratios ($SEM_{Sr/Pb}$:$DMM_{Sr/Pb}$ and $SEM_{Nd/Pb}$:$DMM_{Nd/Pb} \approx 1{:}1$). This is possible if, for instance, the enriched mantle component geochemically resembles the metasomatized lithospheric upper mantle of McDonough (1990), with similarly high Sr/Pb and Nd/Pb ratios to DMM. The strongly hyperbolic mixing trend defined by the primitive-LAG rocks, however, indicates contrasting geochemical parameters, with the ratios $SEM_{Sr/Pb}$:$DMM_{Sr/Pb}$ and $SEM_{Nd/Pb}$:$DMM_{Nd/Pb}$ close to 1:10 and 1:8, respectively. A quantitative evaluation of the contribution of the end-members in the final hybrid depends on the absolute element abundances; that is, whether they are represented by mixing of melts or solids. When we modelled mixing between solid end-members, the samples from Arandjelovac with least radiogenic Sr and Pb, and the most radiogenic Nd isotopic compositions required a source mixing with >95% of DMM in the final melt (not shown), which is geochemicaly unreasonable. Our preferred interpretation of the mixing curves is that they represent mixing of melts, when the proportions of DMM-derived melt (MORB-like) in the final hybrid would be <85% (Fig. 15), because of the higher concentrations of elements involved relative to solid end-members. The behaviour of some of the incompatible elements and their ratios also consistently illustrates the same mixing proportions, with the most enriched end-member showing the highest La/Yb ratios and Nb abundances (Fig. 15c and d). Moreover, the mineral chemistry of the primitive LAG rocks also varies in keeping with the proposed model: the most refractory composition of Cr-spinels [Cr-number = atomic Cr/(Cr + Al) up to 0·95] and lowest TiO_2 content in Cpx occurs in the samples showing the highest degree of hybridization (Arandjelovac).

This type of mixing of melts in the mantle environment is consistent with the vein + wall-rock melting model of Mitchell & Bergman (1991) and Foley (1992*a*), and is in agreement with experimental data, which suggest a

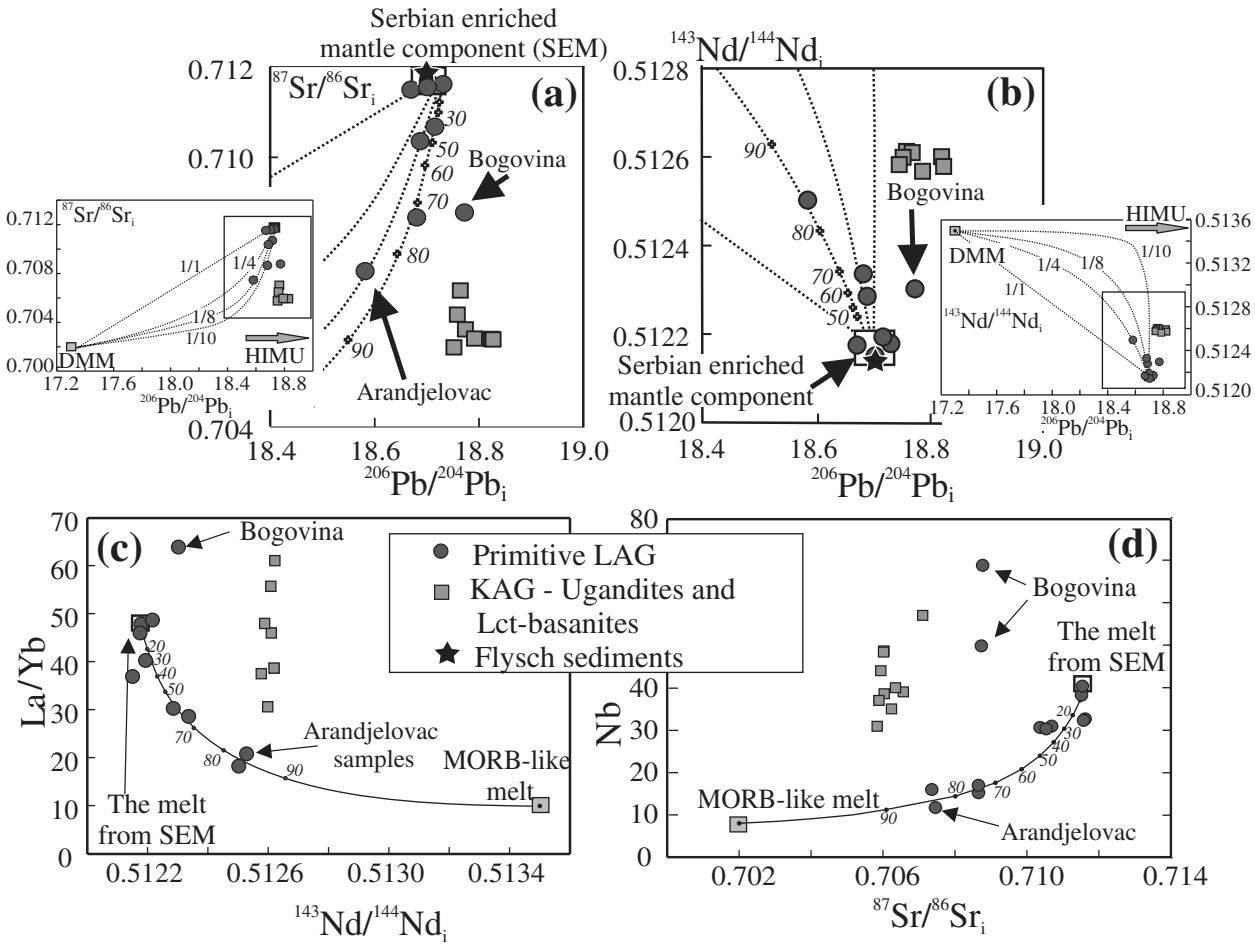

Fig. 15. (a) $^{206}Pb/^{204}Pb_i$ vs $^{87}Sr/^{86}Sr_i$, (b) $^{206}Pb/^{204}Pb_i$ vs $^{143}Nd/^{144}Nd_i$, (c) $^{143}Nd/^{144}Nd_i$ vs La/Yb and (d) $^{87}Sr/^{86}Sr_i$ vs Nb (ppm) for screened samples of Serbian ultrapotassic rocks showing end-member mixing models to explain the isotopic variation of the Serbian ultrapotassic rocks. The numbers on the mixing curves denote different $SEM_{Sr/Pb}$:$DMM_{Sr/Pb}$ and $SEM_{Nd/Pb}$:$DMM_{Nd/Pb}$ ratios. End-members used for modelling: MORB-like melt (Chauvel *et al.*, 1992; Hart *et al.*, 1992): $^{206}Pb/^{204}Pb = 18$, $^{87}Sr/^{86}Sr = 0{\cdot}702$, $^{143}Nd/^{144}Nd = 0{\cdot}51215$, 90 ppm Sr, 7 ppm Nd, 0·3 ppm Pb, 3·25 ppm La, 3·25 ppm Yb; Serbian enriched mantle end-member (SEM) has the isotopic composition of Serbian flysch sediments and trace element content of Ol–Phl–Sa-lamproite sample RoO/1-II: $^{206}Pb/^{204}Pb = 18{\cdot}7$, $^{87}Sr/^{86}Sr = 0{\cdot}71152$, $^{143}Nd/^{144}Nd = 0{\cdot}51219$, 598 ppm Sr, 114·89 ppm Nd, 31 ppm Pb, 80·6 ppm La, 1·75 ppm Yb.

low-pressure origin for Si-rich lamproites (Foley, 1993). Vein material may not be in isotopic equilibrium with the surrounding peridotite. The complex mechanism of melt–solid interaction during the melting process is largely unconstrained and only few theoretical and experimental studies have been carried out (Meen *et al.*, 1989; Foley, 1992*a*; Foley *et al.*, 1999). The alkaline melts produced during the vein melting (in this case derived from the SEM) infiltrate, dissolve and trigger the melting of the depleted peridotite wall-rock. The isotopic effects of melting of exotic veins should be dramatic: the extremely radiogenic Sr and unradiogenic Nd that is characteristic of the lamproites is derived from the vein assemblage. Dissolution of the wall-rock preferentially adds a more refractory component to the melt, resulting in a spectrum of isotopic compositions. The isotopic composition of the melt will be strongly controlled by that of the vein, and only when a large amount of the wall-rock material is involved will it be displaced towards the depleted mantle composition (Meen *et al.*, 1989). This is particularly apparent in the case of the primitive Serbian LAG rocks, which show a wide range of Sr and Nd isotopic compositions (Fig. 15) but very restricted variation in Pb isotopes. The Pb isotopic composition is dominated by the vein-derived end-member, which has a considerably higher Pb concentration than the wall-rocks. The mixing values obtained for primitive LAG rocks indicate that a considerable contribution of melt derived from the wall-rock (~85%) was involved in the petrogenesis of the Arandjelovac samples, which is confirmed by the low HFSE abundances, approaching those of MORB-like melts. This apparently disagrees with typical explanations of

the petrogenesis of potassic lavas as being generated by small degrees of melting of metasomatized mantle sources.

The Bogovina lamproite, the only LAG locality outside the Vardar ophiolitic suture zone, is an exception. In many of the variation diagrams (Fig. 15a–d), the Bogovina samples plot away from the main trends. Although the Bogovina samples show similar patterns in mantle-normalized trace element variation diagrams to those of other primitive LAG rocks (Fig. 8b and c), they show less pronounced Ti and Nb troughs and no Eu trough. Bogovina also shows the crustal Pb signature, but it is deflected slightly towards HIMU (Figs 11b, d and 15a–d). We can speculate that the mantle source of the Bogovina samples experienced multiple metasomatic episodes: first, the major subduction-related metasomatic event of Mesozoic age experienced by other Serbian localities, and a second, later event, explained by percolation of melts related to the Palaeocene–Eocene alkaline basaltic magmatic episode. This younger event would cause the deflection of the isotopic signature towards HIMU and enrichment in TiO_2, Nb and Eu. Multiple mantle metasomatic episodes in the East Serbian lithospheric mantle have been reported recently from mantle xenoliths near Bogovina (Cvetković *et al.*, 2004*b*). It is concluded that the mantle beneath this part of the Balkans records multiple metasomatic imprint via introduction of subduction-related and alkaline mafic melts. However, the existence of only one occurrence of ultrapotassic volcanism in the East Serbian composite terrane is not sufficient to fully evaluate the cause of chemical differences between this and the other volcanics.

The mantle source of the KAG rocks

Ugandites have the lowest SiO_2 and Al_2O_3 contents and contain leucite; nepheline is less abundant than leucite but has an exceptionally high kalsilite component (up to 40 vol. % kalsilite component). The leucite basanites with higher SiO_2 and Al_2O_3 contents contain plagioclase and K-poor nepheline (<15 vol. % kalsilite component) that is almost equal in abundance to leucite. This modal variation reflects the original potassium abundance, which is, however, strongly altered by the analcimization of the most KAG rocks. The compositional and mineralogical variations of the KAG rocks may be attributed to different degrees of partial melting of a relatively uniformly enriched mantle source. The variable HFSE enrichment and LREE/HREE fractionation combined with the limited isotopic variability of the screened KAG rocks (Fig. 14) implies a source that is homogeneous relative to the scale of melting. A relatively uniform enrichment of the KAG mantle source suggests that the metasomatizing agent probably equilibrated with the host peridotite. The lowest degree of melting may explain the ugandites, with higher degrees for leucite basanites. The differences in clinopyroxene chemistry (slope of Al vs Ti) in ugandites and leucite basanites (Fig. 6d) cannot be due to fractionation from common magmas because these clinopyroxenes have similar Mg-number and therefore represent the same degree of differentiation. These differences in Cpx chemistry are better explained by their rocks representing different degrees of melting.

Several geochemical parameters (Ti–Nb, Eu troughs and Pb spikes on normalized trace element variation diagrams) indicate that the KAG source also experienced crustally derived metasomatic imprint. Most notably, Pb isotope systematics indicate a crustal Pb signature, similar to the signature demonstrated by the LAG rocks. However, the KAG samples are characterized by less radiogenic Sr and more radiogenic Nd isotope ratios, which may be explained in two ways. First, the Sr and Nd systematics may indicate metasomatism by a metasomatic agent hosting a different crustal component from that affecting the LAG mantle source. If the metasomatic agent that enriched the KAG mantle source had high Sr and Nd concentrations (which is to be expected), the final isotopic signal should be dominated by the isotopic values of the metasomatic fluid or melt, because of the low abundance of these elements in the mantle. In that case, the KAG rocks should have inherited an isotopic signature of the subducted crustal component. Comparison with the isotope compositions of sediments usually considered to be involved in subduction processes suggests that the most reasonable candidates are oceanic biogenic sediments, including calcareous and siliceous sediments with a significant clay fraction (Ben Othman *et al.*, 1989). Alternatively, the composition of the metasomatic agent that metasomatized the KAG mantle may isotopically resemble that which enriched the LAG source. However, this scenario would require that the KAG source was already metasomatized during an earlier episode that gave rise to an isotopic signature between DM and HIMU-like mantle reservoirs. The ultimate Sr–Nd isotopic signature results from binary mixing, whereas much intense overprinting of the previous isotopic signature would be shown by the Pb isotopes because of the high Pb concentration in the metasomatic agent bearing the crustal component. There are no closer constraints on the isotopic composition of the mantle below the Dinaride part of the Balkans, and we can only speculate about the presence of such a mantle component.

Constraints on the mineralogy of the mantle sources

Mineralogy of the source of the KAG rocks

Given the ultrapotassic character of the KAG rocks, phlogopite and K-richterite are reasonable candidates for K-bearing hydrous phases in the mantle source. Ugandites are interpreted as being produced by the smallest percent of partial melting and have higher

K_2O/Na_2O ratios, more abundant modal leucite and higher kalsilite component in nepheline (up to 40 vol. %) than leucite basanites, implying a greater contribution from a high-K phase in the initial melts. This may be used to discriminate between the two potential mantle K-phases.

Experiments in natural lherzolitic systems (Konzett & Ulmer, 1999) demonstrate that K-richterite is stable between 5·5 and 6·0 GPa at 800°C and between 6·0 and 6·5 GPa at 1100°C but not at lower pressures, restricting it to the coldest regions of subcontinental lithosphere (heat flow $<40\,mW/m^2$). Melts of K-richterite-bearing peridotite are expected to be silica rich because K-richterite, itself a relatively Si-rich mineral, is eliminated soon after the solidus is crossed (Foley *et al.*, 1999; Konzett & Ulmer, 1999). The generally low SiO_2 contents and negative correlation between SiO_2 and K_2O/Na_2O of the KAG rocks suggest that phlogopite, instead of K-richterite, is the K-bearing phase in the mantle source.

We have used the inverse method proposed for estimation of major melting parameters by Treuil & Joron (1975), and improved by Cebria & Lopez Ruiz (1996) and Class & Goldstein (1997), to constrain the mineralogy of the KAG source. This method can be used for the least differentiated samples from a cogenetic suite of rocks, which may be safely considered as representing primitive liquids (i.e. Mg-number $\geq$70; high Ni and Cr) derived from a homogeneous mantle source. Use of the method requires that the melting of a relatively homogeneous mantle source should be the dominant process, and not mixing between various batches of mafic mantle melts derived from chemically different sources. Screened KAG samples (ugandites and leucite basanites) entirely meet these criteria, because they demonstrate consistency in the behaviour of trace elements, which, together with rather uniform Nd–Sr–Pb isotope compositions, reflects homogeneity of the mantle source during the melting process.

During the course of melting, partitioning of a trace element between a melt and the solid residue depends on the mineral phases present. Hence, the bulk solid–melt partition coefficient for various elements is a function of the uptake of the elements in the residual mineralogy. In an element–element diagram (e.g. Nd vs Zr or Nd vs Nb; Fig. 16a and b), the intercept of a linear regression between two elements of the same incompatibility should be zero, and its slope unity, whereas a difference in incompatibility should result in an increase of the intercept on the axis of the more compatible element, and a change of the slope. In an element–element ratio diagram (e.g. Nd vs Nd/Zr, Nd/Nb or Nd/P; Fig. 16c), the intercept of a linear regression between two elements of the same incompatibility should be unity, and its slope zero, whereas a difference in incompatibility should result in a decrease of the intercept and an increase of the slope. The most incompatible element with respect to the residual mineralogy (and not to a normal peridotitic mantle) has a positive intercept in all element–element diagrams (Fig 16a and b) and positive slope in all element–element ratio diagrams (Fig. 16c). The relative degree of incompatibility of other elements may be estimated by comparing their intercepts in element–element diagrams and their slopes in element ratio diagrams plotted against the most incompatible element (Fig. 16d) as has been proposed by Cebria & Lopez Ruiz (1996).

An investigation of plots involving La, Nd, Ce, Pr, Eu, Dy, Yb, Lu, Sc, Nb, Zr, Ti, P, Sr, Th and Ba shows that Nd, Sm and Eu have the most incompatible behaviour relative to the mantle source of the KAG rocks (Fig. 16d). Estimating the relative degree of incompatibility of other elements, comparing their intercepts in element–element diagrams and their slopes in element ratio diagrams plotted against the most incompatible element (in this case Nd) (Fig. 16d) shows that Nd, Sm, Eu and Zr demonstrate similar behaviour, and that incompatibility decreases in the order of Pr, Dy, Th, Ce, Sr, La, Ti, Nb, Sc, Yb, Lu, P and Ba (Fig. 16d). This unusual order of incompatibility results from an atypical residual mineralogy (see also below). The concentration of Nd is highest in the ugandites, confirming that they are produced by the lowest degree of partial melting. Furthermore, we use Nd as an index for the degree of partial melting. Hence, its highest (C^{Nd}_{max}) and lowest (C^{Nd}_{min}) concentrations have been produced by the lowest (F_{low}) and highest (F_{high}) melting degrees, respectively. As has been shown by Maaløe (1994), Cebria & Lopez Ruiz (1996) and Maaløe & Pedersen (2003) for highly incompatible elements, we can approximate the relation $C^{Nd}_{max}/C^{Nd}_{min} = F_{high}/F_{low}$, which enables us to estimate the relative range of the degree of melting for the KAG rocks ($F_{high}/F_{low} = 2{\cdot}21$).

Four major generalizations can be made from this modelling (Fig. 16d): (1) Ba is highly compatible, suggesting the presence of residual phlogopite in the mantle source; (2) the similar compatibility of Nb and Ti and their decoupling from Zr indicates the buffering effect of a Ti-oxide in the source; (3) the high compatibility of P suggests a role for residual apatite; (4) the high compatibility of Yb, Lu and Sc indicates the presence of residual garnet.

To put more quantitative constraints on the presence of residual phases, we further evaluated the mineralogy of the KAG source using the extent of element incompatibility quantified by their enrichment ratios (E). For a particular element j, E is estimated by its relation with the index element, in our case Nd (Fig. 16a and b), according to $E = C^j_{max}/C^j_{min}$. Hence, E depends on concentrations of the element j for the lowest and highest melting degrees, reflecting the bulk partition coefficient during melting. The most incompatible elements have the highest E

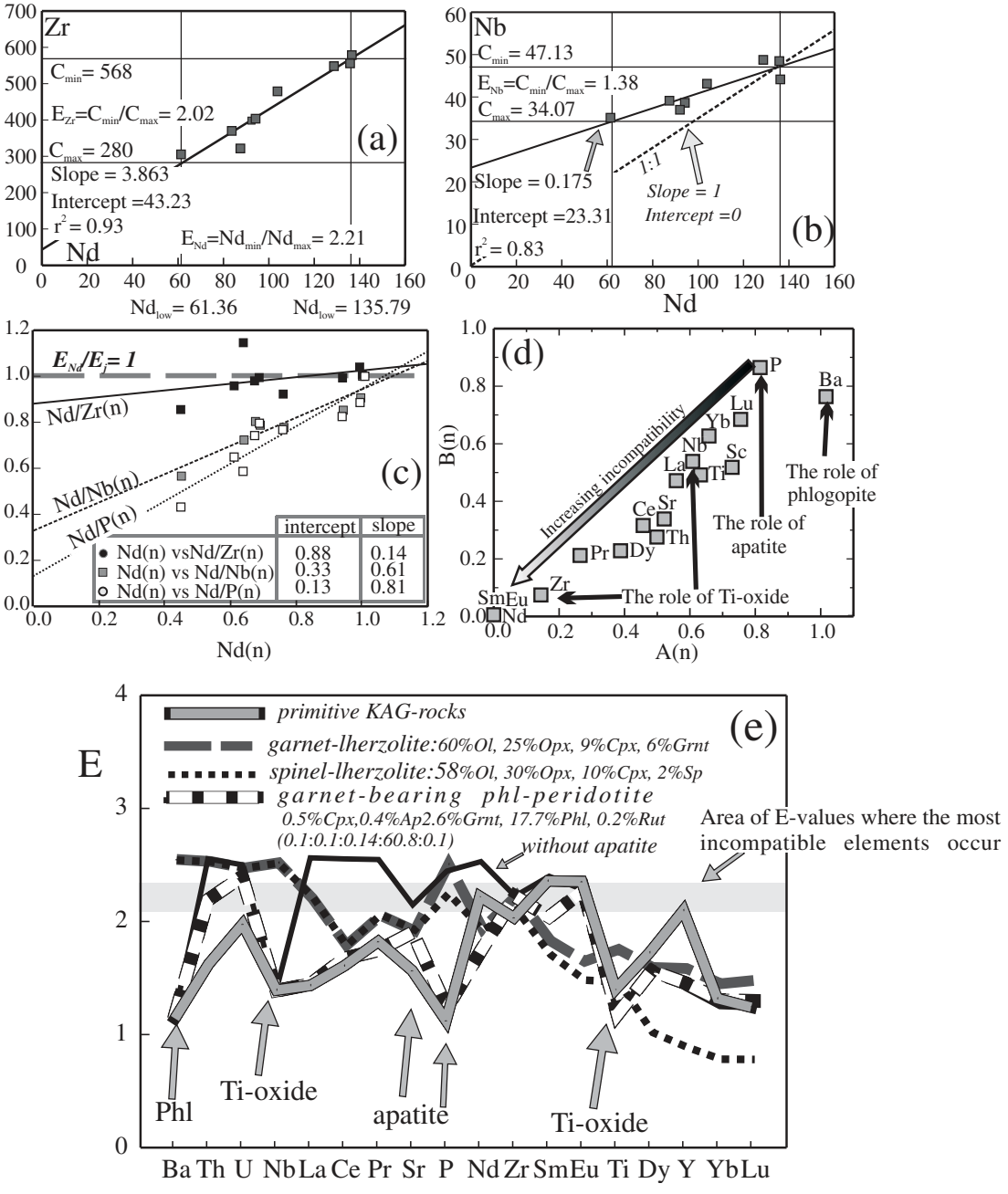

Fig. 16. (a–c) Evaluation of the distribution of Zr, Nb, P and Nd in ugandites and Lct-basanites (KAG), to illustrate the inverse method used to constrain the mineralogy of the KAG source (Treuil & Joron, 1975; Cebria & Lopez Ruiz, 1996; Class & Goldstein, 1997); Nd_n, Zr_n, Nb_n and P_n denote the concentrations, which are normalized relative to the highest concentration of each element. Nd was used as an index for the degree of partial melting as it shows the most incompatible behaviour among La, Nd, Ce, Pr, Sm, Eu, Dy, Yb, Lu, Sc, Nb, Zr, Ti, P, Sr, Th and Ba; C^j_{min} and C^j_{max} denote concentration of element j at low and high degrees of partial melting (lowest and highest Nd concentrations, respectively). The extent of element incompatibility is quantified through its enrichment ratio (E), which is estimated as its relation with the index element, in our case Nd, according to the equation $E = C^j_{min}/C^j_{max}$ (a and b). The estimation of E values for all elements that were using in the evaluation is given in Electronic Appendix 6. (d) Relative degree of incompatibility of trace elements relative to the KAG mantle source mineralogy; the diagram plots the intercepts on element–element diagrams, A(n), and their slopes on ratio–element diagrams plotted against Nd, B(n); A(n) and B(n) are calculated from concentrations normalized relative to the highest concentration of each element. (e) Magma source mineralogy of the KAG rocks. The enrichment ratio (E) pattern for the KAG rocks uses estimated E values from Electronic Appendix 6. Partition coefficients used are presented in Electronic Appendix 7. We also recalculated E values for garnet lherzolite and spinel lherzolite sources with the composition shown in the diagram. The best-fit enrichment ratio pattern for the KAG rocks using a non-modal melting model is a garnet-bearing phlogopite peridotite with 0·5% Cpx, 0·4% Ap, 2·6% Grnt, 17·7% Phl and 0·2% Rut (0·1:0·1:0·14:60·8:0·1). The continuous black line denotes the same modal composition recalculated without apatite.

values. It is important to note that E values are independent of the chemical composition of the source and rely only on the residual mineralogy and degree of melting. A plot of estimated E values for the KAG rocks gives a highly uneven pattern using the common elemental sequence (Fig. 16e).

The enrichment ratio pattern of the KAG rocks confirms the major constraints on the mineralogy of the source made above, with negative anomalies for Ba, P, Ti and HREE reflecting the presence of residual phlogopite, apatite, Ti-oxide and garnet. Further, we modelled a best-fit enrichment ratio pattern for melting of this hypothetical source. The best-fit curve for non-modal batch melting (Shaw, 1970) for different mineral proportions was calculated for garnet-bearing phlogopite peridotite with 0·5% Cpx, 0·4% Ap, 2·6% Grnt, 17·7% Phl and 0·2% Rut, and contributions to the melt are calculated as 0·1 Cpx, 0·1 Ap, 0·14 Grnt, 60·8 Phl and 0·1 Rut (Fig. 16e; see caption for details of modelling and partition coefficients used). The relative amounts of olivine and orthopyroxene are not constrained because of their low partition coefficients. This modelling corresponds to an increase from 4·5 to 11% partial melting from ugandite to leucite basanites.

In this model, about 2% garnet is needed to reproduce the low enrichment ratio for HREE. The presence of garnet in the source may be also recognized by Dy/Yb_N and Tb/Yb_N ratios, which are usually 2·5–1·1 and 1·8, respectively, in liquids derived from the garnet-bearing mantle with Dy/Yb_N and Tb/Yb_N close to unity. Dy/Yb_N and Tb/Yb_N ratios for the KAG rocks are $>1·4$ and $>1·9$, respectively.

The presence of apatite is crucial for a good match to the trace element pattern of the KAG rocks. It is indicated by the compatible character of phosphorus (Fig. 16d) and the presence of a negative anomaly (Fig. 16e). Residual apatite may explain the unusual compatible behaviour of La, Th, U and Sr in the KAG rocks. Our best-fit modelled source composition without apatite (Fig. 16e) clearly illustrates the necessity for apatite. Experiments on partitioning between apatite and melt (Watson & Green, 1981) suggest D values for D_{La}–D_{Sm}–D_{Dy}–D_{Lu} to be as low as 3–5–4–2 for basaltic systems. The partition coefficients we used are measured from spinel lherzolites from Yemen (Chazot *et al.*, 1996) representing hydrous lithospheric mantle peridotite. This study gives much higher partition coefficient values for LREE than HREE.

The decoupling of Nb and Zr is also well modelled, suggesting the presence of a Ti-oxide mineral in the source (Fig. 16a and b). Using available experimental partition coefficients for rutile (Foley *et al.*, 2000), its amount in the source ought to be around 0·2%. Various Ti-oxides are found in the mantle xenoliths including rutile, armalcolite and ilmenite (Harte, 1987; Nixon, 1987; Ionov *et al.*, 1999; Moine *et al.*, 2001; Kalfoun *et al.*, 2002). The hypothesis of a residual Ti-phase during partial melting of the KAG source is, however, apparently inconsistent with high saturation levels of TiO_2 in low-silica melts (Green & Pearson, 1987; Ryerson & Watson, 1987). Green & Pearson (1987) concluded that at 1000°C the saturation level of TiO_2 is ~2·0 wt % at pressures of 20–30 kbar for melts of basaltic composition. Most KAG rocks have TiO_2 concentrations below 2%. A combination of high H_2O contents and thus low temperature, high fO_2, and high alkali and CO_2 contents all may still assist in suppressing the saturation level (Meen *et al.*, 1989). Finally, if phlogopite serves as a major host of Ti and Nb, then there might not be a need for a Ti-rich phase in the source of KAG rocks. For this case we estimate $D_{Nb}^{Phl/melt}$ at around 0·5. However, this is unlikely, despite the high Nb contents reported for phlogopites from mantle xenoliths (Ionov & Hofmann, 1995), as D_{Nb} for phlogopite (Foley *et al.*, 1996; Schmidt *et al.*, 1999; Green *et al.*, 2000) is about an order of magnitude lower (around 0·07).

Mineralogy of the source of the LAG rocks

The geochemical variations, particularly Sr–Nd–Pb isotopes, shown by the LAG rocks cannot result from different degrees of partial melting of a relatively heterogeneous source, and require mixing of distinct melts in the mantle. We interpret coupling of the variable isotopic signatures with REE fractionation and HFSE enrichment of the primitive LAG rocks as being produced by vein + wall-rock melting. The LAG rocks are not suitable for the type of trace element modelling carried out for the KAG because they are produced from mixed mantle sources with large differences in mineralogy and chemical composition. This is in accordance with the guideline that if the source composition of the lavas differs by more that 3%, estimation of major melting parameters using this method yields inaccurate results (Maaløe & Pedersen, 2003).

However, following a similar line of reasoning as for the KAG rocks we can broadly ascertain the mineralogy of the source using trace element behaviour, but without putting quantitative constraints on the melting degree and source mineralogy. Zr has the most incompatible behaviour in the LAG rocks; it shows the widest compositional range and is most enriched in the samples with the highest K_2O abundances that isotopically resemble flysch sediments. Therefore, it may serve as an index for vein + wall-rock melting. Figure 17 illustrates slight differences between the Vardar ophiolitic suture zone samples and the samples from Bogovina, situated in the East Serbian composite terrane. A small compositional gap between these groups also exists in Zr concentration.

Most element–element ratio diagrams (Fig. 17) show linear correlations; only Nb and La show broadly flat patterns. A question arises about the significance of the

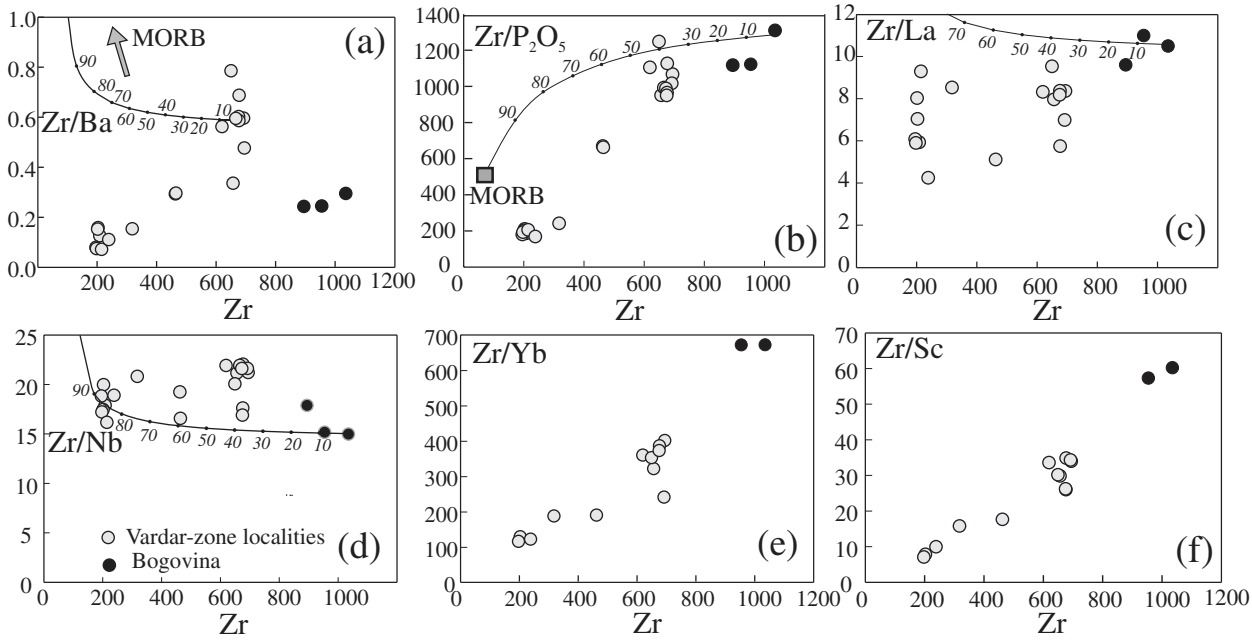

Fig. 17. Zr vs Zr/Ba (a), Zr/P_2O_5 (b), Zr/La (c), Zr/Nb (d), Zr/Yb (e) and Zr/Sc (f) variation diagrams for LAG rocks (screened samples). To illustrate potential mixing relations, we use the compositions of the MORB-like melt of Chauvel *et al.* (1992) and Hart *et al.* (1992) and the most enriched primitive LAG samples. Binary mixing curves of melts derived from distinct sources are displayed. Ticks denote percentage of mixing between end-members.

correlation: whether the residual mineralogy, considered responsible for linear variations in element–element ratio diagrams for the KAG rocks, may also play a role for the LAG rocks. Two interpretations may be proposed for this distribution: (1) it may be consistent with binary mixing of melts derived from distinct sources (according to isotopes, we recognized two potential end-members); (2) the mixing may be accompanied by partial retention of some minerals involved in the melting process, in which case considerable deflection towards lower Zr/C_i should occur. The second case can be viable only if the thermal stability of some minerals from the vein is high enough to allow their persistence until the highest degrees of vein + wall-rock melting. It has been proposed (Foley, 1992*a*) that the presence of residual phases from the vein during vein + wall-rock melting is allowed through the prolonged stability of some non-peridotitic solid solution minerals that have high-temperature end-members, such as phlogopite, amphibole or apatite, because the melting occurs at temperatures lower than their solidus. In the case of primitive LAG rocks, the main candidates are F-rich phlogopite and F-rich apatite (see below).

The high K/Na ratio of LAG rocks indicates that phlogopite rather than K-richterite is the principal potassium mineral in the source (Foley *et al.*, 1999). Given the low estimated oxygen fugacity of the source region of LAG rocks (around FMQ −3 log units fO_2), low H_2O/F and CO_2/CH_4 ratios may be expected. Therefore, the source may contain high-F, low-Al phlogopite that will give rise to perpotassic melts (with K/Al >1) during melting (Foley, 1989). Melting of such phlogopite in a vein should not contribute greatly to the Al content, but would still account for high K and LILE, as well as volatile enrichment. Moreover, its high thermal stability allows it to remain residual.

The LAG rocks, excluding the Bogovina samples, show a linear correlation between Zr and Zr/Ba (Fig. 17a), which is clearly different from the binary mixing relationship shown. This deflection from the mixing hyperbola may be explained by phlogopite remaining residual even at the highest degree of vein melting. The buffering effect of phlogopite may also explain the depleted character of the rocks from Arandjelovac, which are still ultrapotassic. However, the rocks from Bogovina are extremely Ba enriched (around 3000 ppm), which may be an effect of a Ba-enriched accessory phase in the mantle that was completely eliminated at the onset of melting. Alternatively, we cannot exclude hydrothermal alteration as a possible reason for such Ba enrichment.

Similarly, the variation of P_2O_5 and La (Fig. 17b and c) also deviates from the hyperbolic mixing line, indicating the buffering effect of apatite for the primary LAG melts produced by the lowest extent of vein + wall-rock melting. A greater buffering effect is to be expected for F-apatite as a result of its higher thermal stability than OH-apatite, offering a reasonable explanation for the otherwise paradoxical enrichment of P_2O_5 in the most depleted samples. Relatively constant Zr/Nb ratios for

the whole LAG suite argue for the depletion of Nb not being controlled by a residual mineral in the source (Fig. 17d), implying that the Ti–Nb depletion is a feature of the metasomatic agent. Finally, the distribution of HREE and Sc (Fig. 17e and f) is consistent with the interpretation that residual garnet is present at Bogovina, whereas the LAG rocks from the Vardar ophiolitic suture zone are derived from the spinel-lherzolite facies.

Geodynamic significance and concluding remarks

The geodynamic history of the Balkans from the middle Mesozoic to the present consists of crustal shortening and convergence between the African and European plates, comprising periods of subduction, collision and extension (Karamata *et al.*, 1999; Dimitrijević, 2001). The closure of the Vardar branch of Tethys was completed by the end of the Late Cretaceous, resulting in at least two ophiolitic belts of Mesozoic age that make up the dominant features of Balkan geology: the Vardar ophiolitic zone and Dinaride–Hellenide ophiolite belt. The closure of two oceanic areas was accompanied by the subduction of oceanic and perhaps some continental crust. It is generally accepted that the Late Cretaceous–Paleocene volcanic rocks of subduction affinity of the Timok magmatic complex (Fig. 1) resulted from northeastward subduction of the Vardar oceanic plate (Karamata & Djordjević, 1980; Cioflica *et al.*, 1995, 1996). Conversely, such volcanism has not been detected on the Dinaride side. These subduction episodes may have had a major role in the enrichment of the lithospheric mantle of terranes that merged during the collision.

Given the resemblance between the Serbian ultrapotassic volcanics and the much more voluminous Italian ultrapotassic and potassic volcanism, it is interesting to consider what these two spatially adjacent and partly contemporaneous provinces have in common. In Italy, the relationship between the geophysically well-characterized subduction zone environment and a mantle plume postulated by some workers (e.g. Bell, 2002; Bell *et al.*, 2003) is unclear. The magmatism of the Balkan area postdates the latest subduction events by around 30 Myr (Karamata *et al.*, 1997*a*, 1997*b*, 1999), eliminating the possibility that the volcanism is directly related to subduction. Furthermore, there is no evidence to relate this volcanism to mantle plume activity like that which has been proposed by Bell (2002) and Bell *et al.* (2003) to be active under the Tyrrhenian Sea. The alternative explanation proposed for the Italian volcanism related to plume channelling through a subducting slab window (Gasperini *et al.*, 2002) seems also implausible for the Serbian volcanism.

In active rifting zones above a contemporaneous mantle plume, large-scale uplifting of the whole area should be expected, which is not observed in the Balkans. Beginning in the Oligocene, the northern Balkans were characterized by a blocky structure, which was clearly related to major extensional tectonic episodes in the surroundings: Dinaride collapse, Pannonian Basin collapse and Aegean collapse. Both spatially and temporally, the Serbian ultrapotassic volcanism is linked with extensional tectonics, providing a straightforward relationship between geodynamics and volcanism. Our geochemical data also provide further evidence against a plume relationship: the presence of residual phlogopite and apatite in the source strongly suggests a lithospheric origin for the parental magmas. It has been shown that phlogopite is not stable under the thermal conditions of a mantle plume (Class & Goldstein, 1997). Finally, none of the isotopic compositions of the Serbian ultrapotassic volcanics show any affinity with the mantle component HIMU, unlike those of some Italian volcanoes (Fig. 11).

There is general agreement (Marović *et al.*, 1998, 1999, 2000, 2001, 2002) that Tertiary tectonic activity in this part of the Balkan Peninsula resulted from three competing factors: (1) isostatic reaction and collapse of the Dinaride orogen; (2) NW movement of the Adriatic plate and collision with the Dinaride orogen; (3) extensional processes related to the opening of the Pannonian and Aegean basins. The interplay of these factors resulted in extensional and compressional episodes in the northern Balkan Peninsula from Oligocene to Pliocene times (Fig. 2) accompanied by voluminous intermediate to acid magmatism and associated basaltic volcanism (Cvetković *et al.*, 2004*a*). The onset of ultrapotassic volcanism at around 30 Ma (Fig. 2) is coincident with the activation of new fractures oriented WNW–ESE and west–east (e.g. the Zvornik and Sava lines), instead of former old NNW–SSE to north–south faults or terrane boundaries. This resulted in simultaneous magmatic activity at Bogovina, Rudnik, Ozrem, Boljkovac, Mionica and Veliki Majdan, transecting the main axis of the Balkan Peninsula including the Vardar ophiolitic suture zone, the Jadar Block and the East Serbian composite terrane. This is a very pronounced feature of Serbian ultrapotassic volcanism, emphasizing the connection between the timing of magmatism and changes in the regional stress field. These magmas indicate a post-collisional, relaxational stress regime, which is an optimal geodynamic setting for generating ultrapotassic melts (Mitchell & Bergman, 1991; Vaughan, 1996; Vaughan & Scarrow, 2003). In spite of later displacements of the tectonic units in Miocene times (Balla, 1986), the linearity of the oldest ultrapotassic volcanics does not seem to be accidental. Ultrapotassic volcanism could be regarded as the starting point of an isostatic reaction and the collapse of the Dinarides that provided the necessary conditions for Late Paleogene–Early Neogene magmatism. The distribution of ultrapotassic volcanism resembles the extent of the

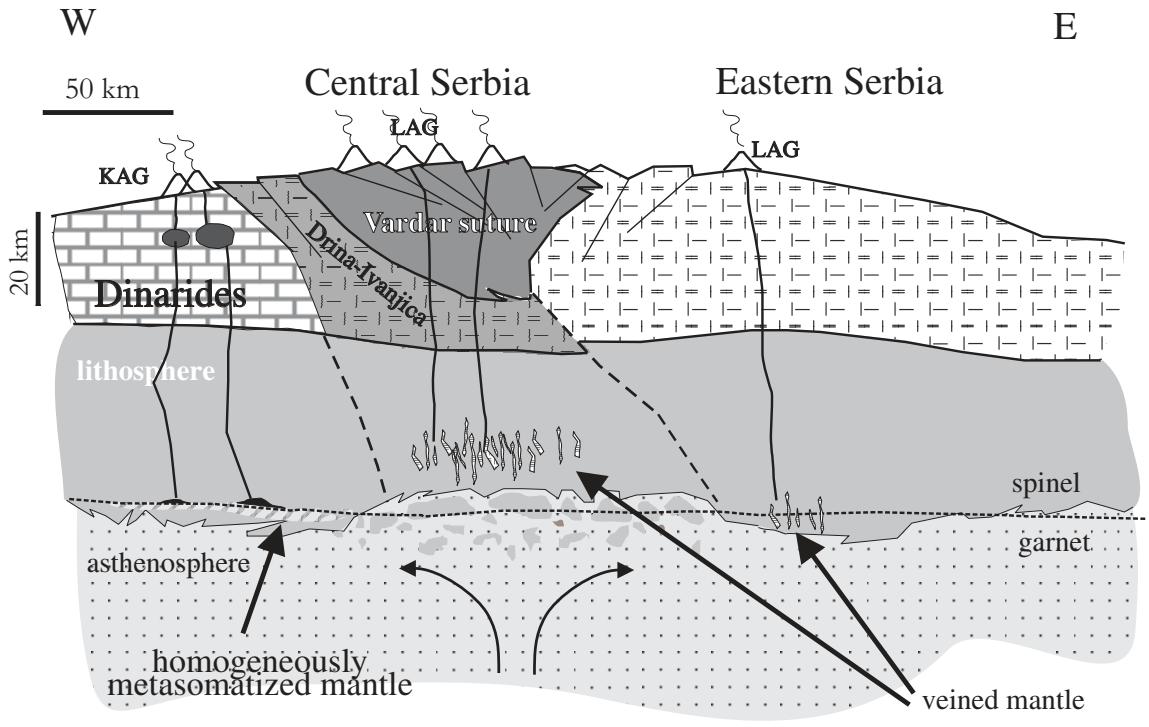

Fig. 18. Geodynamic model to illustrate the origin of Tertiary ultrapotassic volcanism in Serbia, in response to the orogenic collapse. Differences in the scale and the character of mantle heterogeneity in the various terranes are the major reason for the geochemical variability of the erupted magmas. Vardar suture—the Vardar ophiolitic suture zone; Dinarides—the Dinaride ophiolite belt terrane; Drina–Ivanjica—the Drina–Ivanjica terrane.

Oligocene–Early Miocene Dinaride–Kraishtide lacustrine province of Marović *et al.* (1998, 1999) or Krstić (2001), which is interpreted as a result of a wide dextral wrench corridor that occurred along the axis of the collapsing Dinaride orogen. Figure 18 illustrates the geodynamic situation during Serbian ultrapotassic volcanism as being triggered mostly by the collapse of the Dinaride orogen. The Vardar ophiolitic suture zone is shown as a simple rootless suture unit (Dinter, 1998), although some consider it to have originally consisted of different domains or lithospheric blocks (Karamata *et al.*, 1999). Rough approximations of crustal and lithospheric thickness are based on estimates for recent continental crust in former Yugoslavia (Aljinović, 1987). The extensional episode with its surface expression in the pull-apart basins and lacustrine provinces (Djurdjević, 1992; Obradović *et al.*, 1994) corresponds at both regional and local levels to the ultrapotassic magmatism. The younger magmatic ages (around 22 Ma) were partly contemporaneous with the westward displacement and clockwise rotation of the Tisza–Alcapa domain (Balla, 1986; Csontos *et al.*, 1992; Csontos, 1995) that resulted in the Middle Miocene extension and collapse in the Pannonian Basin. Finally, the youngest tectonic movements related to rotation of the external Albano-Hellenides along the Scutari–Peć line, initiated by the Late Miocene–Pliocene extension of the Aegean Basin (Kissel *et al.*, 1995; Marović *et al.*, 1998), gave rise to the youngest ultrapotassic volcanism at around 5 Ma.

The spatial distribution and geochemical features of the two Serbian ultrapotassic suites are discontinuous even within the same magmatic cycle. This may reflect the different lithospheric blocks on which they occur. If this is correct, the spatial separation of the two ultrapotassic suites, regardless of age, implies their derivation from different lithospheric mantle domains. This idea, although not fully constrained, is supported by the general geology of the area. The Balkans are composed of a number of micro-terranes, of different age, origin and provenance. The Pan-African affinity of the Dinaride basement (Ilić *et al.*, in preparation), together with previous geotectonic interpretations, implies different provenance for the two terranes (Dinarides and Vardar) in which the two ultrapotassic magmatic suites occur. However, there is a complete lack of deep seismic data on the structure of the Vardar ophiolitic suture zone to allow further constraint on the structure and composition of the lower crust and mantle.

The close isotopic resemblance of the Serbian ultrapotassic rocks to Mesozoic flysch sediments from the central Serbian suture zone lends support to the interpretation

that the enrichment of their mantle sources is probably related to Mesozoic subduction. The occurrence of a crustal signature in the source of the ultrapotassic magmas from all the lithospheric segments suggests that the mantle below the Dinarides was also affected by subduction. During subsequent convective thinning of the lithospheric mantle and advection in the region of the thermal boundary layer, these enriched lithospheric domains were exposed to the hot asthenosphere, giving rise to melting. Our results suggest zonation of metasomatic assemblages in the lithospheric upper mantle. For the central and eastern Serbian units, a phlogopite-bearing refractory spinel lherzolite (Central Serbia) and garnet lherzolite (easternmost LAG rocks) source with phlogopite and apatite situated in veins is most probable. The spatial distribution of the LAG magmatism is along a NW–SE-trending line striking roughly parallel to the Zvornik line (Fig. 1); this lineament probably represents a fundamental fracture zone that allowed migration of melts from metasomatized lithosphere domains. The western terranes host the KAG volcanics, which appear to be derived from homogeneously metasomatized phlogopite + apatite + Ti-oxide + garnet-bearing mantle peridotite. These volcanics may be regarded as counterparts of the Italian low-silica 'leucite-bearing' rocks (Conticelli *et al.*, 2002), suggesting a common geodynamic history of their sources (Dinarides and Apennines) and a similar pre-eruptive mantle metasomatic event.

ACKNOWLEDGEMENTS

D.P. is greatly indebted to the late Milivoje Jovanović for his close collaboration and guidance during the fieldwork. The authors are very grateful to O. Appelt and D. Rhede for assistance with the microprobe analyses. Professor Dr. Mahmut Tarkian and Barbara Cornelisen from Mineralogisch–Petrographisches Institut Hamburg provided access to the microprobe for D.P., making possible very helpful early reconnaissance study. We thank Sandro Conticelli, Nick Rodgers and an anonymous reviewer for very constructive and helpful reviews that extensively improved the paper. Finally, during thorough editorial handling, Marjorie Wilson substantially improved the presentation of our arguments in the manuscript. This research has been supported by the Deutsche Forschungsgemeinschaft (DFG) within the project Fo 181-15. We also acknowledge the support of the European Community Access to Research Infrastructure action of the Improving Human Potential Programme, contract HPRICT-199900008 awarded to Professor B. J. Wood (EU Geochemical Facility, University of Bristol).

SUPPLEMENTARY DATA

Supplementary data for this paper are available at *Journal of Petrology* online.

REFERENCES

Aljinović, B. (1987). On certain characteristics of the Mohorovicic discontinuity in the region of Yugoslavia. *Acta Geologica* **55**, 13–18.

Altherr, R., Meyer, H.-P., Holl, A., Volker, F., Alibert, C., McCulloch, M. T. & Majer, V. (2004). Geochemical and Sr–Nd–Pb isotopic characteristics of Late Cenozoic leucite lamproites from the East European Alpine belt (Macedonia and Yugoslavia). *Contributions to Mineralogy and Petrology* **147**, 58–73.

Andersen, D. J. & Lindsley, D. H. (1988). Internally consistent solution models for Fe–Mg–Mn–Ti oxides; Fe–Ti oxides. *American Mineralogist* **73**, 714–726.

Andersen, D. J., Lindsley, D. H. & Davidson, P. M. (1993). QUILF; a Pascal program to assess equilibria among Fe–Mg–Mn–Ti oxides, pyroxenes, olivine and quartz. *Computers and Geosciences* **19**, 1333–1350.

Anderson, D. L. (1995). Lithosphere, asthenosphere and perisphere. *Reviews of Geophysics* **33**, 125–149.

Arai, S. (1994). Compositional variation of olivine–chromian spinel in Mg-rich magmas as a guide to their residual spinel peridotites. *Journal of Volcanology and Geothermal Research* **59**, 279–293.

Araujo, A. L. N., Carlson, R. W., Gaspar, J. C. & Bizzi, L. A. (2001). Petrology of kamafugites and kimberlites from the Alto Paranaíba Alkaline Province, Minas Gerais, Brazil. *Contributions to Mineralogy and Petrology* **142**, 163–177.

Arndt, N. T., Naldrett, A. J. & Pyke, D. R. (1977). Komatiitic and iron-rich tholeiitic lavas of Munro Township, Northeast Ontario. *Journal of Petrology* **18**, 319–369.

Balla, Z. (1986). Palaeotectonic reconstruction of the central Alpine–Mediterranean belt for the Neogene. In: *Tectonics of the Eurasian Fold Belts*. Amsterdam: Elsevier, pp. 213–243.

Ballhaus, C., Berry, R. F. & Green, D. H. (1991). High pressure experimental calibration of the olivine–orthopyroxene–spinel oxygen geobarometer; implications for the oxidation state of the upper mantle. *Contributions to Mineralogy and Petrology* **107**, 27–40.

Barnes, S. J. & Roeder, P. L. (2001). The range of spinel compositions in terrestrial mafic and ultramafic rocks. *Journal of Petrology* **42**, 2279–2302.

Bell, K. (2002). The isotope geochemistry of the mantle below Italy. *EUROCARB Workshop, Italy, 7–10 June 2002, Chieti; Abstracts*, pp. 16–18.

Bell, K., Castorina, F., Rosatelli, G. & Stoppa, F. (2003). Large scale, mantle plume activity below Italy: isotopic evidence and volcanic consequences. European Geosciences Union, General Assembly 2003, Nice. CD with abstracts. European Geophysical Society.

Benito, R., López-Ruiz, J., Cebriá, J. M., Hertogen, J., Doblas, M., Oyarzun, R. & Demaiffe, D. (1999). Sr and O isotope constraints on source and crustal contamination in the high-K calc-alkaline and shoshonitic Neogene volcanic rocks of SE Spain. *Lithos* **46**, 773–802.

Ben Othman, D., White, W. M. & Patchett, J. (1989). The geochemistry of marine sediments, island arc magma genesis, and crust–mantle recycling. *Earth and Planetary Science Letters* **94**, 1–21.

Cameron, W. E., McCulloch, M. T. & Walker, D. A. (1983). Boninite petrogenesis; chemical and Nd–Sr isotopic constraints. *Earth and Planetary Science Letters* **65**, 75–89.

Campbell, I. H. (2001). Identification of ancient mantle plumes. In: Ernst, R. & Buchan, K. L. (eds) *Mantle Plumes; their Identification through Time. Geological Society of America, Special Papers* **352**, 5–21.

Campbell, I. H., Naldrett, A. J. & Roeder, P. L. (1979). Nickel activity in silicate liquids; some preliminary results. *Canadian Mineralogist* **17**, 495–505.

Carlson, R. W., Esperanca, S. & Svisero, D. P. (1996). Chemical and Os isotopic study of Cretaceous potassic rocks from southern Brazil. *Contributions to Mineralogy and Petrology* **125**, 393–405.

Carmichael, I. S. E., Lange, R. A. & Luhr, J. F. (1996). Quaternary minettes and associated volcanic rocks of Mascota, western Mexico; a consequence of plate extension above a subduction modified mantle wedge. *Contributions to Mineralogy and Petrology* **124**, 302–333.

Cebria, J. M. & Lopez Ruiz, J. (1996). A refined method for trace element modelling of nonmodal batch partial melting processes; the Cenozoic continental volcanism of Calatrava, central Spain. *Geochimica et Cosmochimica Acta* **60**, 1355–1366.

Cebria, J. M. & Wilson, M. (1995). Cenozoic mafic magmatism in Western/Central Europe: a common European Asthenospheric Reservoir? *Terra Abstracts, EUG*, **8**, 162.

Chauvel, C., Hofmann, A. W. & Vidal, P. (1992). HIMU-EM; the French Polynesian connection. *Earth and Planetary Science Letters* **110**, 99–119.

Chazot, G., Menzies, M. A. & Harte, B. (1996). Determination of partition coefficients between apatite, clinopyroxene, amphibole and melt in natural spinel lherzolites from Yemen; implications for wet melting of the lithospheric mantle. *Geochimica et Cosmochimica Acta* **60**, 423–437.

Cioflica, G., Jude, R., Lupulescu, M. & Palaseanu, M. (1995). Late Cretaceous–Eocene arc magmatism in the western part of the South Carpathians, Romania. *Geological Society of Greece, Special Publication, Proceedings of XV Congress of the CBGA* **4/2**, 495–500.

Cioflica, G., Jude, R., Lupulescu, M. & Ducea, M. (1996). Lower crustal origin of the late Cretaceous–Eocene arc magmatism in the western part of the South Carpathians, Romania. In: Knežević-Djordjević, V. & Krstić, B. (eds) *Terranes of Serbia*. Belgrade: Faculty of Mining and Geology, University of Belgrade, pp. 103–107.

Class, C. & Goldstein, S. L. (1997). Plume–lithosphere interactions in the ocean basins; constraints from the source mineralogy. *Earth and Planetary Science Letters* **150**, 245–260.

Conticelli, S. (1998). The effect of crustal contamination on ultrapotassic magmas with lamproitic affinity: mineralogical, geochemical and isotope data from the Torre Alfina lavas and xenoliths, Central Italy. *Chemical Geology* **149**, 51–81.

Conticelli, S. & Peccerillo, A. (1992). Petrology and geochemistry of potassic and ultrapotassic volcanism in central Italy: petrogenesis and inferences on the evolution of the mantle sources. *Lithos* **28**, 221–240.

Conticelli, S., Manetti, P. & Menichetti, S. (1992). Mineralogy, geochemistry and Sr-isotopes in orendites from South Tuscany, Italy; constraints on their genesis and evolution. *European Journal of Mineralogy* **4**, 1359–1375.

Conticelli, S., D'Antonio, M., Pinarelli, L. & Civetta, L. (2002). Source contamination and mantle heterogeneity in the genesis of Italian potassic and ultrapotassic volcanic rocks: Sr–Nd–Pb isotope data from Roman Province and Southern Tuscany. *Mineralogy and Petrology* **74**, 189–222.

Csontos, L. (1995). Tertiary tectonic evolution of the Intra-Carpathian area: a review. *Acta Vulcanologica* **7**, 1–15.

Csontos, L., Nagymarosy, A., Horvath, A. & Kovacs, M. (1992). Tertiary evolution of the Intra-Carpathian area: a model. *Tectonophysics* **208**, 221–241.

Cvetković, V., Knežević, V. & Pécskay, Z. (2000). Tertiary igneous formations of the Dinarides, Vardar zone and adjacent regions: from recognition to petrogenetic implications. In: Karamata, S. & Janković, S. (eds) *Geology and Metallogeny of the Dinarides and the Vardar Zone*. Banja Luka-Srpsko Sarajevo: Academy of Sciences and Arts of the Republic of Srpska, pp. 245–253.

Cvetković, V., Prelević, D., Downes, H., Jovanović, M., Vaselli, O. & Pécskay, Z. (2004*a*). Origin and geodynamic significance of Tertiary post-collisional basaltic magmatism in Serbia (Central Balkan Peninsula). *Lithos* **73**, 161–186.

Cvetković, V., Downes, H., Prelević, D., Jovanović, M. & Lazarov, M. (2004*b*). Characteristics of the lithospheric mantle beneath East Serbia inferred from ultramafic xenoliths in Paleogene basanites. *Contributions to Mineralogy and Petrology* **148**, 335–357.

Di Battistini, G., Montanini, A., Vernia, L., Bargossi, G. M. & Castorina, F. (1998). Petrology and geochemistry of ultrapotassic rocks from the Montefiascone Volcanic Complex (Central Italy): magmatic evolution and petrogenesis. *Lithos* **43**, 169–195.

Di Battistini, G., Montanini, A., Vernia, L., Venturelli, G. & Tonarini, S. (2001). Petrology of melilite-bearing rocks from the Montefiascone Volcanic Complex (Roman Magmatic Province): new insights into the ultrapotassic volcanism of Central Italy. *Lithos* **59**, 1–24.

Dimitrijević, M. D. (2001). Dinarides and the Vardar Zone: a short review of the geology. *Acta Vulcanologica* **13**, 1–8.

Dinter, D. A. (1998). Late Cenozoic extension of the Alpine collisional orogen, northeastern Greece: origin of the north Aegean basin. *Geological Society of America Bulletin* **110**, 1208–1230.

Djurdjević, J. (1992). Sedimentology of the Neogene lake basins, on the example of the Pranjani basin. M.Sc. thesis, University of Belgrade, 193 pp.

Downes, H., Kostoula, T., Jones, A. P., Beard, A. D., Thirlwall, M. F. & Bodinier, J. L. (2002). Geochemistry and Sr–Nd isotopic compositions of mantle xenoliths from the Monte Vulture carbonatite–melilitite volcano, central southern Italy. *Contributions to Mineralogy and Petrology* **144**, 78–92.

Eggler, D. H. (1974). Effect of CO_2 on the melting of peridotite. *Carnegie Institution of Washington, Yearbook* **73**, 215–224.

Eggler, D. H. (1983). Upper mantle oxidation state: evidence from olivine–orthopyroxene–ilmenite assemblages. *Geophysical Research Letters* **10**, 365–368.

Ellam, R., Hawkesworth, C., Menzies, M. & Rogers, N. (1989). The volcanism of southern Italy: role of subduction and the relationship between potassic and sodic alkaline volcanism. *Journal of Geophysical Research* **94**, 4589–4601.

Falloon, T. J. & Danyushevsky, L. V. (2000). Melting of refractory mantle at 1·5, 2 and 2·5 GPa under anhydrous and H_2O-undersaturated conditions: implications for the petrogenesis of high-Ca boninites and the influence of subduction components on mantle melting. *Journal of Petrology* **41**, 257–283.

Foley, S. F. (1985). The oxidation state of lamproitic magmas. *Tschermaks Mineralogische und Petrographische Mitteilungen* **34**, 217–238.

Foley, S. F. (1989). Experimental constraints of phlogopite chemistry in lamproites; 1, The effect of water activity and oxygen fugacity. *European Journal of Mineralogy* **1**, 411–426.

Foley, S. F. (1992*a*). Vein-plus-wall-rock melting mechanisms in the lithosphere and the origin of potassic alkaline magmas. *Lithos* **28**, 435–453.

Foley, S. F. (1992*b*). Petrological characterization of the source components of potassic magmas: geochemical and experimental constraints. *Lithos* **28**, 187–204.

Foley, S. F. (1993). An experimental study of olivine lamproite—first results from the diamond stability field. *Geochimica et Cosmochimica Acta* **57**, 483–489.

Foley, S. F. & Jenner, G. A. (2004). Trace element partitioning in lamproitic magmas—the Gaussberg olivine leucitite. *Lithos* **75**, 19–38.

Foley, S. F. & Venturelli, G. (1989). High K_2O rocks with high MgO, high SiO_2 affinities. In: Crawford, A. J. (ed.) *Boninites and Related Rocks*. London: Unwin Hyman, pp. 72–88.

Foley, S. F., Taylor, W. R. & Green, D. H. (1986). The role of fluorine and oxygen fugacity in the genesis of the ultrapotassic rocks. *Contributions to Mineralogy and Petrology* **94**, 183–192.

Foley, S. F., Venturelli, G., Green, D. H. & Toscani, L. (1987). The ultrapotassic rocks: characteristics, classification and constraints for petrogenetic models. *Earth-Science Reviews* **24**, 81–134.

Foley, S. F., Jackson, S. E., Fryer, B. J., Greenough, J. D. & Jenner, G. A. (1996). Trace element partition coefficients for clinopyroxene and phlogopite in an alkaline lamprophyre from Newfoundland by LAM-ICP-MS. *Geochimica et Cosmochimica Acta* **60**, 629–638.

Foley, S. F., Musselwhite, D. S. & van der Laan, S. R. (1999). Melt compositions from ultramafic vein assemblages in the lithospheric mantle; a comparison of cratonic and non-cratonic settings. In: Gurney, J. J., Gurney, J. L., Pascoe, M. D. & Richardson, S. H. (eds) *The J. B. Dawson Volume; Proceedings of the VIIth International Kimberlite Conference; Volume 1*. Cape Town: Red Roof Design, pp. 238–246.

Foley, S. F., Barth, M. G. & Jenner, G. A. (2000). Rutile/melt partition coefficients for trace elements and an assessment of the influence of rutile on the trace element characteristics of subduction zone magmas. *Geochimica et Cosmochimica Acta* **64**, 933–938.

Fraser, K., Hawkesworth, C., Erlank, A., Mitchell, R. & Scott-Smith, B. (1985). Sr, Nd and Pb isotope and minor element geochemistry of lamproites and kimberlites. *Earth and Planetary Science Letters* **76**, 57–70.

Gasperini, D., Blichert-Toft, J., Bosch, D., Moro, A. D., Macera, P. & Albarède, F. (2002). Upwelling of deep mantle material through a plate window: evidence from the geochemistry of Italian basaltic volcanics. *Journal of Geophysical Research* **107**, 2367.

Gaul, O. F., Griffin, W. L., O'Reilly, S. Y. & Pearson, N. J. (2000). Mapping olivine composition in the lithospheric mantle. *Earth and Planetary Science Letters* **182**, 223–235.

Green, T. H. & Pearson, N. J. (1987). An experimental study of Nb and Ta partitioning between Ti-rich minerals and silicate liquids at high pressure and temperature. *Geochimica et Cosmochimica Acta* **51**, 55–62.

Green, T. H., Blundy, J. D., Adam, J. & Yaxley, G. M. (2000). SIMS determination of trace element partition coefficients between garnet, clinopyroxene and hydrous basaltic liquids at 2–7·5 GPa and 1080–1200°C. In: Austrheim, H. & Griffin, W. L. (eds) *Element Partitioning in Geochemistry and Petrology; Special Volume in Honour of Brenda B. Jensen*. Amsterdam: Elsevier, pp. 165–187.

Harangi, S. (2001). Neogene magmatism in the Alpine–Pannonian Transition Zone—a model for melt generation in a complex geodynamic setting. *Acta Vulcanologica* **13**, 25–39.

Hart, S. R. (1984). A large-scale isotope anomaly in the Southern Hemisphere mantle. *Science* **309**, 753–757.

Hart, S. R., Hauri, E. H., Oschmann, L. A. & Whitehead, J. A. (1992). Mantle plumes and entrainment; isotopic evidence. *Science* **256**, 517–520.

Harte, B. (1987). Metasomatic events recorded in mantle xenoliths; an overview. In: Nixon, P. H. (ed.) *Mantle Xenoliths*. Chichester: John Wiley, pp. 625–640.

Hoch, M., Rehkamper, M. & Tobschall, H. J. (2001). Sr, Nd, Pb and O isotopes of minettes from Schirmacher Oasis, East Antarctica: a case of mantle metasomatism involving subducted continental material. *Journal of Petrology* **42**, 1387–1400.

Holmes, A. & Harwood, H. F. (1937). *The Volcanic Area of Bufumbira. Part II: The Petrology of the Volcanic Field of Bufumbira, South-West Uganda. Geological Survey of Uganda Memoir*.

Ilić, A., Neubauer, F. & Handler, R. (2005). Late Paleozoic–Mesozoic tectonics of Dinarides revisited: implications from $^{40}Ar/^{39}Ar$ dating of detrital white micas. *Geology* (in press).

Ionov, D. A. & Hofmann, A. W. (1995). Nb–Ta-rich mantle amphiboles and micas; implications for subduction-related metasomatic trace element fractionations. *Earth and Planetary Science Letters* **131**, 341–356.

Ionov, D. A., Grégoire, M. & Prikhodko, V. S. (1999). Feldspar–Ti-oxide metasomatism in off-cratonic continental and oceanic upper mantle. *Earth and Planetary Science Letters* **165**, 37–44.

Jaques, A. L., Lewis, J. D., Smith, C. B., Gregory, G. P., Ferguson, J., Chappell, B. W. & McCulloch, M. T. (1984). The diamond-bearing ultrapotassic (lamproitic) rocks of the West Kimberley region, Western Australia. In: Kornprobst, J. (ed.) *Proceedings of the 3rd International Kimberlite Conference*. Amsterdam: Elsevier, pp. 225–254.

Kalfoun, F., Ionov, D. & Merlet, C. (2002). HFSE residence and Nb/Ta ratios in metasomatised, rutile-bearing mantle peridotites. *Earth and Planetary Science Letters* **199**, 49–65.

Kamenetsky, V. S., Crawford, A. J. & Meffre, S. (2001). Factors controlling chemistry of magmatic spinel: an empirical study of associated olivine, Cr-spinel and melt inclusions from primitive rocks. *Journal of Petrology* **42**, 655–671.

Kamenetsky, V. S., Sobolev, A. V., Eggins, S. M., Crawford, A. J. & Arculus, R. J. (2002). Olivine-enriched melt inclusions in chromites from low-Ca boninites, Cape Vogel, Papua New Guinea; evidence for ultramafic primary magma, refractory mantle source and enriched components. In: Hauri, E. H., Kent, A. J. R. & Arndt, N. (eds) *Melt Inclusions at the Millennium; Toward a Deeper Understanding of Magmatic Processes*. Amsterdam: Elsevier, pp. 287–303.

Karamata, S. & Djordjević, P. (1980). Origin of the Upper Cretaceous and Tertiary magmas in the Eastern part of Yugoslavia. *Bulletin de l'Académie des Serbe des Sciences et des Arts, Classe des Sciences Mathématiques et Naturelles, Sciences Naturelles* **LXXII**, 99–108.

Karamata, S. & Krstić, B. (1996). Terranes of Serbia and neighboring areas. In: Knežević-Djordjević, V. & Krstić, B. (eds) *Terranes of Serbia*. Belgrade: Faculty of Mining and Geology, University of Belgrade, pp. 25–40.

Karamata, S., Steiger, R., Djordjević, P. & Knezević, V. (1990). New data on the origin of granitic rocks from western Serbia. *Bulletin de l'Académie des Serbe des Sciences et des Arts, Classe des Sciences Mathématiques et Naturelles, Sciences Naturelles* **32**, 1–9.

Karamata, S., Knežević, V., Pécskay, Z. & Djordjević, M. (1997*a*). Magmatism and metallogeny of the Ridanj–Krepoljin belt (eastern Serbia) and their correlation with northern and eastern analogues. *Mineralium Deposita* **32**, 452–458.

Karamata, S., Krstić, B., Dimitrijević, D. M., Dimitrijević, M. N., Knežević, V., Stojanov, R. & Filipović, I. (1997*b*). Terranes between the Moesian Plate and the Adriatic Sea. In: *IGCP Project No. 276; Paleozoic Geodynamic Domains and their Alpidic Evolution in the Tethys*. Athens: Laboratoire de Géologie de l'Université, pp. 429–477.

Karamata, S., Dimitrijević, N. M. & Dimitrijević, D. M. (1999). Oceanic realms in the central part of the Balkan Peninsula during the Mesozoic. *Slovak Geological Magazine* **5**, 173–177.

Keith, T. E. C., Thompson, J. M. & Mays, R. E. (1983). Selective concentration of cesium in analcime during hydrothermal alteration, Yellowstone National Park, Wyoming. *Geochimica et Cosmochimica Acta* **47**, 795–804.

Kissel, C., Speranza, F. & Milićević, V. (1995). Paleomagnetism of external southern and central Dinarides and northern Albanides: implications for the Cenozoic activity of the Scutari–Pec transverse zone. *Journal of Geophysical Research* **100**, 14999–15007.

Konzett, J. & Ulmer, P. (1999). The stability of hydrous potassic phases in lherzolitic mantle—an experimental study to 9·5 GPa in simplified and natural bulk compositions. *Journal of Petrology* **40**, 629–652.

Kretz, R. (1983). Symbols for rock-forming minerals. *American Mineralogist* **68**, 277–279.

Krstić, N. (2001). Timing of the Neogene geotectonic events in the Carpatho-Balkanidic and Dinaridic Alps with adjoining regions. *PANCARDI 2001, Sopron, Abstracts*, p. 25.

Kuehner, S., Edgar, A. & Arima, M. (1981). Petrogenesis of the ultrapotassic rocks from the Leucite Hills, Wyoming. *Amererican Mineralogist* **66**, 663–677.

Le Maitre, R. W. (ed.) (2002). *Igneous Rocks: a Classification and Glossary of Terms: Recommendations of the International Union of Geological Sciences Subcommission on the Systematics of Igneous Rocks*. Cambridge: Cambridge University Press, 236 pp.

Maaløe, S. (1994). Estimation of the degree of partial melting using concentration ratios. *Geochimica et Cosmochimica Acta* **58**, 2519–2525.

Maaløe, S. & Pedersen, R. B. (2003). Two methods for estimating the degree of melting and trace element concentrations in the sources of primary magmas. *Chemical Geology* **193**, 155–166.

Marović, M., Djoković, I. & Toljić, M. (1998). Genesis of the neotectonic structures of Serbia. *Annales Géologiques de la Peninsule Balkanique* **LXII**, 25–47.

Marović, M., Krstić, N., Stanić, S., Cvetković, V. & Petrović, M. (1999). The evolution of Neogene sedimentation provinces of Central Balkan Peninsula. *Bulletin of Geoinstitute* **36**, 25–94.

Marović, M., Djoković, I., Pešić, L., Toljić, M. & Gerzina, N. (2000). The genesis and geodynamics of Cenozoic sedimentation provinces of the central Balkan Peninsula. *Geotectonics* **34**, 415–427.

Marović, M., Mihailović, D., Djoković, I., Gerzina, N. & Toljić, M. (2001). Wrench tectonic of the Paleogene–Lower Miocene basins of Serbia between the central part of the Vardar Zone and the Moesian Plate. *PANCARDI 2001, Sopron, Abstracts*, p. 28.

Marović, M., Djoković, I., Pešić, L., Radovanović, S., Toljić, M. & Gerzina, N. (2002). Neotectonics and seismicity of the southern margin of the Pannonian Basin in Serbia. *EGU Stephan Mueller Special Publication Series* **3**, 1–19.

McDonough, W. (1990). Constraints on the composition of the continental lithospheric mantle. *Earth and Planetary Science Letters* **101**, 1–18.

McDonough, W. F. & Sun, S. S. (1995). The composition of the Earth. In: McDonough, W. F., Arndt, N. T. & Shirey, S. (eds) *Chemical Evolution of the Mantle. Chemical Geology*. Amsterdam: Elsevier, pp. 223–253.

Meen, J. K., Ayers, J. C. & Fregeau, E. J. (1989). A model of mantle metasomatism by carbonated alkaline melts; trace-element and isotopic compositions of mantle source regions of carbonatite and other continental igneous rocks. In: Bell, K. (ed.) *Carbonatites; Genesis and Evolution*. London: Unwin Hyman, pp. 464–499.

Miller, C., Schuster, R., Klötzli, U., Frank, W. & Purtscheller, F. (1999). Post-collisional potassic and ultrapotassic magmatism in SW Tibet: geochemical and Sr–Nd–Pb–O isotopic constraints for mantle source characteristics and petrogenesis. *Journal of Petrology* **40**, 1399–1424.

Mitchell, R. H. (1995). Melting experiments on a sanidine phlogopite lamproite at 4–7 GPa and their bearing on the sources of lamproitic magmas. *Journal of Petrology* **36**, 1455–1474.

Mitchell, R. H. & Bergman, S. C. (1991). *Petrology of Lamproites*. New York: Plenum.

Mitchell, R. H., Platt, R. G. & Downey, M. (1987). Petrology of lamproites from Smoky Butte, Montana. *Journal of Petrology* **28**, 645–677.

Moine, B. N., Grégoire, M., O'Reilly, S. Y., Sheppard, S. M. F. & Cottin, J. Y. (2001). High field strength element fractionation in the upper mantle: evidence from amphibole-rich composite mantle xenoliths from the Kerguelen Islands (Indian Ocean). *Journal of Petrology* **42**, 2145–2167.

Murck, B. W. & Campbell, I. H. (1986). The effects of temperature, oxygen fugacity and melt composition on the behaviour of chromium in basic and ultrabasic melts. *Geochimica et Cosmochimica Acta* **50**, 1871–1887.

Murphy, D. T., Collerson, K. D. & Kamber, B. S. (2002). Lamproites from Gaussberg, Antarctica: possible transition zone melts of Archaean subducted sediments. *Journal of Petrology* **43**, 981–1001.

Nelson, D. R. (1992). Isotopic characteristics of potassic rocks; evidence for the involvement of subducted sediments in magma genesis. *Lithos* **28**, 403–420.

Nelson, D. R., McCulloch, M. T. & Sun, S. S. (1986). The origins of ultrapotassic rocks as inferred from Sr, Nd and Pb isotopes. *Geochimica et Cosmochimica Acta* **50**, 231–245.

Nixon, P. H. (1987). *Mantle Xenoliths*. Chichester: John Wiley.

Obradović, J., Djurdjević, C. J., Vasić, N. & Grubin, N. (1994). Facies and characteristics of some Neogene lacustrine sediments in Serbia. *Sedimentary Facies and Palaeogeography* **14**, 12–27.

Peccerillo, A. (1985). Roman comagmatic province (central Italy); evidence for subduction-related magma genesis. *Geology (Boulder)* **13**, 103–106.

Peccerillo, A. (1990). On the origin of the Italian potassic magmas—comments. *Chemical Geology* **85**, 183–196.

Peccerillo, A. (1992). Potassic and ultrapotassic rocks: compositional characteristics, petrogenesis and geologic significance. *Episodes—Journal of International Geoscience* **15**, 243–251.

Peccerillo, A. (1995). Mafic calc-alkaline to ultrapotassic magmas in central–southern Italy; constraints on evolutionary processes and implications for source composition and conditions of magma generation. In: *Proceedings of the Symposium on the Physics and the Chemistry of the Upper Mantle*. Rio de Janeiro: Academia Brasileira de Ciencias, pp. 171–189.

Peccerillo, A. (1998). Relationships between ultrapotassic and carbonate-rich volcanic rocks in central Italy: petrogenetic and geodynamic implications. *Lithos* **43**, 267–279.

Peccerillo, A. (1999). Multiple mantle metasomatism in central–southern Italy: geochemical effects, timing and geodynamic implications. *Geology* **27**, 315–318.

Peccerillo, A. (2003). Plio-Quaternary magmatism in Italy. *Episodes—Jornal of International Geoscience* **26**, 222–226.

Perini, G. & Conticelli, S. (2002). Crystallization conditions of leucite-bearing magmas and their implications on the magmatological evolution of ultrapotassic magmas: the Vico Volcano, Central Italy. *Mineralogy and Petrology* **74**, 253–276.

Poustovetov, A. A. & Roeder, P. L. (2001). The distribution of Cr between basaltic melt and chromian spinel as an oxygen geobarometer. *Canadian Mineralogist*, **39**, pp. 309–317.

Prelević, D., Cvetković, V. & Foley, S. F. (2001*a*). Composite igneous intrusions from Serbia: two case studies of interaction between lamprophyric and granitoid magmas. *Acta Vulcanologica* **13**, 145–157.

Prelević, D., Cvetković, V., Foley, S. F., Jovanović, M. & Melzer, S. (2001*b*). Tertiary ultrapotassic–potassic rocks from Serbia, Yugoslavia. *Acta Vulcanologica* **13**, 101–115.

Prelević, D., Foley, S. F. & Cvetković, V. (2002*a*). A Serbian ultrapotassic province reminiscent of central–southern Italy. In: *EUROCARB Workshop, Italy, 7–10 June 2002, Chieti; Abstracts*, pp. 23–25.

Prelević, D., Foley, S. F. & Cvetković, V. (2002*b*). Petrology, geochemistry and geodynamic significance of the Serbian ultrapotassic igneous province. *Berichte der Deutschen Mineralogischen Gesellschaft, Beihefte zum European Journal of Mineralogy* **14**, 133.

Prelević, D., Foley, S. F., Romer, R. & Cvetković, V. (2003). Serbian Tertiary ultrapotassic province—petrology, geochemistry and geodynamic significance. In: *Proceedings of the 8th International Kimberlite Conference*, Victoria, BC, 22–27 June 2003, FLA_0165.

Prelević, D., Foley, S. F., Cvetković, V. & Romer, R. L. (2004*a*). Origin of minette by mixing of lamproite and dacite magmas in Veliki Majdan, Serbia. *Journal of Petrology* **45**, 759–792.

Prelević, D., Foley, S. F., Cvetković, V. & Romer, R. L. (2004*b*). The analcime problem and its impact on the geochemistry of ultrapotassic rocks from Serbia. *Mineralogical Magazine* **68**, 621–636.

Redkin, A. F. & Hemley, J. J. (2000). Experimental Cs and Sr sorption on analcime in rock-buffered systems at 250–300°C and P_{sat} and the thermodynamic evaluation of mineral solubilities and phase relations. *European Journal of Mineralogy* **12**, 999–1014.

Righter, K. & Rosas-Elguera, J. (2001). Alkaline lavas in the volcanic front of the Western Mexican Volcanic Belt: geology and petrology of the Ayutla and Tapalpa volcanic fields. *Journal of Petrology* **42**, 2333–2361.

Rogers, N. W., Hawkesworth, C. J., Parker, R. J. & Marsh, J. S. (1985). The geochemistry of potassic lavas from Vulsini, central Italy and implications for mantle enrichment processes beneath the Roman region. *Contributions to Mineralogy and Petrology* **90**, 244–257.

Romer, R. L., Foerster, H. J. & Breitkreuz, C. (2001). Intracontinental extensional magmatism with a subduction fingerprint; the Late Carboniferous Halle volcanic complex (Germany). *Contributions to Mineralogy and Petrology* **141**, 201–221.

Ryerson, F. J. & Watson, E. B. (1987). Rutile saturation in magmas; implications for Ti–Nb–Ta depletion in island-arc basalts. *Earth and Planetary Science Letters* **86**, 225–239.

Sato, M. (1978). Oxygen fugacity of basaltic magmas and the role of gas-forming elements. *Geophysical Research Letters* **5**, 447–449.

Schmidt, K. H., Bottazzi, P., Vannucci, R. & Mengel, K. (1999). Trace element partitioning between phlogopite, clinopyroxene and leucite lamproite melt. *Earth and Planetary Science Letters* **168**, 287–299.

Shaw, D. M. (1970). Trace element fractionation during anatexis. *Geochimica et Cosmochimica Acta* **34**, 237–243.

Stoppa, F. & Cundari, A. (1995). A new Italian carbonatite occurrence at Cupaello (Rieti) and its genetic significance. *Contributions to Mineralogy and Petrology* **122**, 275–288.

Sun, S. S. & McDonough, W. F. (1989). Chemical and isotopic systematics of oceanic basalts; implications for mantle composition and processes. In: Saunders, A. D. & Norry, M. J. (eds) *Magmatism in the Ocean Basins. Geological Society, London, Special Publications* **42**, 313–345.

Tappe, S., Foley, S. F. & Pearson, D. G. (2003). The kamafugites of Uganda: a mineralogical and geochemical comparison with their Italian and Brazilian analogues. *Periodico di Mineralogia* **72**, 51–77.

Terzić, M. & Svešnjikova, E. V. (1991). Age of leucite-bearing rocks in Yugoslavia. *Comptes Rendus des Séances de la Société Serbe de Géologie* 283–287.

Thy, P., Stecher, O. & Korstgard, J. A. (1987). Mineral chemistry and crystallization sequences in kimberlite and lamproite dikes from the Sisimiut area, central West Greenland. *Lithos* **20**, 391–417.

Treuil, M. & Joron, J. L. (1975). Utilisation des éléments hydromagmatophiles pour la simplification de la modelisation quantitative des processus magmatiques; exemples de l'Afar et la Dorsale Medioatlantique. In: *Societa Italiana di Mineralogia e Petrologia; Atti della Riunione; Tavola Rotonda. Geochimica e Geochimica Isotopica.* **56**, 125–174.

Turner, S., Arnaud, N., Liu, J., Rogers, N., Hawkesworth, C., Harris, N., Kelley, S., van Calsteren, P. & Deng, W. (1996). Post-collision, shoshonitic volcanism on the Tibetan Plateau: implications for convective thinning of the lithosphere and the source of ocean island basalts. *Journal of Petrology* **37**, 45–71.

Turner, S., Platt, J. P., George, R. M. M., Kelley, S. P., Pearson, D. G. & Nowell, G. M. (1999). Magmatism associated with orogenic collapse of the Betic–Alboran domain, SE Spain. *Journal of Petrology* **40**, 1011–1036.

Vaselli, O., Downes, H., Thirlwall, M. F., Dobosi, G., Coradossi, N., Seghedi, I., Szakacs, A. & Vannucci, R. (1995). Ultramafic xenoliths in Plio-Pleistocene alkali basalts from the eastern Transylvanian Basin; depleted mantle enriched by vein metasomatism. *Journal of Petrology* **36**, 23–53.

Vasković, N., Jović, V. & Matović, V. (1996). Petrochemical characteristics of Tertiary volcanic rocks from Avala Mt. *Annales Géologiques de la Peninsule Balkanique* **LX/2**, 291–312.

Vaughan, A. P. M. (1996). A tectonomagmatic model for the genesis and emplacement of Caledonian calc-alkaline lamprophyres. *Journal of the Geological Society, London* **153**, 613–623.

Vaughan, A. P. M. & Scarrow, J. H. (2003). K-rich mantle metasomatism control of localization and initiation of lithospheric strike-slip faulting. *Terra Nova* **15**, 163–169.

Venturelli, G., Capedri, S., Battistini, G. D., Crawford, A., Kogarko, L. & Celestini, S. (1984*a*). The ultrapotassic rocks from southeastern Spain. *Lithos* **17**, 37–54.

Venturelli, G., Thorpe, R., Piaz, G. D., Moro, A. D. & Potts, P. (1984*b*). Petrogenesis of calc-alkaline, shoshonitic and associated ultrapotassic Oligocene volcanic rocks from the Northwestern Alps, Italy. *Contributions to Mineralogy and Petrology* **86**, 209–220.

Venturelli, G., Mariani, E. S., Foley, S. F., Capedri, S. & Crawford, A. J. (1988). Petrogenesis and conditions of crystallization of Spanish lamproitic rocks. *Canadian Mineralogist* **26**, 67–79.

Venturelli, G., Capedri, S., Barbieri, M., Toscani, L., Mariani, E. S. & Zerbi, M. (1991). The Jumilla lamproite revisited—a petrological oddity. *European Journal of Mineralogy* **3**, 123–145.

Vollmer, R. (1976). Rb–Sr and U–Th–Pb systematics of alkaline rocks; the alkaline rocks from Italy. *Geochimica et Cosmochimica Acta* **40**, 283–295.

Vollmer, R. (1989). On the origin of the Italian potassic magmas; 1, A discussion contribution. *Chemical Geology* **74**, 229–239.

Vollmer, R. (1991). On the origin of the Italian potassic magmas; a one-dimensional diffusion-controlled model of source metasomatism. *Earth and Planetary Science Letters* **107**, 487–498.

von Quadt, A., Peytcheva, I., Heinrich, C., Frank, M., Cvetković, V. & Banješević, M. (2003). Evolution of the Cretaceous magmatism in the Apuseni–Timok–Srednogorie metallogenic belt and implications for the geodynamic reconstructions: new insight from geochronology, geochemistry and isotope studies. *Final GEODE-ABCD Workshop, Programme and Abstracts*, 60 pp.

Watson, E. B. & Green, T. H. (1981). Apatite/liquid partition coefficients for the rare earth elements and strontium. *Earth and Planetary Science Letters* **56**, 405–421.

Wendlandt, R. F. (1991). Oxygen diffusion in basalt and andesite melts; experimental results and discussion of chemical versus tracer diffusion. *Contributions to Mineralogy and Petrology* **108**, 463–471.

Wilson, M. & Bianchini, G. (1999). Tertiary–Quaternary magmatism within the Mediterranean and surrounding regions. In: Durand, B., Jolivet, L., Horvath, F. & Seranne, M. (eds) *The Mediterranean Basins; Tertiary Extension within the Alpine Orogen. Geological Society, London, Special Publications* **156**, 141–168.

Wilson, M. & Downes, H. (1991). Tertiary–Quaternary extension-related alkaline magmatism in western and central Europe. *Journal of Petrology* **32**, 811–849.

Wilson, M. & Patterson, R. (2001). Intraplate magmatism related to short-wavelength convective instabilities in the upper mantle: evidence from the Tertiary–Quaternary volcanic province of western and central Europe. In: Ernst, R. & Buchan, K. L. (eds) *Mantle Plumes: their Identification through Time. Geological Society of America, Special Papers* **352**, 37–58.

Woolley, A. R., Bergman, S. C., Edgar, A. D., Le Bas, M. J., Mitchell, R., H., Rock, N. M. S. & Scott Smith, B. H. (1996). Classification of lamprophyres, lamproites, kimberlites, and kalsilitic, melilitic, and leucitic rocks. *Canadian Mineralogist* **34**, 175–186.

Zindler, A. & Hart, S. (1986). Chemical geodynamics. *Annual Review of Earth and Planetary Sciences* **14**, 493–571.